

ACTA UNIVERSITATIS SZEGEDIENSIS

PARS CLIMATOLOGICA
SCIENTIARIUM NATURALIUM
CURAT: JÁNOS UNGER

ACTA CLIMATOLOGICA
TOMUS LI-LII.

SZEGED (HUNGARIA)

2018

Editor-in-chief

JÁNOS UNGER

Editorial board

ILONA BÁRÁNY-KEVEI

ANITA BOKWA

TAMÁS GÁL

ÁGNES GULYÁS

PAVEL KONSTANTINOV

ATTILA KOVÁCS

RÓBERT MÉSZÁROS

STEVAN SAVIĆ

NÓRA SKARBIT

Technical editor

TAMÁS GÁL

Publisher

University of Szeged, Faculty of Sciences and Informatics
(H-6720 Szeged, Aradi vértanúk tere 1.)

The issues are available on
www.clima.u-szeged.hu/acta-climatologica

Acta Universitatis Szegediensis: **ISSN 0324-6523**

Acta Climatologica: **ISSN 0563-0614**

CONTENTS

Bokwa A, Dobrovolný P, Gál T, Geletič J, Gulyás Á, Hajto MJ, Holec J, Hollósi B, Kielar R, Lehnert M, Skarbit N, Šťastný P, Švec M, Unger J, Walawender JP, Žuvela-Aloise M: Urban climate in Central European cities and global climate change	7
Unger J, Skarbit N, Gál T: Absolute moisture content in mid-latitude urban canopy layer, Part 1: a literature review	37
Unger J, Skarbit N, Gál T: Absolute moisture content in mid-latitude urban canopy layer, Part 2: results from Szeged, Hungary	47
Molnár G, Gál T, Gyöngyösi AZ: Evaluation of a WRF-LCZ system in simulating urban effects under non-ideal synoptic patterns	57

URBAN CLIMATE IN CENTRAL EUROPEAN CITIES AND GLOBAL CLIMATE CHANGE*

A BOKWA¹, P DOBROVOLNÝ², T GÁL³, J GELETIČ², Á GULYÁS³, M J HAJTO⁴,
J HOLEC⁷, B HOLLÓSI⁵, R KIELAR⁴, M LEHNERT⁶, N SKARBIT³, P ŠTASTNÝ⁷, M
ŠVEC⁷, J UNGER³, J P WALAWENDER^{4,1} and M ŽUVELA-ALOISE⁵

¹Jagiellonian University, Institute of Geography and Spatial Management, Gronostajowa St. 7, 30-387 Kraków, Poland

²Global Change Research Centre AS CR, Belidla St. 986/4a, 603 00 Brno, Czech Republic

³Department of Climatology and Landscape Ecology, University of Szeged, Egyetem u. 2., 6720 Szeged, Hungary

⁴Institute of Meteorology and Water Management - National Research Institute, Piotra Borowego St. 14, 30-215 Kraków, Poland

⁵Zentralanstalt für Meteorologie und Geodynamik, Hohe Warte St. 38, 1190 Vienna, Austria

⁶Palacký University Olomouc, Krizkovského St. 511/8, 77147 Olomouc, Czech Republic

⁷Slovak Hydrometeorological Institute, Jeseniova St. 17, 83315 Bratislava, Slovakia

E-mail: anita.bokwa@uj.edu.pl

Summary: Urban areas are among those most endangered with the potential global climate changes. The studies concerning the impact of global changes on local climate of cities are of a high significance for the urban inhabitants' health and wellbeing. This paper is the final report of a project (Urban climate in Central European cities and global climate change) with the aim to raise the public awareness on those issues in five Central European cities: Szeged (Hungary), Brno (Czech Republic), Bratislava (Slovakia), Kraków (Poland) and Vienna (Austria). Within the project, complex data concerning local geomorphological features, land use and long-term climatological data were used to perform the climate modelling analyses using the model MUKLIMO_3 provided by the German Weather Service (DWD).

Key words: urban climate, climate change, urban climate model, heat load

1. INTRODUCTION

Global climate changes affect the environment in global, regional and local scales. Urban climate is a local scale phenomenon but it has direct and significant impact on 54% of the total global population living in cities (data of 2014). The global urban population is expected to grow further, approximately 1.84% per year between 2015 and 2020, 1.63% per year between 2020 and 2025, and 1.44% per year between 2025 and 2030 (Urban population growth 2015). Parallel, the global mean surface temperature change for the period 2016–2035 relative to 1986–2005 will likely be in the range of 0.3°C to 0.7°C, and relative to the average from year 1850 to 1900, global surface temperature change by the end of the 21st century is projected to likely exceed 1.5°C (IPCC 2013). Urban areas are among those most endangered with the potential global climate changes. The heat load in cities is supposed to get intensified as global temperature increase will be superimposed on air temperature modifications characteristic for urban areas, e.g. the Urban Heat Island (UHI) effect. Those phenomena might have far-reaching health effects (e.g. Baccini et al. 2008). Therefore, the

* This paper is the edited version of the final report of the Urban climate in Central European cities and global climate change project, submitted in 2015.

studies concerning the impact of global changes on local climate of cities are of a high significance for the urban inhabitants' health and wellbeing. In order to plan and undertake the mitigation actions in particular cities, it is necessary to recognize the possible range of heat load increase, in terms of both its magnitude and spatial extent.

The present paper shows the prediction of urban heat load increase by 2100 in five Central European cities: Kraków (Poland), Bratislava (Slovakia), Brno (Czech Republic), Szeged (Hungary) and Vienna (Austria). The heat load is defined as the mean annual number of the summer days, i.e. days with maximum temperature $\geq 25^{\circ}\text{C}$. Numerous previous studies, completed for the cities mentioned, allowed to achieve the recognition of their present urban climate features (e.g. Unger et al. 2011, Unger et al. 2014, Dobrowolný et al. 2012, Dobrowolný 2013, Lapin and Melo 2011, Auer et al. 1989, Böhm 1998, Walawender et al. 2014, Bokwa 2010a, 2010b, Bokwa et al. 2015). The cities are located in large river valleys and the diversified relief is an important local climate factor (except Szeged, located in flat area), even though the cities are not placed in the mountains. The historical urban infrastructure of Kraków, Bratislava, Brno and Szeged has been significantly modified first due to the destruction during the Second World War and then due to spatial development during the communistic times. For example, unlike in most cities located in USA or West Europe, areas with high buildings can be found in the suburbs, while city centres comprise of 2-3-storey historical buildings. Therefore, urban climate of the cities included in the study is an outcome of complex interactions between land use/land cover and land forms. The modelling approach used is designed to evaluate possible changes in urban heat load under future climate conditions, taking under consideration the role of the relief in controlling the urban climate which is a unique feature comparing to other similar tools available. The long-perspective aim of the study is to compare the values and spatial extent of the expected heat load increase among the cities included in the study, find the factors controlling those patterns and provide the city planners with information which can be implemented in the future urban development plans.

2. THE STUDY AREAS AND METHODS

In the present study, the analyses were performed for five cities, located in Central Europe. The basic features of the cities are described in Table 1.

Table 1 Basic data concerning the cities included in the study

City (country)	Area (km²)	Altitude range (m a.s.l.)	Population (year)
Kraków (Poland)	327	145-459	761,870 (2014)
Bratislava (Slovakia)	368	126-450	419,670 (2014)
Brno (Czech Republic)	230	200-525	377,400 (2015)
Szeged (Hungary)	281	46-143	162,500 (2015)
Vienna (Austria)	414	141-581	1,812,600 (2015)

Kraków is a city in southern Poland, on the river Vistula. The city is located in a concave landform, i.e. in the river valley passing from west to east. The historical city centre is placed on the bottom of the river Vistula valley (at about 200 m a.s.l.), on a limestone tectonic horst (Wawel Hill), emerging from the river valley. To the north of the river Vistula and the city centre is the Kraków-Częstochowa Upland, built of limestone and marls, and its parts located close to Kraków reach up to 300 m a.s.l. The southern borders of the city run

partially in the Carpathian Foothills, built of Flysch rocks, with an elevation up to 370 m a.s.l. in the area neighbouring Kraków. The river Vistula valley is narrow in the western part of Kraków (about 1 km) and widens to about 10 km in the eastern part. In the western part of the valley, there are several limestone tectonic horsts, reaching about 350 m a.s.l., so the city area is not surrounded by hills only from the east. The urbanized areas can be found in the river valley with its terraces and in convex landforms to the south and north of the city centre. Height differences between the valley floor and the hilltops next to the city borders are about 100 m, and the built-up areas do not reach those hilltops. Within the city borders, built-up areas cover 43.0% of the area, while agricultural and semi-natural areas amount to 41.3%, and the remaining (green and water) areas cover 15.7%. In the valley floor, many different land use types can be distinguished, while in the convex landforms south and north of the valley, only a few land use types can be found (Bokwa et al. 2015).

Bratislava is located in south-western Slovakia and it occupies both banks of the River Danube and the left bank of the River Morava. It is the country's largest city, situated only 60 km from the Austrian capital Vienna. Bordering Austria and Hungary, it is the only national capital that borders two independent countries (Swire 2006). The city has a total area of 368 km². The historic city center is located between the Danube and south-eastern slopes of the Carpathian mountain range – Malé Karpaty. Several city districts or boroughs are not directly connected to the historical center, but are located more separately and connected to Bratislava through narrow urban regions. The largest and most distinct borough of Bratislava situated on the right bank of Danube is Petržalka. Significant feature in the region of Bratislava is the mentioned Malé Karpaty mountain range in the northern and western parts of the city. Several city boroughs are found on both sides of the mountain ridge and are situated at foothill or directly on its slopes. The most of city districts are however located in the lowlands, to the east and southeast at Podunajská nížina lowland and to the northwest at Záhorská nížina lowland. The city's lowest point is at the Danube at 126 m a.s.l., and the highest point is Devínska Kobyla at 514 m. Complex orographic conditions in the Bratislava region generate a distinct and variable nature of the climate in the city and its surroundings. Especially the Malé Karpaty mountain range is affecting overall air circulation and thereby affecting most of climate characteristics in the city.

Brno is situated in the south-eastern part of the Czech Republic and it is the second-largest city in the country. Brno area is characterized by a basin position with complex terrain. Altitudes range from 190 m to 479 m, with the higher elevations lying largely in the western and northern parts of the region. Lower and flatter terrain is typical of the southern and eastern parts of the study area. There is a large water reservoir (area approximately 2.6 km²) located on the north-west border of the built-up part. The study area lies in one of the warmest and the driest regions in the Czech Republic. Mean annual temperature stands at 9.4°C, while mean annual precipitation is around 500 mm (1961–2000 reference period).

Szeged is located in the Pannonian Plain in Central Europe. According to the climate classification system developed by Köppen, it belongs to temperate warm climate with a rather uniform annual distribution of precipitation (Kottek et al. 2006). The urbanized area covers only about 40 km² of the city. The Tisza River is the axis of the town and the city has a regular avenue-boulevard structure. It is characterized by densely built up center, blocks of flats in the northern part, large area of family houses and warehouses mostly in western part (Unger 2004). In the study area, several database and input material is available from earlier studies, e.g. parameters used in the LCZ system and a set of other data (Rapid eye satellite images, CORINE land cover, road database, etc.) (Lelovics et al. 2014).

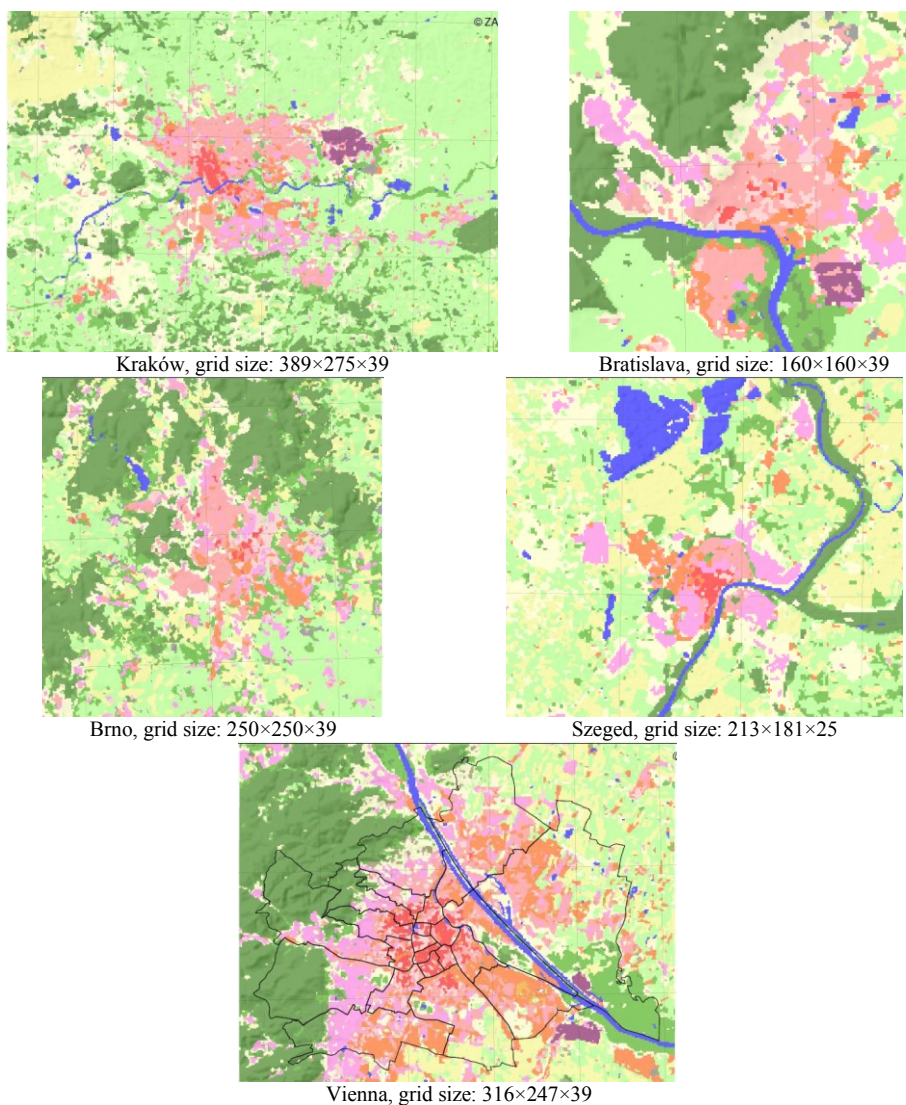


Fig. 1 Land use/land cover for the cities studied and their surroundings, presented with the LCZ method

Vienna is the capital city of Austria and the largest city used in this study. It is located at the easternmost extension of the Alps in a transition zone to the Pannonian Plain with the Danube River passing through the city. The City of Vienna covers an area of 41,487 ha from which 35.6% are buildings, 45.5% are green areas, 4.6% is water and 14.3% are traffic surfaces. The highest elevation is the Hermannskogel in Wienerwald (543 m) and the lowest point (151 m) is in the Lobau, east of the city center (Stadt Wien 2015). The urbanized area is characterized by the historical center surrounded by a green belt, dense built-up areas in the inner districts and low-density residential areas on the hillsides in the western part of the

city and in the flat terrain in the south and east direction. Most of the industrial areas are located in the eastern and southern part of the city.

In each of the cities studied, the land use pattern is different. In order to obtain comparable data on land use/land cover for all the cities, the method of Local Climate Zones was used (see section 4.2). The results are presented in Fig. 1.

Table 2 presents the share of particular LCZ classes in each city and its surroundings (i.e. in the domains shown in Fig. 1). It can be seen that some LCZ classes cannot be found or their share is very little in all cities: 1 (compact high-rise), 4 (open high-rise), 7 (lightweight low-rise), B (scattered trees), G (water). There is no one single LCZ that would have a dominating share in all cities; on the contrary, the land use/land cover structure is different for each city. Additionally, Fig. 1 shows that the spatial pattern of particular LCZ is different in each city, i.e. there are no regular zones surrounding the urban core area but there is a mosaic of various LCZ types.

Table 2 Share (%) of particular LCZ classes in the total area of the domain taken into analyses for each city studied

City	LCZ classes														
	1	2	3	4	5	6	7	8	9	10	A	B	C	D	E
Kraków	-	0.6	0.2	-	6.5	2.9	0.0	1.8	14.4	0.6	8.3	8.1	-	50.1	0.3
Bratislava	-	0.7	2.8	-	13.0	6.2	-	5.2	15.4	24.1	4.7	-	20.9	1.4	2.9
Brno	-	0.6	7.4	-	4.3	5.0	1.4	3.3	6.8	32.6	20.7	-	6.7	3.2	7.6
Szeged	-	0.7	0.4	-	3.6	5.1	-	4.8	16.4	6.4	8.5	-	23.5	-	27.1
Vienna	-	2.1	2.6	-	8.8	8.5	0.2	10.6	11.4	0.6	21.9	7.2	0.7	12.7	0.1

3. METEOROLOGICAL DATA

Meteorological data were used in the study for several purposes. In each city, daily data from a rural and from an urban station were used, for a period of 30 years (1971–2000 and 1981–2010), concerning air temperature, humidity and wind speed and direction. The stations are listed in Table 3.

Table 3 Meteorological stations used in the study

City	Station name	Land use	Coordinates	Altitude (m a.s.l.)
Bratislava	Bratislava, airport	Rural	48°10'N, 17°12'E	128
	Bratislava, Mlynská dolina	Urban	48°09'N, 17°04'E	180
Brno	Brno, Tuřany airport	Rural	49°09'N, 16°41'E	241
	Brno, Mendel Sqr.	Urban	49°11'N, 16°36'E	206
Kraków	Balice airport	Rural	50°04'N, 19°47'E	241
	Botanical Garden	Urban	50°03'N, 19°57'E	206
Szeged	HMS meteorological station	Rural	46°15'N, 20°05'E	79
	HMS climate station	Urban	46°15'N, 20°08'E	81
Vienna	Groß Enzersdorf	Rural	48°11'N, 16°33'E	153
	Innere Stadt	Urban	48°11'N, 16°22'E	177

The usage of meteorological data in cuboid method (section 4.1) was connected first with establishment of the threshold values; daily data from the 30-year period were used to obtain for each city, for the rural station, the lowest (cmin) and the highest (cmax) values of mean daily air temperature (T), relative humidity (rh) and wind speed (v), at which, at the urban station, the maximum air temperature was $\geq 25^{\circ}\text{C}$. The combinations of those threshold

values made the corners of a “cuboid” (Fig. 2), constructed separately for each city. Then the 30-year data were used to obtain the spatial pattern of mean annual number of days with $t_{max} \geq 25^\circ\text{C}$ for each city, for the areas presented in Fig. 1, with the usage of MUKLIMO_3 and the cuboid method. The 30-year data were also used as a reference series for the comparison with modelled data, for each city.

4. METHODS

4.1. MUKLIMO

MUKLIMO_3 (in German: 3D Mikroskaliges Urbanes KLima MOdell) is a non-hydrostatic micro-scale model with z-coordinates, which solves the Reynolds-averaged Navier–Stokes equations to simulate atmospheric flow fields in presence of buildings (Sievers and Zdunkowski 1985, Sievers 1990, 1995). The thermo-dynamical version of the model includes prognostic equations for atmospheric temperature and humidity, the parameterization of unresolved buildings, short-wave and long-wave radiation, balanced heat and moisture budgets in the soil (Sievers et al. 1983) and a vegetation model based on Siebert et al. (1992). The numerical approach for the calculation of short-wave irradiances at the ground, the walls and the roof of buildings in an environment with unresolved built-up is described by Sievers and Früh (2012). The flow between buildings is parameterized through a porous media approach for unresolved buildings (Gross 1989). The model uses high-resolution orography and land use distribution data. For each land use class, a set of parameters is defined to describe land use properties and urban structures: fraction of built area (γ_b), mean building height (h_b), wall area index (w_b), fraction of pavement of the non-built area (v), fraction of tree cover (σ_t) and fraction of low vegetation of the remaining surface (σ_c), height (h_c) (Table 4) and leaf area index (LAI_c) of the canopy layer as well as mean height (h_t) and leaf area index (LAI_t) of the trees with separated values for the tree trunk and the tree crown area. The model does not include cloud processes, precipitation, horizontal runoff or anthropogenic heat.

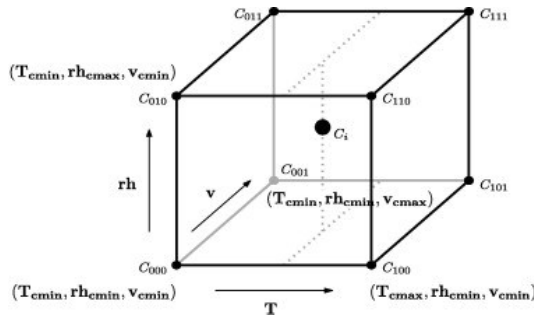


Fig. 2 The concept of the cuboid method (Žuvela-Aloise et al. 2014, Früh et al. 2011)

Table 4 Parameters for land cover properties in MUKLIMO_3 model: fraction of built area (γ_b), mean building height (h_b), wall area index (w_b), fraction of pavement (v), fraction of tree cover (σ_t), fraction of low vegetation (σ_c), tree height (h_t) and height of the low vegetation (h_c). Fractions γ_b and σ_t are relative to the total grid cell area. Fraction v is relative to the area without buildings and trees and σ_c is relative to the remaining surface

Land use class		γ_b (%)	h_b (m)	w_b	v (%)	σ_t (%)	σ_c (%)	h_t (m)	h_c (m)
1	Compact high-rise								
2	Compact midrise	0.40	15.00	3.42	0.60	0.00	0.80	0	0.30
3	Compact low-rise	0.40	8.40	2.40	0.40	0.00	0.80	0	0.30
4	Open high-rise								
5	Open midrise	0.20	18.60	4.40	0.60	0.00	0.80	0	0.30
6	Open low-rise	0.20	6.50	2.10	0.40	0.00	0.70	0	0.30
7	Lightweight low-rise	0.75	3.00	1.80	0.20	0.00	0.30	0	0.30
8	Large low-rise	0.30	7.00	2.00	0.80	0.00	0.80	0	0.30
9	Sparsely built	0.10	6.00	2.10	0.20	0.00	0.80	0	0.30
10	Heavy industry	0.30	7.00	2.00	0.80	0.00	0.80	0	0.30
A	Dense trees	0.00	0.00	0.00	0.00	0.80	0.90	17	0.50
B	Scattered trees	0.00	0.00	0.00	0.00	0.40	0.90	9	0.50
C	Bush, scrub	0.00	0.00	0.00	0.00	0.40	0.90	1.5	0.50
D	Low plants	0.00	0.00	0.00	0.00	0.00	1.00	0	0.50
E	Bare rock or paved	0.00	0.00	0.00	0.95	0.00	0.01	0	0.30
F	Bare soil or sand	0.00	0.00	0.00	0.00	0.00	0.01	0	0.30
G	Water	0.00	0.00	0.00	-1.00	0.00	0.01	0	0.30

In order to calculate climatic indices, such as the mean annual number of summer days, the dynamical modelling approach is combined with the so-called “cuboid method” (Früh et al. 2011, Žuvela-Aloise et al. 2014). The cuboid method refers to a tri-linear interpolation of meteorological fields derived by single-day simulations from an urban climate model. The simulations are performed for a set of idealized weather patterns for potential situations where a heat load exceedance in the urban centre could occur. Eight simulations with duration of 24 hours for two prevailing wind directions are calculated representing the cuboid corners (Fig. 2). Calculation of climatic indices for 30-year climatic periods is based on maximum temperature fields from the 8 single-day simulations using daily time series of T, rh and v, including hourly wind direction from a reference station as input.

4.2. Local Climate Zones

The Local Climate Zone (LCZ) classification (Stewart and Oke 2012) is an outstanding concept for the climate-related classification of urban areas in global scale. Although it was originally designed for meta-data communication in observational urban heat island studies, its possible applications are numerous. One of the most important ones is the possibility to use these zones for the input of different climate or weather models in order to better represent urban areas. The use of this concept in these models is advantageous because this classification is based on the thermal characteristics of the urban areas, and it is connected to the most obvious alteration of the climate in urban areas, the urban heat island (Stewart 2011). Fig. 3 contains the LCZ classes and definitions.


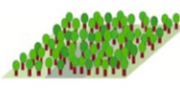



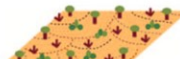



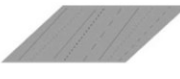
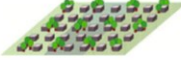

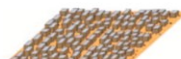




Built types	Definition	Land cover types	Definition
1. Compact high-rise 	Dense mix of tall buildings to tens of stories. Few or no trees. Land cover mostly paved. Concrete, steel, stone, and glass construction materials.	A. Dense trees 	Heavily wooded landscape of deciduous and/or evergreen trees. Land cover mostly pervious (low plants). Zone function is natural forest, tree cultivation, or urban park.
2. Compact midrise 	Dense mix of midrise buildings (3–9 stories). Few or no trees. Land cover mostly paved. Stone, brick, tile, and concrete construction materials.	B. Scattered trees 	Lightly wooded landscape of deciduous and/or evergreen trees. Land cover mostly pervious (low plants). Zone function is natural forest, tree cultivation, or urban park.
3. Compact low-rise 	Dense mix of low-rise buildings (1–3 stories). Land cover mostly paved. Stone, brick, tile, and concrete construction materials.	C. Bush, scrub 	Open arrangement of bushes, shrubs, and short, woody trees. Land cover mostly pervious (bare soil or sand). Zone function is natural scrubland or agriculture.
4. Open high-rise 	Open arrangement of tall buildings to tens of stories. Abundance of pervious land cover (low plants, scattered trees). Concrete, steel, stone, and glass construction materials.	D. Low plants 	Featureless landscape of grass or herbaceous plants/crops. Few or no trees. Zone function is natural grassland, agriculture, or urban park.
5. Open midrise 	Open arrangement of midrise buildings (3–9 stories). Abundance of pervious land cover (low plants, scattered trees). Concrete, steel, stone, and glass construction materials.	E. Bare rock or paved 	Featureless landscape of rock or paved cover. Few or no trees or plants. Zone function is natural desert (rock) or urban transportation.
6. Open low-rise 	Open arrangement of low-rise buildings (1–3 stories). Abundance of pervious land cover (low plants, scattered trees). Wood, brick, stone, tile, and concrete construction materials.	F. Bare soil or sand 	Featureless landscape of soil or sand cover. Few or no trees or plants. Zone function is natural desert or agriculture.
7. Lightweight low-rise 	Dense mix of single-story buildings. Few or no trees. Land cover mostly hard-packed. Lightweight construction materials (e.g., wood, thatch, corrugated metal).	G. Water 	Large, open water bodies such as seas and lakes, or small bodies such as rivers, reservoirs, and lagoons.
8. Large low-rise 	Open arrangement of large low-rise buildings (1–3 stories). Few or no trees. Land cover mostly paved. Steel, concrete, metal, and stone construction materials.	VARIABLE LAND COVER PROPERTIES	
9. Sparsely built 	Sparse arrangement of small or medium-sized buildings in a natural setting. Abundance of pervious land cover (low plants, scattered trees).	Variable or ephemeral land cover properties that change significantly with synoptic weather patterns, agricultural practices, and/or seasonal cycles.	
10. Heavy industry 	Low-rise and midrise industrial structures (towers, tanks, stacks). Few or no trees. Land cover mostly paved or hard-packed. Metal, steel, and concrete construction materials.	b. bare trees	Leafless deciduous trees (e.g., winter). Increased sky view factor. Reduced albedo.
		s. snow cover	Snow cover > 10 cm in depth. Low admittance. High albedo.
		d. dry ground	Parched soil. Low admittance. Large Bowen ratio. Increased albedo.
		w. wet ground	Waterlogged soil. High admittance. Small Bowen ratio. Reduced albedo.

Fig. 3 Local Climate Zones classes and definitions (Stewart and Oke 2012)

The LCZ system was initially designed for the classification of urban measurement sites (Stewart and Oke 2012), but meanwhile several methods for LCZ mapping have been proposed (Bechtel and Daneke 2012, Lelovics et al. 2014, Geletič and Lehnert 2016, Bechtel

et al. 2015). Our study concentrates on 5 different cities and for each city different databases and surface data are available. For this reason we had to choose a simple method for mapping, moreover the same method had to be used in all of the cities. Therefore, the same input data needed had to be available in all cities. The only suitable method in this situation is the Bechtel-method. It applies free-access satellite images, free software and it can be handled without expert remote sensing knowledge. The methodology uses two software packages: Google Earth and SAGA-GIS. As an input data, it applies globally available Landsat satellite images. The workflow consist two main steps (Bechtel et al. 2015).

First, typical LCZ areas (training areas) have to be located in the study area; this part is carried out in Google Earth. The training areas are stored in a kml file containing a set of polygons for the different LCZ types and also a rectangle defining the border of the examined area. This kml file is used for the second part of the process which is carried out in SAGA-GIS. Secondly, in SAGA-GIS the Landsat images and the vector file (containing the training areas) have to be preprocessed. The Landsat scene is cut with the border of study area in order to decrease the computation time, and the imagery is resampled to 100 m from the original 30 m to get a representation of the spectral signal of local scale urban structures rather than smaller objects. Finally, the classification is conducted with the built in random forest classifier based on the Landsat images and the training area polygons. The classifier calculates the most likely LCZ type and the probabilities for all LCZ classes for each pixel.

For the study areas included in the present paper, we used all spectral bands of 19 Landsat 7 and 8 images (Bratislava: 3 images, Brno: 4, Kraków: 4, Szeged: 5, Vienna: 3). The use of multiple images from different seasons is advantageous, as with more spectral information the classification gives better results. The scenes were obtained from USGS (earthexplorer.usgs.gov). The criterion of the selection of these images was to ensure the absence of clouds. The LCZ classification outcome for particular cities is shown in Fig. 1.

4.3. EURO-CORDEX

Climate models provide key information on the impacts of 21st century climate change but are limited in their capacity to represent the relatively small scales needed for decision making on adaptation. Large collaborative research projects such as EURO-CORDEX (Jacob et al. 2013) have generated climate change scenarios via Regional Climate Models (RCMs). EURO-CORDEX simulations use the new Representative Concentration Pathways (RCPs) defined in the Fifth Assessment Report of the IPCC (Moss et al. 2010, IPCC 2013). RCPs do not identify socioeconomic scenarios; they express the change in radiative forcings, introduced by altered land use patterns at the end of the twenty-first century relative to pre-industrial conditions (Table 5). For instance, the EURO-CORDEX simulations consider the RCPs scenarios corresponding to stabilization of radiative forcing after the 21st century at 4.5 Wm⁻² (RCP4.5) (Smith and Wigley 2006, Clarke et al. 2007, Wise et al. 2009), rising radiative forcing crossing 8.5 Wm⁻² at the end of 21st century (RCP8.5) (Riahi et al. 2007), and peaking radiative forcing within the 21st century at 3.0 Wm⁻² and declining afterwards (RCP2.6) (van Vuuren et al. 2007).

The EURO-CORDEX simulations not only consider the new RCP scenarios, they increase the spatial resolution based on multiple dynamical and empirical-statistical downscaling. The members of the ensemble are forced by multiple global climate models from the Coupled Model Intercomparison Project (CMIP5) and the simulations focus on grid-sizes of about 12 km (0.11°, EUR-11) and 50 km (0.44°, EUR-44) for the complete European model domain.

Table 5 Characteristics of the new Representative Concentration Pathways (RCPs)

Name	Radiative forcing	CO ₂ eq. (ppm)	Temp. anomaly (°C)	Pathway	SRES temp. eq.	Number of experiments
RCP8.5	8.5 Wm ⁻² in 2100	1370	4.9	Rising	SRES A1FI	7
RCP4.5	4.5 Wm ⁻² past 2100	650	2.4	Stabilization without overshoot	SRES B1	7
RCP2.6	2.6 Wm ⁻² by 2100	490	1.5	Peak and decline	None	1

For this study, five different GCMs and three different RCMs have been used for the establishment of one simulation for RCP2.6 and seven simulations for RCP4.5 and RCP8.5 for the EUR-11 domain (Table 6). All changes in output variables (mean temperature, relative humidity, wind speed and direction) have been analysed for the city areas using daily data for three time periods: 1971–2000, 2021–2050 and 2071–2100.

Table 6 GCM-RCM model chains used to generate the different climate change projections used in this study

Model	RCP2.6	RCP4.5	RCP8.5
	Near-surface temperature [K]		
	Near-surface relative humidity [%]		
	Eastward Near-Surface Wind [ms ⁻¹]		
	Northward Near-Surface Wind [ms ⁻¹]		
EUR-11_CNRM-CERFACS-CNRM-CM5_*_SMHI-RCA4		✓	✓
EUR-11_ICHEC-EC-EARTH_*_SMHI-RCA4	✓	✓	✓
EUR-11_ICHEC-EC-EARTH_*_KNMI-RACMO22E		✓	✓
EUR-11_ICHEC-EC-EARTH_*_DMI-HIRHAM5		✓	✓
EUR-11_IPSL-IPSL-CM5A-MR_*_SMHI-RCA4		✓	✓
EUR-11_MPI-M-MPI-ESM-LR_*_SMHI-RCA4		✓	✓
EUR-11_MOHC-HadGEM2-ES_*_SMHI-RCA4		✓	✓

The outputs of the climate models do not offer perfect results as they describe complex processes and interactions. We can observe systematic errors in the outputs. To minimize this error we should use error correction processes. There are abundant of known processes, in this study we used a bias correction method.

The applied correction method is based on that we can completely describe the statistical properties of given datasets with their distribution and probability functions. So we can say that two data series are the same if their distribution and probability functions are the same (Formayer and Haas 2009). Thus if we want to correct a dataset based on its statistical properties we have to achieve that the distribution function will be the same of the measurements. Therefore to apply this method we should have dataset from measurements for a given time period. For this common period we suit the distribution functions of the measurement and the model with correction factors and we assume that the deviation will be permanent. In case of temperature the correction factors are the deviations of the percentiles.

In this study we used the 1971–2000 time period as reference period. We calculated the 1% percentiles and their deviation for the datasets of the measurement and the model simulations. We corrected the temperature datasets for the 2021–2050 and 2071–2100 periods based on the deviation of the reference period. In case of the relative humidity we took into consideration the corrected temperature data. The other correction that we made is

the correction of the temperature gradient in height. We surveyed the altitude for each city and for each grid points which are the nearest to the city in the model outputs. We calculated the deviation and took into account the decrease of the temperature in height applying the $0.65^{\circ}\text{C} / 100 \text{ m}$ value.

4.4. Estimation of the change in heat load

For the present study, the heat load is expressed in the mean annual number of days with maximum air temperature $\geq 25^{\circ}\text{C}$, i.e. summer days. The change in the heat load due to predicted climate changes is then defined as the difference in the mean annual number of summer days between a 30-year period representing the present conditions, 1971–2000, and two periods representing future conditions: 2021–2050 and 2071–2100. Therefore, first the spatial pattern on mean annual number of summer days, for each city and period considered, was obtained with the usage of MUKLIMO_3 and cuboid method. For each of the two future periods (2021–2050 and 2071–2100), the calculations were made separately for each climate scenario (i.e. RCP2.6, RCP4.5 and RCP8.5). For RCP2.6, the results obtained with one model were used, while for RCP4.5 and RCP8.5, mean values from seven models were used (see Table 6). The comparative analysis of the patterns allows to define areas in particular cities which are and/or are supposed to be the “hot spots” and “cold spots”, and which might experience the largest and the smallest changes in the heat load in the future. The changes of the heat load can be also calculated separately for areas with particular LCZ type in order to show whether all kinds of land use/land cover will react to the climatic changes in a similar way. For each city and period, mean, maximum and minimum number of summer days for the whole domain considered was calculated. The mean value is representative for the whole area, while maximum and minimum values describe extreme conditions occurring in the area and constitute the range of the phenomenon’ variability. The changes can be expressed in absolute numbers or in percentage; the latter is especially useful in comparative studies between the cities.

5. RESULTS

5.1. Reference

The map of the summer days calculated using the measured climate data in *Szeged* has a characteristic spatial pattern (Fig. 4). In the city center, we find the highest values (about 100–110 days) in the time period 1981–2010. In the less dense

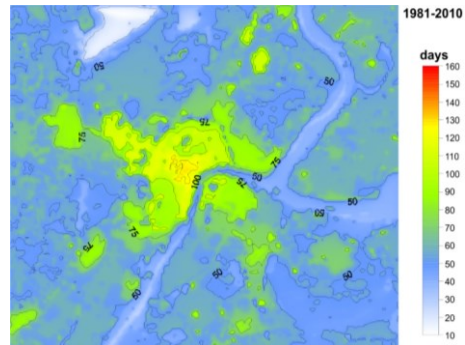


Fig. 4 Mean annual number of summer days in Szeged in the period 1981–2010 using the measured data

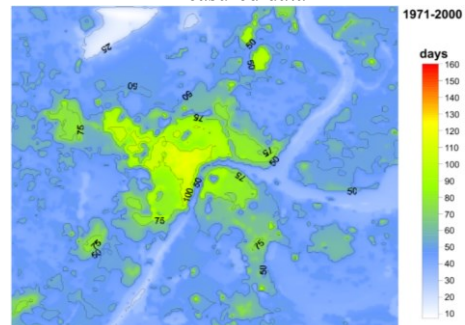


Fig. 5 Mean annual number of summer days in Szeged in the period 1971–2000 using the data of the climate models

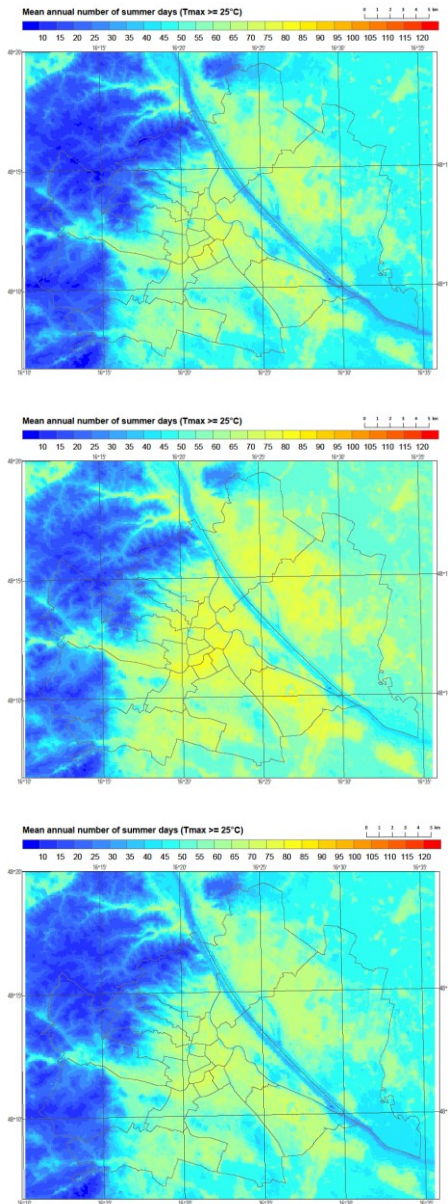


Fig. 6 Mean annual number of summer days in Vienna in the period 1971–2010 (top) and 1981–2010 (center) using the measured data and 1971–2000 (bottom) using the data of the climate models

landforms we found less number of summer days, in open midrise areas about 90–100 days, open low-rise areas 70–80 days. In rural areas there was only 60–70 days.

The time period 1971–2000 is the standard reference time for climate models. Fig. 5 shows the map for this period calculated using the climate data from climate models. It has almost similar spatial pattern to the one of 1981–2010. In the city center, there are the highest values (about 90–100 days), in open midrise areas about 80–90 days, in open low-rise areas 70–80 days, and in rural areas only 60–70 days.

In case of *Vienna*, the reference simulation shows a typical spatial distribution with the maximum heat load in densely built-up areas in the city center and in residential areas in the flat terrain north-east of the river Danube (Fig. 6). Both orography and land use distribution influence the thermal characteristics. Due to the orography and prevailing winds from the northwest and southeast, the heat load in the residential areas located on the hill slopes in the west is lower than the heat load in the same type of built-up in the flat terrain located southward and eastward of the city center. The spatial pattern in the simulations for the periods 1971–2000 and 1981–2010, based on the measured data, is similar. However, the more recent climate period indicates a warming trend, which is found in observational time series. The simulation for the time period 1971–2000 based on climate model data is similar to the simulation based on the observational data for the same time period. The simulation based on the climate model data is further use as the reference for evaluation of future climate changes.

Fig. 7 presents distribution of summer days in *Brno* as simulated with MUKLIMO model for recent climate. Spatial distribution of this variable reflects well the role of the main natural and anthropogenic factors that form urban

climate conditions, the number of summer days varies from 20–30 in northern and western parts in higher elevations to more than 100 in the city center. Spatial distribution of summer days within the Brno cadastral correlate well with density of buildings. The highest values are typical for the city center, but also for the Brno exhibition area (located south-east from the center) and also for relatively large areas of former factories (north-west of city center). Three maps on Fig. 7 for three successive 30-year long periods also well document gradual rising of air temperatures in this area. This increasing trend is statistically significant especially for summer months and on average it reaches $0.5^{\circ}\text{C} / 10$ years in the period 1961–2010.

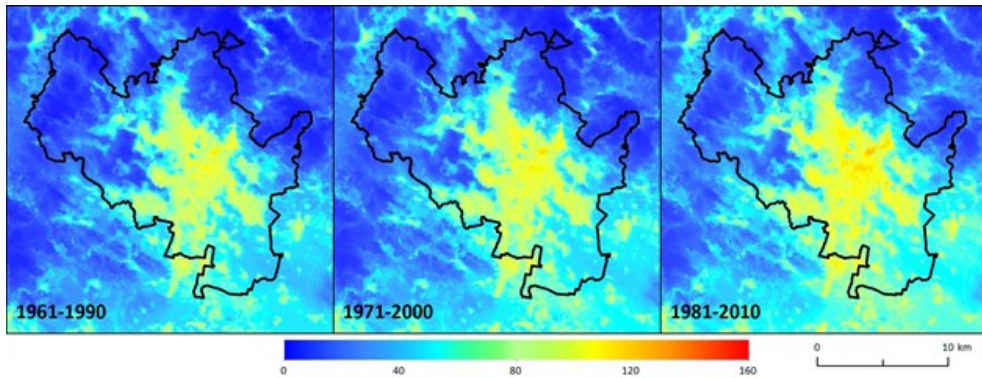


Fig. 7 Mean annual number of summer days simulated using the data of the climate models in Brno for in three different reference periods (1961–1990, 1971–2000, 1981–2010)

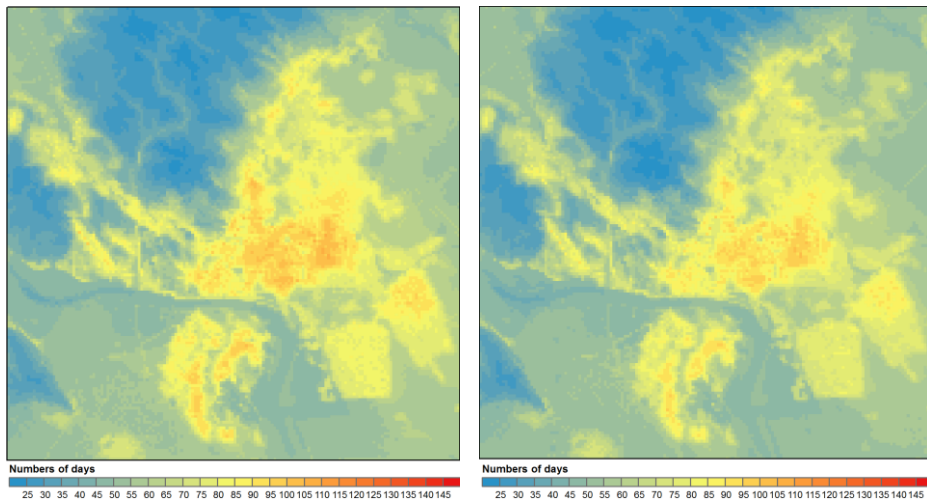


Fig. 8 Mean annual number of summer days in Bratislava in the period 1981–2010 using the measured data (left) and in the period 1971–2000 using the data of the climate models (right)

In *Bratislava*, reference simulation also shows a considerable influence of terrain, as there is an evident connection between lower heat load and higher altitude, while there are also clearly defined most compact built-up urbanized areas. There is an obvious spatial

distribution of highest number of summer days with higher values in most compact urban areas in the center, as well as in residential districts to the south and industrial to the east. The spatial pattern also clearly shows the impact of the mountain range and forested areas in the north and west with the lowest observed values. The simulations for the periods 1971–2000 and 1981–2010 (Fig. 8) share a similar spatial pattern, but there are slightly higher values in case of 1981–2010 period related to the warming in recent years and partly due to the different form of input (climate model vs. real station measurements). Difference between simulation of 1971–2000 based on climate model data and 1981–2010 based on real observation however is not overly significant. For both simulations the highest values are in the range of about 100–110 days, and the lowest at only 20–30 days.

In *Kraków*, the data for the reference period 1971–2000 show that in the most densely urbanized areas, mean annual number of summer days was about 60 days (in 1981–2010: about 66) while e.g. in forested areas located within the city borders the number was below 5 days (1981–2010: 5.6; Fig. 9). Large differences are also seen in rural areas between valleys and hilltops nearby; the values for the valleys were significantly larger. As suburban areas tend to develop intensively, relatively large values of the number of summer days can be also observed in areas surrounding the city, especially in small cities like *Wieliczka* or *Skawina*. The area of the *Vistula* river bottom is rather diversified in terms of the index discussed, as there are the most urbanized areas located, together with large areas of urban green and water areas.

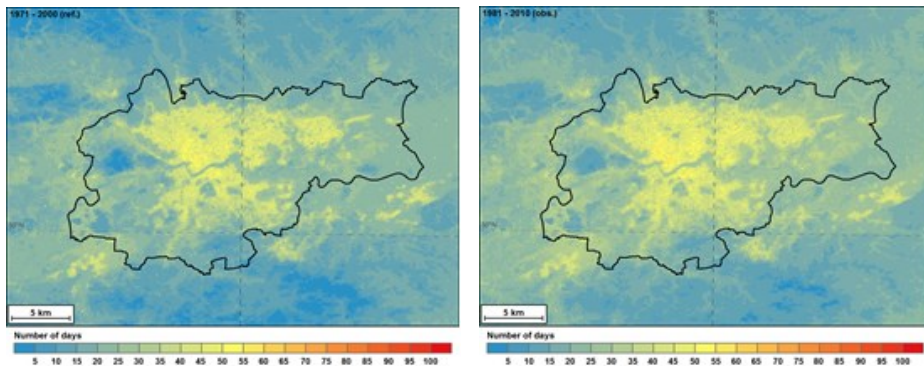


Fig. 9 Mean annual number of summer days in *Kraków* in the period 1971–2000 using the data of the climate models (left) and in the period 1981–2010 using the observations (right)

5.2. Validation

In *Szeged*, for the validation, we compared the data from the map of summer days, from the points located closest to the two meteorological stations in *Szeged*, with the data available from those stations. The data from the rural station is a mean value for 1981–2010, in urban station is a mean value for 1999–2010. In rural station the model resulted 54 summer days and based on the measurements there was 89 days. For the urban site the values are more similar, based on the measurements there is 94 days and the model gives 108 days.

In case of *Vienna*, the model results for the time period 1981–2010 are compared to 7 monitoring stations which have more than 10 years of measurements. The model results for the urban station *Vienna Innere Stadt* agree well with the observations. Mean annual number of summer days in the model is 79.4, while observed value is 72.3 summer days in average

for the period 1985–2010. At the rural station Groß Enzersdorf, an average of 65.7 summer days is observed. The model results yield a value of 56.8 summer days, which underestimates the measured value by 14%. However, the comparison between stations in different environment shows variable model performance. The best agreement is found for the station Vienna Hohe Warte (-5%) located in residential areas in northwestern part of the city. In comparison with the station Groß Enzersdorf, the results for the airport station Schwechat

representative for the rural environment as well, show a slight overestimation (68.5 summer days in the model compared to the 62.8 summer days in monitoring records). The reason for variable model performance could be the simplified land use distribution when using LCZ classification, which might not be representative for different micro-environments in Vienna.

In case of *Brno*, direct validation of simulated number of summer days can be done only for Brno, Tuřany station (Fig. 10). This station is located at the Brno airport in south-east part of the cadastral area and unfortunately, this station is neither typical urban nor typical rural station. From Fig. 10 it follows that model MUKLIMO 3D in general overestimates the number of summer days and this overestimation is about 50–60%. However, it must be stressed that this type of validation that is based on only one station may be biased or not well representative, because the found difference may be influenced due to many factors, e.g. proper classification of LCZ in this area.

For the city of *Bratislava*, the model in selected rural location within the modeled region shows on average 56 summer days for 1981–2010 period, while according to the measurements at respective rural station the mean annual number of summer day was 69 summer days. As for urban location (within the airport area) the model states that there was on average 72 summer days during year and according to the measurements at local station in 1981–2010 period the mean annual number of summer days was 54. In both rural and urban locations the mean annual number of summer days for 1981–2010 period presented by model, was therefore lower than values provided by station measurements.

In case of *Kraków*, data from the two stations mentioned in table 3 (Balice airport, rural station and Botanical Garden, urban station) were used for comparison with the data generated with the model. The data presented in Table 7 show that the model shows lower values than measured, as already mentioned for other cities. However, the tendencies of changes are predicted correctly; the measurements show that the difference in the number of summer days between the urban and rural station decreased from 12.1 days (1971–2000) to 10.2 days (1981–2010) and the modelled values are 15.3 and 14.3 days.

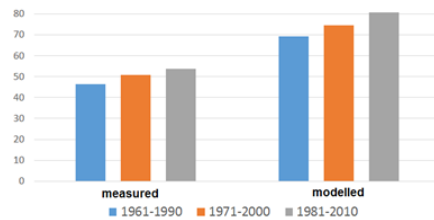


Fig. 10 Mean numbers of summer days as measured (left) and simulated with the MUKLIMO 3D model (right) in Brno area for three different periods representing recent climate

Table 7 Mean annual number of summer days at the rural (Balice airport) and urban (Botanical Garden) stations in Kraków, according to measurements and modelled values

Station	Period	1971–2000		1981–2010	
		measured	modelled	measured	modelled
Balice airport		38.1	28.6	46.2	31.3
Botanical Garden		50.2	43.9	56.4	45.6

5.3. Future scenarios

In this section, the predictions of heat load changes in 2021–2050 and 2071–2100 are presented. First the data for each city is analyzed and then an attempt of comparative analysis of all the cities is undertaken.

In *Szeged*, in the period 2021–2050, the number of summer days is supposed to increase compared to the present conditions. The spatial pattern is supposed to remain unchanged. The highest number of summer days is expected to be found in the city center. However, in case of RCP2.6 and RCP4.5, the number of summer days in the city centre is supposed to reach about 120 days, while in case of RCP8.5 it is 130 days (Fig. 11).

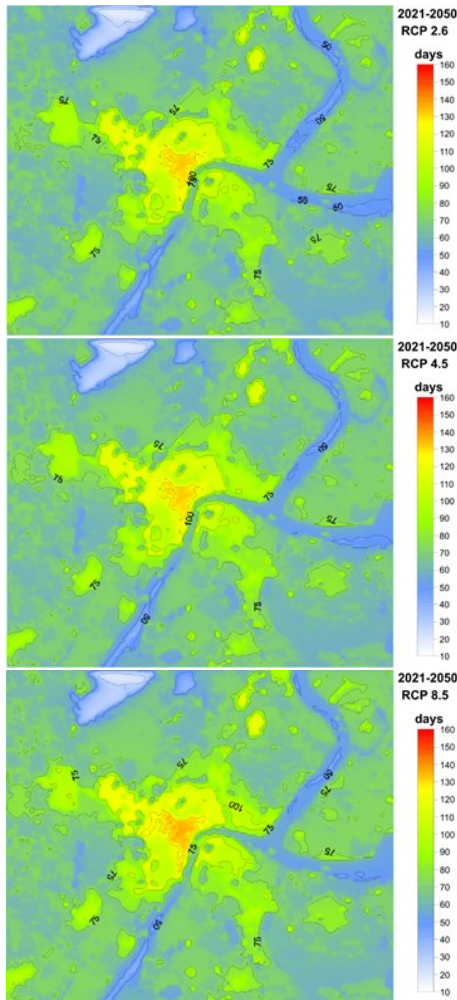


Fig. 11 Mean annual number of summer days in Szeged in the period 2021–2050 using the model simulations for the RCP2.6 (top) RCP4.5 (center) and RCP8.5 (bottom) scenarios

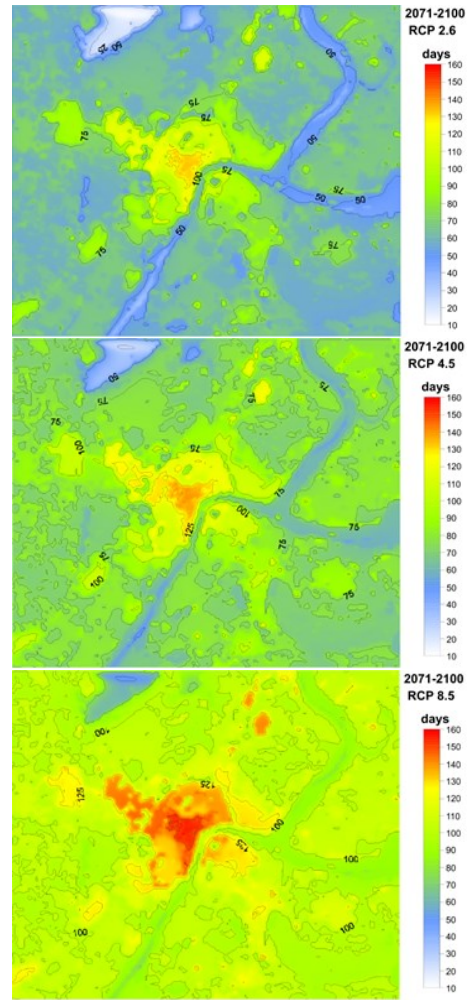


Fig. 12 Mean annual number of summer days in Szeged in the period 2071–2100 using the model simulations for the RCP2.6 (top) RCP4.5 (center) and RCP8.5 (bottom) scenarios

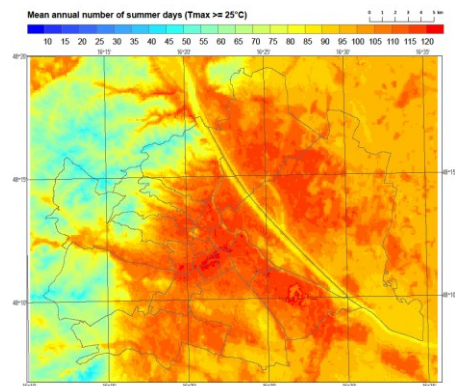
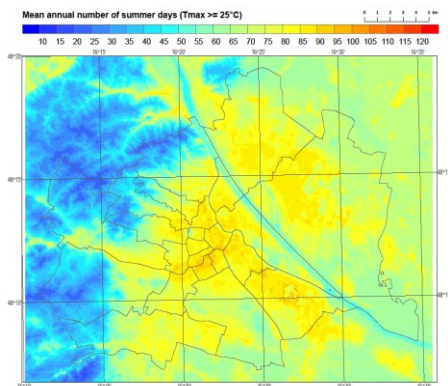
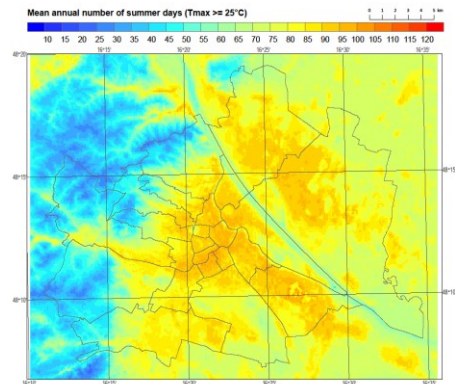
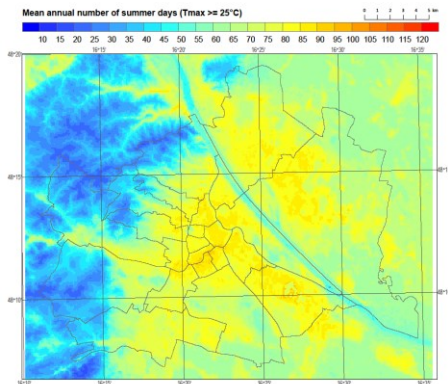
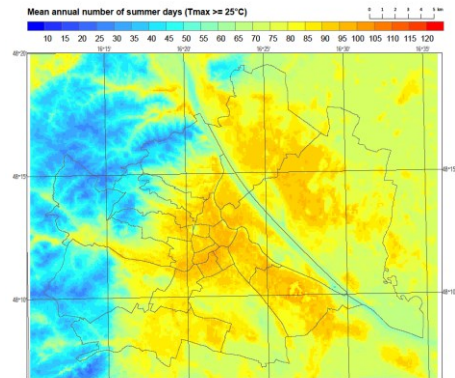
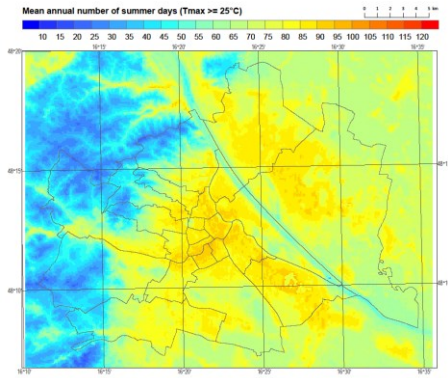


Fig. 13 Mean annual number of summer days in Vienna in the period 2021–2050 using the model simulations for the RCP2.6 (top) RCP4.5 (center) and RCP8.5 (bottom) scenarios

Fig. 14 Mean annual number of summer days in Vienna in the period 2071–2100 using the model simulations for the RCP2.6 (top) RCP4.5 (center) and RCP8.5 (bottom) scenarios

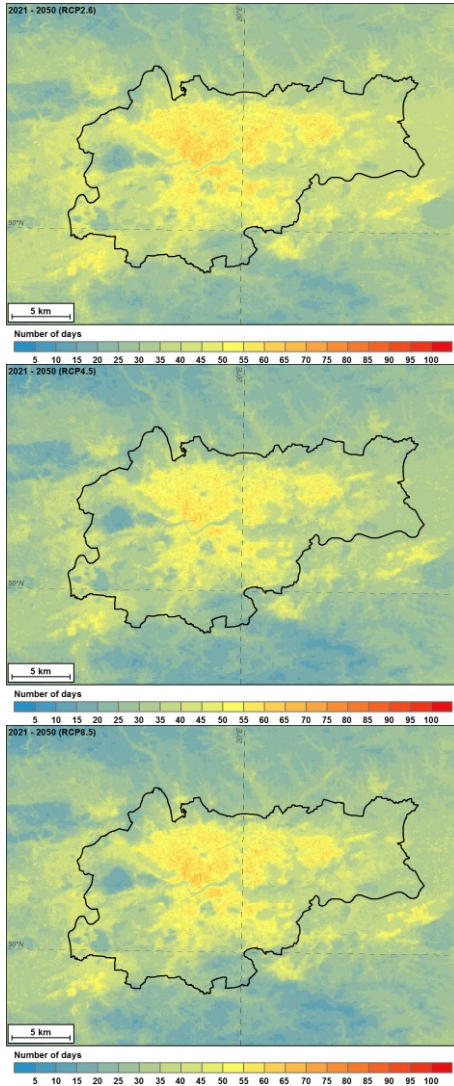


Fig. 15 Mean annual number of summer days in Kraków in the period 2021–2050 using the model simulations for the RCP2.6 (top), RCP4.5 (center) and RCP8.5 (bottom) scenarios

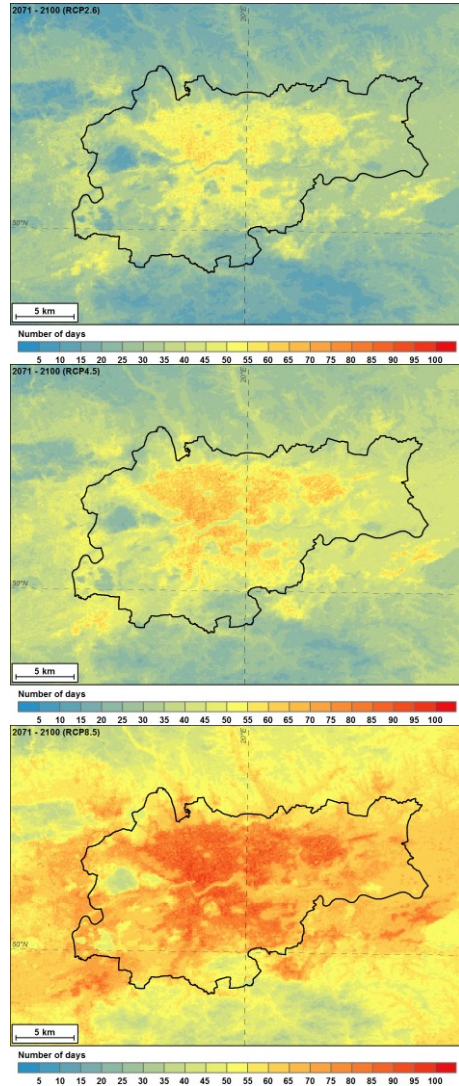


Fig. 16 Mean annual number of summer days in Kraków in the period 2071–2100 using the model simulations for the RCP2.6 (top), RCP4.5 (center) and RCP8.5 (bottom) scenarios

For the end of the century (2071–2100) the number of summer days is significantly different in different RCPs. The spatial patterns are basically similar in each case, because the urban effects are similar, i.e. it is assumed in the present analysis that the land use/land cover remains unchanged. In the case of RCP2.6 (Fig. 12) there is no change compared to 2021–2050 (Fig. 11). RCP4.5 represents a moderate change in the number of summer days,

the highest values are around 140 days. RCP8.5 is the worst scenario and the results differ significantly from the other scenarios and time periods, because the highest values are around 160 days (Fig. 12) and even in the rural areas the numbers of summer days are higher than the numbers of summer days in the urban areas in the present climate conditions (Figs. 4, 5).

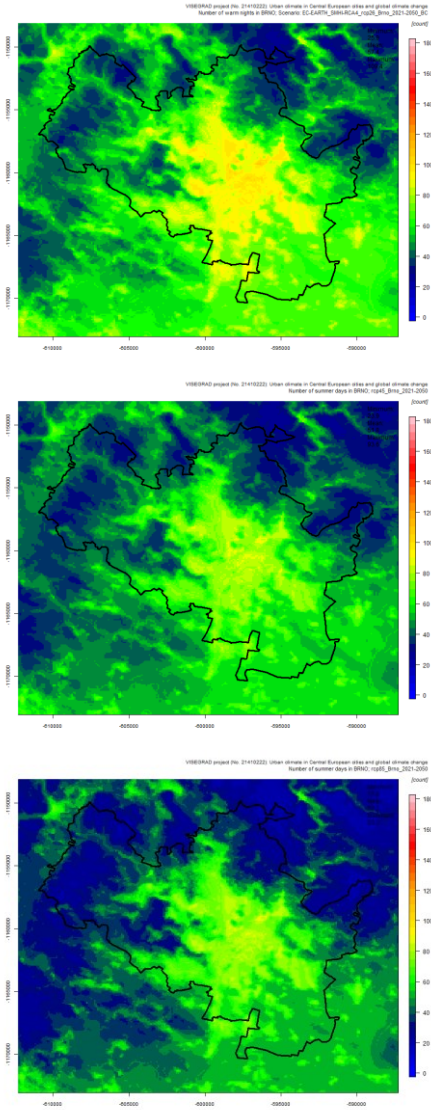


Fig. 17 Mean annual number of summer days in Brno in the period 2021–2050 using the model simulations for the RCP2.6 (top), RCP4.5 (center) and RCP8.5 (bottom) scenarios

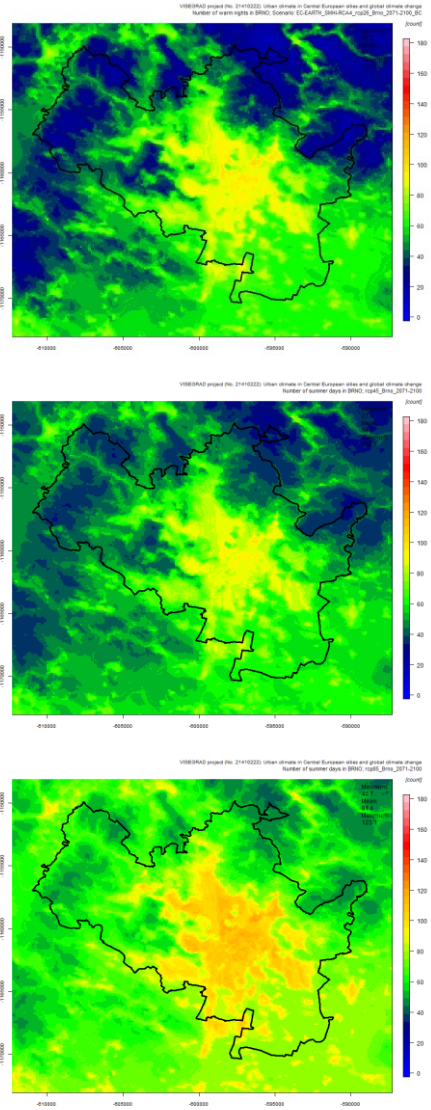


Fig. 18 Mean annual number of summer days in Brno in the period 2071–2100 using the model simulations for the RCP2.6 (top), RCP4.5 (center) and RCP8.5 (bottom) scenarios

In case of *Vienna*, the model results for the time period 2021–2050 show moderate increase in the number of summer days compared to the reference simulation (Fig. 13). The intensity of warming and the spatial pattern do not vary much between different climate scenarios. For the end of the century (2071–2100) the increase in number of summer days is substantially different for each RCP scenario (Fig. 14). Minimal change is found for the RCP2.6 compared to the 2021–2050 simulation. The RCP4.5 indicates an intermediate change, while the RCP8.5 scenarios shows extreme increase in the number of summer days. The highest values are around 120 days compared to about 70 days found in the reference simulation.

In *Kraków*, for the period 2021–2050, all scenarios show a slight increase in the mean annual number of summer days; the mean value for the whole domain is expected to increase by about 10 days and reach the value of about 30 days (Fig. 15). In case of the period 2071–2100 (Fig. 16), the uncertainty of predictions increases, and mean values vary depending on the scenario chosen from 30 to 65 days. For both periods considered, the spatial pattern shows the impact of both land use/land cover and relief on the thermal conditions. The highest numbers of summer days can be found in densely built-up areas, located in the valley floor, and in urban areas located close to Kraków borders. The lowest values are observed for forested areas. Additionally, in rural areas surrounding Kraków, larger numbers of summer days can be found in the valleys than at the hilltops nearby. Green urban areas located between strongly urbanized parts of the city show smaller number of summer days than built-up areas.

In case of *Brno*, the model results for the middle of this century (2021–2050) show about 40% increase in the number of summer days compared to the reference simulation for RCP4.5, RCP8.5 scenarios (Fig. 17). Distinctly higher number of summer days show RCP2.6 scenario (increase about 60% compared to recent climate). This difference, however, is related to the fact that lower number of regional model outputs was used for RCP2.6 scenario. Simulated numbers of summer days are compared to the reference Brno, Tuřany station. Thus there is and an increase from about 37 days (1971–2000) to 52 days (2021–2050) in case of scenarios RCP4.5 and RCP8.5 and 57 days (2021–2050) in case of RCP2.6. Quite different results as for individual scenarios were found for the Brno climate simulations of the end of the 21 century (2071–2100) – see Fig. 18. While RCP2.6 scenario predicts on average 52 summer days in Brno area, RCP4.5 scenario predicts slightly higher – 59 summer days (that is 60% increase compared to the present). Significantly higher number of summer days can be seen for the RCP8.5 scenario; 81 summer days represents 120% of the present value.

In case of *Bratislava*, there is a moderate increase in the number of summer days in the study area for the time period 2021–2050 compared to the reference simulation (Fig. 19). The scenarios show that mean number of days for the whole region would increase by around 20 days. The maximum number of summer days in 2021–2050 period for the worst RCP8.5 scenario could be 130 days, which is about 26 more summer days annually compared to the reference simulation of 1971–2000. In the later 2071–2100 period the average and maximum number of summer days within the modeled region as well as their spatial distribution have greater variance depending on the input scenario (Fig. 20). Mean values in this period calculated for the whole region vary depending on the scenario from 78 to 119 days. The model yields a maximum value of 148 summer days for RCP8.5 scenario compared to about 100 days found in the reference simulation.

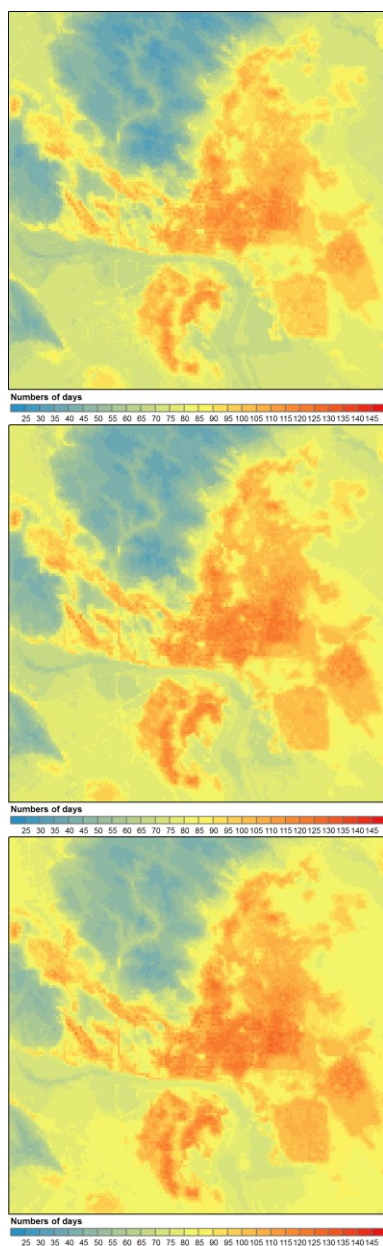


Fig. 19 Mean annual number of summer days in Bratislava in the period 2021–2050 using the model simulations for the RCP2.6 (top), RCP4.5 (center) and RCP8.5 (bottom) scenarios

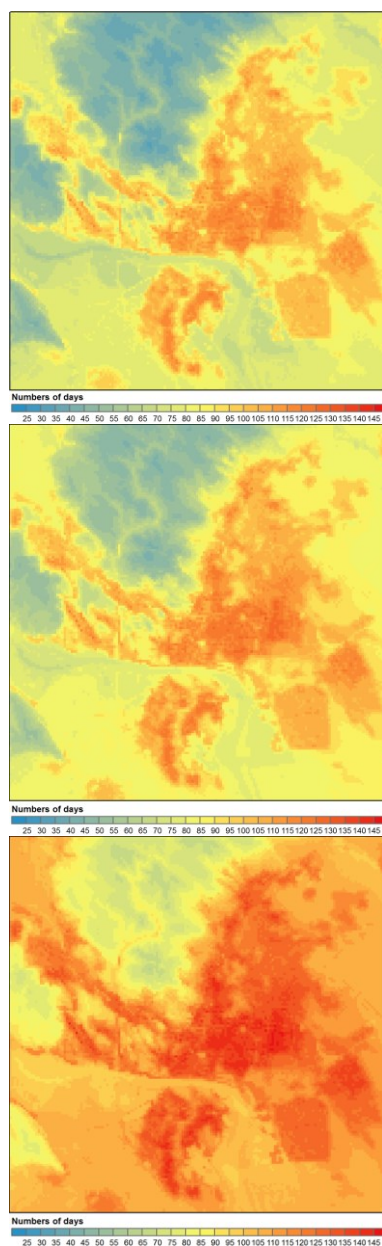


Fig. 20 Mean annual number of summer days in Bratislava in the period 2071–2100 using the model simulations for the RCP2.6 (top), RCP4.5 (center) and RCP8.5 (bottom) scenarios

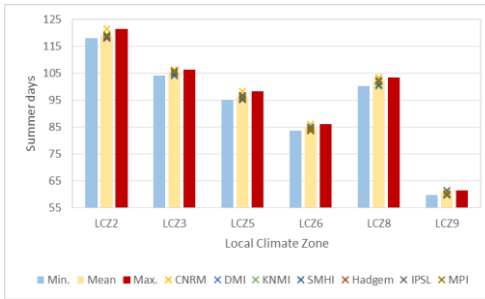


Fig. 21 Maximum, mean and minimum of mean annual number of summer days in Szeged in the period 1971–2000 using the applied climate models in different LCZ classes

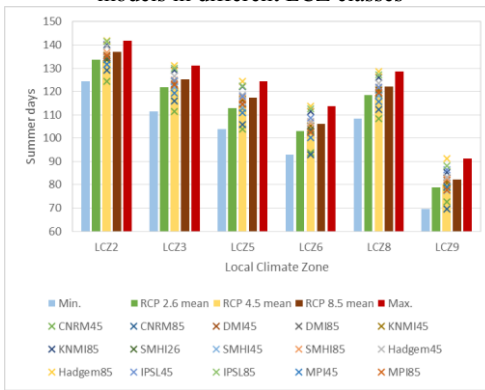


Fig. 22 Maximum, mean of the different RCPs and minimum of mean annual number of summer days in the period 2021–2050 using the applied climate models in different LCZ classes in Szeged

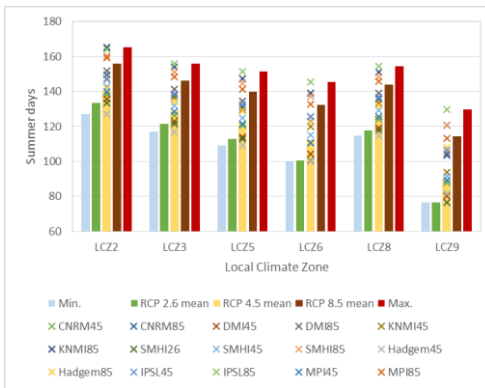


Fig. 23 Maximum, mean of the different RCPs and minimum of mean annual number of summer days in the period 2071–2100 using the applied climate models in different LCZ classes in Szeged

5.4. Changes of heat load in land use types

In order to analyze the heat load change in connection with land use/land cover, the following procedure was used. One or a few points were found for each LCZ in each city.

Those were the points in the centers of the largest homogenous LCZ areas of the city. For those points, maximum, minimum and mean values of mean annual number of summer days were compared, using data from the EURO-CORDEX climate models (see section 4.3) downscaled with cuboid method (see section 4.1). The procedure allows to compare the absolute or relative (% change) values of the cities for different 30-year periods. The procedure is shown using the example of Szeged and Brno.

In Szeged, the intra urban difference is significant in the present climate conditions, LCZ9 (sparsely built) and LCZ6 (open low-rise) have less summer days. LCZ2 (compact mid-rise) has two times more summer days than LCZ9 (Fig. 21).

The intra urban differences remain the same in the period 2021–2050 (Fig. 22) or 2071–2100 (Fig. 23). In the period 2021–2050, the minimum predicted number of summer days occur in LCZ9 and the maximum in LCZ2. Difference between models is almost the same as the difference between LCZs except LCZ9. In period 2071–2100 the thresholds of the different models are increasing.

Relative values were calculated for the minimum, maximum and mean of model results for particular LCZ type. In case of RCP2.6, 4.5 and 8.5 the reference value was the model mean for 1971–2000. The results show that the highest increase is predicted in LCZ9 or LCZ6 (Figs. 24, 25). Those are the areas with less dense built-up than the city centre, so the increase in built-up area share in those parts of the city can cause serious hazards for the inhabitants, due to the increase of the heat load. The differences in

relative change (Figs. 24, 25) are not enough to distinguish the differences in the number of the summer days between LCZs (Figs. 22, 23).

Similar analysis was performed for Brno and the results are shown in Figs. 26–30. In 1971–2000, the highest mean values were observed for LCZ2 (compact mid-rise) and LCZ 8 (large low-rise). The highest increase is predicted in LCZ9, like in the case of Szeged.

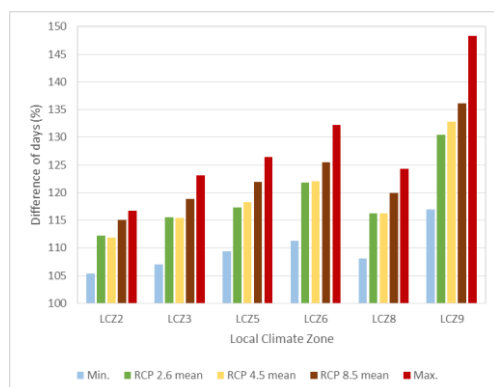


Fig. 24 Change of maximum, mean of the different RCPs and minimum of mean annual number of summer days in the period 2021–2050 using the applied climate models in different LCZ classes compared to 1971–2000 (min., mean and max., respectively) in Szeged

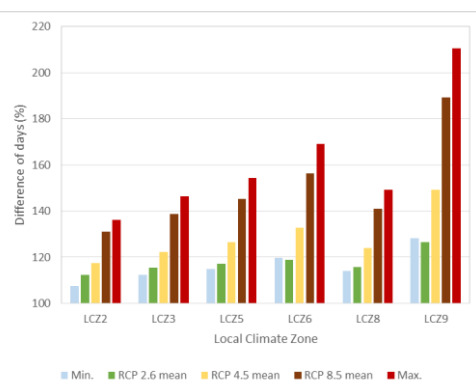


Fig. 25 Change of maximum, mean of the different RCPs and minimum of mean annual number of summer days in the period 2021–2050 using the applied climate models in different LCZ classes compared to 1971–2000 (min., mean and max., respectively) in Szeged

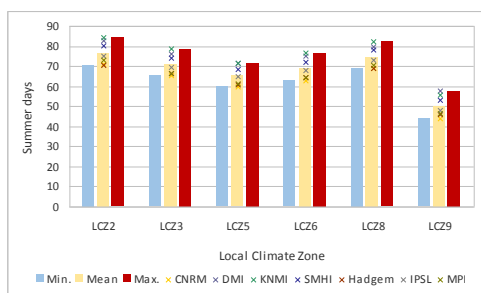


Fig. 26 Maximum, mean and minimum of mean annual number of summer days in Brno in the period 1971–2000 using the applied climate models in different LCZ classes

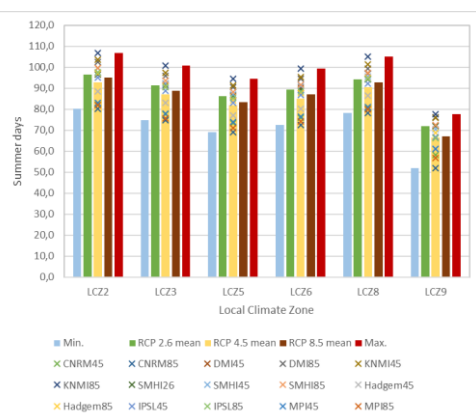


Fig. 27 Maximum, mean of the different RCPs and minimum of mean annual number of summer days in the period 2021–2050 using the applied climate models in different LCZ classes in Brno

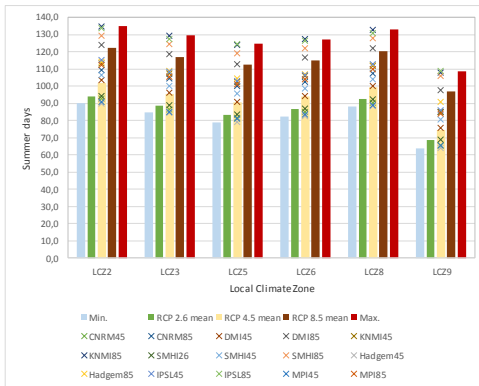


Fig. 28 Maximum, mean of the different RCPs and minimum of mean annual number of summer days in the period 2071–2100 using the applied climate models in different LCZ classes in Brno

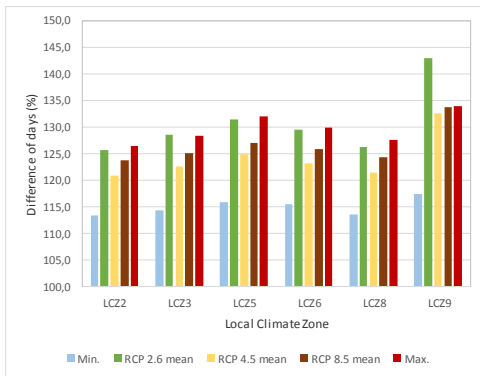


Fig. 29 Change of maximum, mean of the different RCPs and minimum of mean annual number of summer days in the period 2021–2050 using the applied climate models in different LCZ classes compared to 1971–2000 (min., mean and max., respectively) in Brno

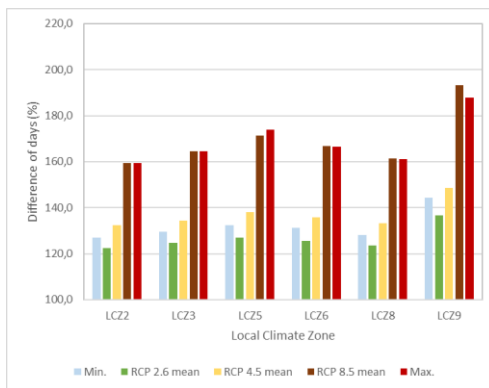


Fig. 30 Change of maximum, mean of the different RCPs and minimum of mean annual number of summer days in the period 2071–2100 using the applied climate models in different LCZ classes compared to 1971–2000 (min., mean and max., respectively) in Brno

6. DISCUSSION

The results obtained for particular cities can be compared in order to formulate the features characteristic for the cities in the whole region of Central Europe. The predictions for the period 2021–2050 show a rather slight increase in the mean annual number of summer days, while for the period 2071–2100, the predicted values are much larger. The scenario RCP2.6 is the most optimistic one in terms of future CO₂ concentration and impact, but unfortunately the chances that it will be realized are rather modest. Therefore, the predictions for the period 2071–2100, for the scenarios RCP4.5 and RCP8.5 were analyzed further. Tables 8,

9 and 10 present the characteristic values for each city and scenario, in relation to the reference period 1971–2000. The values in Table 8 refer to the results shown in Figs. 11–20.

Table 8 shows large differences among the cities in the mean number of summer days in the reference period 1971–2000 (mean values for the whole domains). Cities located in the southern part of Central Europe (represented by Szeged) have on average twice as much summer days than cities located north of the Carpathian Mts. (represented by Kraków). It is a result of climatic variability of Central Europe, linked to the transitional character of all elements of the natural environment. The Carpathian Mts. constitute a significant climatic barrier. South of that mountain chain, the impact of the Mediterranean Sea is one of the factors controlling climatic conditions while north of the Carpathians, polar air masses

(maritime from the west and continental from the east) decide about large weather variability and more severe climatic conditions.

Table 8 Mean annual number of summer days, 1971–2000 and 2071–2100 (RCP4.5 and RCP8.5)

City	Mean			Min			Max		
	1971– 2000	2071–2100 RCP4.5	2071–2100 RCP8.5	1971– 2000	2071–2100 RCP4.5	2071–2100 RCP8.5	1971– 2000	2071–2100 RCP4.5	2071–2100 RCP8.5
Kraków	20.3	37.8	59.2	4.0	14.8	28.7	61.1	78.6	100.3
Brno	37.2	59.3	81.4	10.5	27.4	40.7	83.4	102.1	123.1
Vienna	45.4	70.0	93.4	7.2	21.3	40.0	82.8	107.8	128.8
Bratislava	56.4	85.9	107.8	20.6	42.4	65.0	104.1	131.2	148.9
Szeged	50.1	79.1	104.3	7.8	24.3	78.5	123.4	142.8	159.1

Explanations: mean – mean value for the whole domain of a certain city (see Fig. 1), min – the lowest value found in a domain, max – the highest value found in the domain

Additionally, data from Table 8 show that the difference in mean annual number of days (mean values for the whole domain) between Szeged and Kraków might increase in the future: for 1971–2000 it was about 30 days, while for 2071–2100 it is predicted to increase up to about 41–45 days, depending on the scenario. Minimum and maximum values shown in table 8 are much more dependent on local land use/land cover variability than on general climatic conditions; those values represent areas in each city where extremely low or high values can occur. But those values also show the range of the values that can be experienced in each city. For the reference period, the largest difference was noted for Szeged (about 166 days) while the smallest for Kraków (57 days). In all cities, maximum and minimum values are predicted to increase, but the changes in the range of the values (i.e. the difference between the maximum and minimum value) shows no uniform tendency. In Kraków, Brno and Vienna the range is predicted to increase in comparison to 1971–2000 (by 2–15 days, depending on the scenario used), in Bratislava it is predicted to be almost unchanged, and in Szeged – it might decrease even by 35 days. The decrease for Szeged might constitute a particular hazard for the inhabitants.

Tables 9 and 10 show the absolute and relative changes of the values shown in Table 8. Relative values (in %) in table 10 show a larger increase in mean values for the whole domain in the north of the region (Kraków and Brno: 192 and 119% for RCP8.5) than in the south (Szeged: 108% for RCP8.5). An interesting feature is the difference in most values between Vienna and Bratislava, as they are located so close to each other. On one hand, Bratislava is a much smaller city than Vienna, so the impact of built-up area on urban climate is smaller, too. On the other hand, each city is located in different environmental conditions, including relief, which is a significant element controlling urban climate. From all the cities considered, Szeged is the only one located in a flat area and it is also the smallest city comparing to the others. Even though the absolute number of summer days (mean for the whole domain) is predicted to be the highest there in 2071–2100, the relative increase is comparable to Vienna or Brno, while for Kraków the values of relative increase are the highest. The indices discussed above allow to see the regional dimension of the predicted heat load increase. The local dimension can be discussed for each city in terms e.g. of the spatial planning. As mentioned in the introduction section, all cities studied except Szeged are located in a complicated relief conditions. The figures presented in section 3 show that concave land forms (e.g. valley bottoms) experience larger numbers of summer days than nearby hilltops. It is a phenomenon well known from the studies on the climate of the mountains. Even though the cities considered are not located in the mountains, the differences

in relative altitude are large enough to contribute to the generation of the processes known from mountainous areas (e.g. katabatic flows, air temperature inversions). However, those processes can be observed mainly during the night time, while the present study concerns the daytime and the occurrence of the maximum temperature $\geq 25^{\circ}\text{C}$. During the day time, there are no such large differences in air temperature between valleys and hilltops as during the night but valley floors tend to have higher maximum air temperature and that is also visible in the data presented above.

Table 9 Increase (in number of days) of mean annual number of summer days in the periods 1971–2000 and 2071–2100 (RCP4.5 and RCP8.5)

City	Mean			Min			Max		
	1971–2000	2071–2100 RCP4.5	2071–2100 RCP8.5	1971–2000	2071–2100 RCP4.5	2071–2100 RCP8.5	1971–2000	2071–2100 RCP4.5	2071–2100 RCP8.5
Kraków	20.3	17.5	38.9	4.0	10.8	24.7	61.1	17.5	39.2
Brno	37.2	22.1	44.2	10.5	16.9	30.2	83.4	18.7	39.7
Vienna	45.4	24.6	48.0	7.2	14.1	32.8	82.8	25	46
Bratislava	56.4	29.5	51.4	20.6	21.8	44.4	104.1	27.1	44.8
Szeged	50.1	29.0	54.2	7.8	16.5	70.7	123.4	19.4	35.7

Explanations: mean – mean value for the whole domain of a certain city (see Fig. 1), min – the lowest value found in a domain, max – the highest value found in the domain

Table 10 Increase (in %) of mean annual number of summer days, in the periods 1971–2000 and 2071–2100 (RCP4.5 and RCP8.5)

City	Mean			Min			Max		
	1971–2000	2071–2100 RCP4.5	2071–2100 RCP8.5	1971–2000	2071–2100 RCP4.5	2071–2100 RCP8.5	1971–2000	2071–2100 RCP4.5	2071–2100 RCP8.5
Kraków	20.3	86	192	4.0	270	618	61.1	29	64
Brno	37.2	59	119	10.5	161	288	83.4	22	48
Vienna	45.4	54	106	7.2	196	456	82.8	30	56
Bratislava	56.4	52	91	20.6	106	215	104.1	26	43
Szeged	50.1	58	108	7.8	212	906	123.4	16	29

Explanations: mean – mean value for the whole domain of a certain city (see Fig. 1), min – the lowest value found in a domain, max – the highest value found in the domain

7. CONCLUSIONS

According to the predictions presented, an increase in heat load, expressed in mean annual number of summer days, is expected in urban areas of Central Europe. Mean values for particular study areas are expected to increase by 2100, comparing to 1971–2000, by 20–50 days, depending on the scenario used. The regional spatial pattern of the predicted values of mean annual number of summer days shows dependence on latitude, i.e. for cities located in the northern part of the study area, the values are lower than for cities located in the south. The difference for mean values, for particular study areas, reaches about 40 days. The local spatial pattern shows the impact of both land use/land cover and relief. The largest values of mean annual number of summer days are observed in areas with intense built-up which are located in the valley floors. In rural areas, larger values are observed in the valleys than in the hill tops. The differences between the places with the lowest value and the largest value in particular cities reach 60–100 days, depending on the scenario used.

The results obtained might be useful e.g. in spatial planning in particular cities, but they should be also used for a long-term education of local communities. The predicted changes call for preparedness and planning of the mitigation actions. Those are actions which cannot be realized without a relatively high level of public awareness of the issue discussed. First of all, the density of existing built-up structures should not be increased as it might generate in the future the intensification of the heat load. New buildings should be located in areas located well above the river valley floor, so as to avoid the enhancement of heat load increase by overlapping effect of both relief and land use. Additionally, each city should elaborate a “strategy of shading”, e.g. by increasing the number of trees. Urban green areas may contribute to the decrease of heat load only when they are arranged in such a way as to increase the city albedo, i.e. reflect the solar radiation and do not allow it to be absorbed by the urban structures.

The area of Central Europe is very diversified in terms of the natural environment conditions. Effects of factors of regional importance are modified significantly by the impact of various local conditions. The results presented above for the five cities of Central Europe show, on one hand, the high diversity of the region, but on the other hand, they present a tendency common for the whole area of Central Europe, namely the predicted increase in the heat load in urban areas. Those results are in accordance with results available for the whole continent. Therefore, further research on potential consequences of that phenomenon is needed, together with the transfer of this scientific knowledge to the decision makers, responsible for spatial planning and citizens’ health and well-being.

Acknowledgements: The project “Urban climate in Central European cities and global climate change” (<http://www.klimat.geo.uj.edu.pl/urbanclimate/index.html>) has been realized within the framework of the International Visegrad Fund’s Standard Grant No. 21410222 in the years 2014–2015. The study was supported by National Research, Development and Innovation Office (NKFI K-120346).

REFERENCES

- Auer I, Böhm R, Mohnl H (1989) Eine anwendungsorientierte Klimatographie. Magistrat der Stadt Wien, Wien
- Baccini M, Biggeri A, Accetta G, Kosatsky T, Katsouyanni K, Analitis A, Anderson HR, Bisanti L, D’Ippoliti D, Danova J, Forsberg B, Medina S, Paldy A, Rabczenko D, Schindler C, Michelozzi P (2008) Heat effects on mortality in 15 European cities. *Epidemiology* 19:711-719
- Bechtel B, Daneke C (2012) Classification of local climate zones based on multiple earth observation data. *J-STARS* 5:1191-1202
- Bechtel B, Alexander PJ, Böhner J, Ching J, Conrad O, Feddema J, Mills G, See L, Stewart I (2015) Mapping local climate zones for a worldwide database of the form and function of cities. *ISPRS Int J Geo-Inf* 4: 199-219
- Böhm R (1998) Urban bias in temperature time series: a case study for the City of Vienna, Austria. *Climatic Change* 38:113-128
- Bokwa A (2010a) Effects of air pollution on precipitation in Kraków (Cracow), Poland in the years 1971–2005. *Theor Appl Climatol* 101:289-302
- Bokwa A (2010b) Wieloletnie zmiany struktury mezoklimatu miasta na przykładzie Krakowa. [Multi-annual changes of the urban mesoclimate structure using an example of Kraków (in Polish)] Institute of Geography and Spatial Management, Jagiellonian University, Kraków
- Bokwa A, Hajto MJ, Walawender JP, Szymanowski M (2015) Influence of diversified relief on the urban heat island in the city of Kraków, Poland. *Theor Appl Climatol* 122:365-382
- Clarke L, Edmonds J, Jacoby H, Pitcher H, Reilly J, Richels R (2007) Scenarios of Greenhouse Gas Emissions and Atmospheric Concentrations. Sub-report 2.1A of Synthesis and Assessment Product 2.1 by the U.S. Climate Change Science Program and the Subcommittee on Global Change Research. Department of Energy, Office of Biological & Environmental Research, Washington D.C.

- Dobrovolný P, Řezníčková L, Brázdil R, Krahula L, Zahradníček P, Hradil M, Doleželová M, Šálek M, Štěpánek P, Rožnovský J, Valášek H, Kirchner K, Kolečka J (2012) Klima Brna. Víceúrovňová analýza městského klimatu. [The Climate of Brno. Multilevel analysis of urban climate (in Czech)] Masaryk University, Brno
- Dobrovolný P (2013) The surface urban heat island in the city of Brno (Czech Republic) derived from land surface temperatures and selected reasons for its spatial variability. *Theor Appl Climatol* 112:89-98
- Formayer H, Haas P (2009) Correction of RegCM3 model output data using a rank matching approach applied on various meteorological parameters. In: Deliverable D3.2 RCM output localization methods (BOKU-contribution of the FP 6 CECILIA project)
- Früh B, Becker P, Deutschländer T, Hessel JD, Kossmann M, Mieskes I, Namyslo J, Roos M, Sievers U, Steigerwald T, Turau H, Wienert U (2011) Estimation of climate-change impacts on the urban heat load using an urban climate model and regional climate projections. *J Appl Meteor Climatol* 50:167-184
- Gross G (1989) Numerical simulation of the nocturnal flow systems in the Freiburg area for different topographies. *Beitr Phys Atmos* 62:57-72
- IPCC (2013) Climate Change 2013: The Physical Science Basis. Contribution of Working Group I to the Fifth Assessment Report of the Intergovernmental Panel on Climate Change. Cambridge University Press, Cambridge, New York
- Jacob D, Petersen J, Eggert B, Alias A, Christensen OB, Bouwer L, Braun A, Colette A, Déqué M, Georgievski G, Georgopoulou E, Gobiet A, Menut L, Nikulin G, Haensler A, Hempelmann N, Jones C, Keuler K, Kovats S, Kröner N, Kotlarski S, Kriegsmann A, Martin E, Meijgaard E, Moseley C, Pfeifer S, Preuschmann S, Radermacher C, Radtke K, Rechid D, Rounsevell M, Samuelsson P, Somot S, Soussana JF, Teichmann C, Valentini R, Vautard R, Weber B, Yiou P (2013) EURO-CORDEX: new high-resolution climate change projections for European impact research Regional Environmental Change. Springer, Berlin, Heidelberg
- Kottek M, Grieser J, Beck C, Rudolf B, Rubel F (2006) World Map of the Köppen-Geiger climate classification updated. *Meteorol Z* 15:259-263
- Lapin M, Melo M (2011) Climate change and its possible impacts on the urban areas in SW Slovakia. Institute of Geography and Spatial Management, Jagiellonian University, Kraków
- Geletič J, Lehnert M (2016). GIS-based delineation of local climate zones: The case of medium-sized Central European cities. *Moravian Geogr Rep* 24:2-12
- Lelovics E, Unger J, Gál T, Gál CV (2014) Design of an urban monitoring network based on Local Climate Zone mapping and temperature pattern modelling. *Clim Res* 61: 51-62
- Moss RH, Edmonds JA, Hibbard KA, Manning MR, Rose SK, van Vuuren DP, Carter TR, Emori S, Kainuma M, Kran T, Mehl GA, Mitchell JFB, Nakicenovic N, Riahi K, Smith SJ, Stouffer RJ, Thomson AM, Weyant JP, Wilbanks TJ (2010) The next generation of scenarios for climate change research and assessment. *Nature* 463:747-756
- Riahi K, Gruebner A, Nakicenovic N (2007) Scenarios of long-term socio-economic and environmental development under climate stabilization. *Technol Forecast Socl* 74:887-935
- Siebert J, Sievers U, Zdunkowski W (1992) A one-dimensional simulation of the interaction between land surface processes and the atmosphere. *Bound-Lay Meteorol* 59:1-34
- Sievers U, Forkel R, Zdunkowski W (1983) Transport equations for heat and moisture in the soil and their application to boundary layer problems. *Beitr Phys Atmos* 56:58-83
- Sievers U, Zdunkowski W (1985) A numerical simulation scheme for the albedo of city street canyons. *Bound-Lay Meteorol* 33:245-257
- Sievers U (1990) Dreidimensionale Simulationen in Stadtgebieten. *Umwelt-meteorologie, Schriftenreihe Band 15: Sitzung des Hauptausschusses II am 7. und 8. Juni in Lahnstein. Kommission Reinhaltung der Luft im VDI und DIN, Düsseldorf*
- Sievers U (1995) Verallgemeinerung der Stromfunktionsmethode auf drei Dimensionen. *Meteorol Z* 4:3-15
- Sievers U, Früh B (2012) A practical approach to compute short-wave irradiance interacting with subgrid-scale buildings. *Meteorol Z* 21:349-364
- Smith SJ, Wigley TML (2006) Multi-gas forcing stabilization with the MiniCAM. *Energy J* 27:373-391
- Stadt Wien (2015) Wirtschaft, Arbeit und Statistik (Magistratsabteilung 23): Wien in Zahlen 2015. Stadt Wien, Wien
- Stewart ID (2011) A systematic review and scientific critique of methodology in modern urban heat island literature. *Int J Climatol* 31:200-217
- Stewart ID, Oke TR (2012) Local Climate Zones for urban temperature studies. *B Am Meteorol Soc* 93:1879-1900
- Swire D (2006) Bratislava Blast. In: *Finance New Europe*
- Unger J (2004) Intra-urban relationship between surface geometry and urban heat island: review and new approach. *Clim Res* 27:253-264

- Unger J, Savić S, Gál T (2011) Modelling of the annual mean urban heat island pattern for planning of representative urban climate station network. *Adv Meteorol* 2011:398613
- Unger J, Savić S, Gál T, Milošević D (2014) Urban climate and monitoring network system in Central European cities. University of Novi Sad, University of Szeged, Novi Sad, Szeged
- Urban population growth (2015) Global Health Observatory (GHO) data. World Health Organization
- van Vuuren DM, den Elzen P, Lucas B, Eickhout B, Strengers B, van Ruijven S, Wonink R, van Houdt (2007) Stabilizing greenhouse gas concentrations at low levels: an assessment of reduction strategies and costs. *Climatic Change* 109:77-94
- Walawender JP, Szymanowski M, Hajto MJ, Bokwa A (2014) Land surface temperature patterns in the urban agglomeration of Kraków (Poland) derived from Landsat-7/ETM+ Data. *Pure Appl Geophys* 171:913-940
- Wise MA, Calvin KV, Thomson AM, Clarke LE, Bond-Lamberty B, Sands RD, Smith SJ, Janetos AC, Edmonds JA (2009) Implications of limiting CO₂ concentrations for land use and energy. *Science* 324:1183-1186
- Žuvela-Aloise M, Koch R, Neureiter A, Böhm R, Buchholz S (2014) Reconstructing urban climate of Vienna based on historical maps dating to the early instrumental period. *Urban Clim* 10:490-508

ABSOLUTE MOISTURE CONTENT IN MID-LATITUDE URBAN CANOPY LAYER, PART 1: A LITERATURE REVIEW

J UNGER, N SKARBIT and T GÁL

*Department of Climatology and Landscape Ecology, University of Szeged, Egyetem u. 2., 6720 Szeged, Hungary,
E-mail: unger@geo.u-szeged.hu*

Summary: This part of the study on absolute moisture content in the mid-latitude urban canopy layer first gives a comparison on intra-urban relative and absolute humidity patterns showing an example based on a long dataset. The comparison clearly demonstrates the usefulness of the utilization of absolute measure opposite to the temperature dependent relative one. This supports the earlier statements found in the literature albeit these statements are based on only case studies or short datasets. Then a short overview follows which presents the main results of studies about urban absolute moisture content. These studies focused mainly on urban-rural and less on intra-urban humidity differences. The scale differences are used for the grouping of studies based on the number of available measurement sites as well as their spatial distribution and density in the investigated urban regions.

Key words: relative humidity, vapor pressure, other humidity measures, urban-rural differences, intra-urban differences

1. INTRODUCTION

Urban regions modify the originally natural landscapes which means transformation in their radiative, thermal, moisture and aerodynamic characteristics reflecting in datasets of different climate parameters (temperature, humidity, precipitation, wind, etc.) (Oke 1987). It has long been known in the related literature that the relative humidity (RH , %) is generally lower in the near-surface air in the built-up areas (urban canopy layer, UCL) relative to their surroundings, especially in the evening/night hours because of the temperature-dependence of RH . It is mainly explained by the developing urban heat island phenomenon, that is the momentary urban RH pattern is the mirror image of this and it is calling as “urban dry island – UDF ” (Moriwaki et al. 2013, Cuadrat et al. 2015). Therefore, the extent of this negative RH deviation is closely related to the strength of the heat island and its daily variation (e.g. Ackerman 1987, Oke et al. 2017).

In contrast, if we are interested in not the relative but the absolute amount of air moisture (moisture content of air) and its urban-rural or intra-urban differences or patterns, we need to use other measures (e.g. vapor pressure – e , dew point temperature – T_d , absolute humidity/vapor density – p_v , specific humidity – q) having other units instead of % (hPa/mmHg/mb, °C/°F, gm^{-3} , gkg^{-1} , respectively) (Oke et al. 2017). Moriwaki et al. (2013) summarized the importance of the spatial and temporal distribution of air moisture mentioning that local severe rainfall is occasionally caused by the urbanization induced convergence of water vapor, as well as the humidity level can influence the plants life, the thermal comfort and health of people living in urban environment.

As our study has general and specific aims we split it into two parts. The first (recent) part is organized as follows:

(1) Presentation of the mean summer patterns of relative and absolute amount of air humidity (in parallel to temperature) in a city's *UCL* as an example in order to compare the two types of vapor content measures and their usefulness.

(2) Compilation of a short overview on the main results of earlier studies related to urban absolute moisture content of cities in mid-latitude climate regions (Köppen types C and D, Kottek et al. 2006). These studies are divided into two groups according to their scales. Studies in the first group are on urban-rural (larger scale) differences while the second group contains studies on humidity patterns and their intra-urban (smaller scale) differences.

In the second part of our study we will show the results about the absolute moisture content of the urban canopy layer in Szeged, Hungary based on a rather long (three years) and detailed intra-urban dataset (see Unger et al. 2018).

2. COMPARISON OF URBAN PATTERNS OF MEAN RELATIVE AND ABSOLUTE MOISTURE CONTENT

In this section we compare the mean summer patterns of relative and absolute amount (vapor pressure) of air humidity as well as temperature.

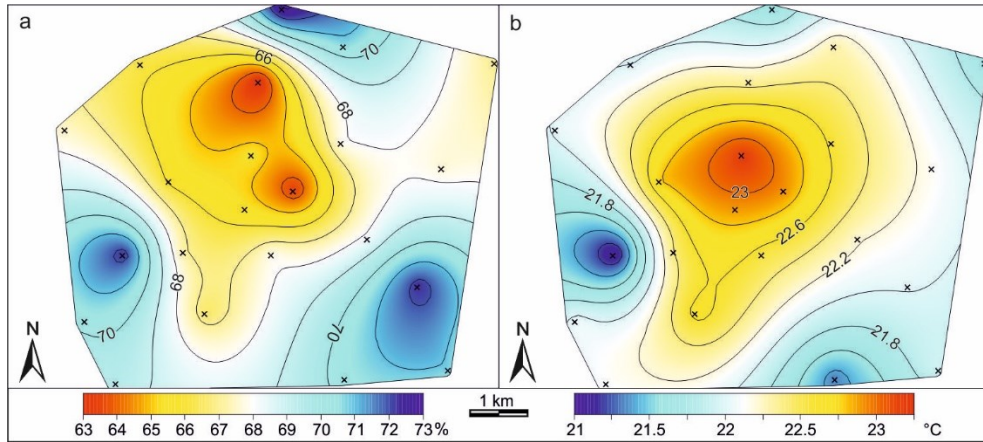


Fig. 1 Mean summer patterns of (a) relative humidity and (b) temperature in the urban area of Szeged, Hungary (June 2014 – May 2017)

As we mentioned in the previous section the urban *RH* pattern is the mirror image of the urban thermal field in the *UCL*, since the *RH* is the ratio of the vapor pressure and the vapor saturation pressure and the last one is the function of the temperature (*T*). Now we support this statement, not just based on a momentary situation, but taking the averages of a longer period (nine months) based on a three-year dataset of an urban meteorological station network from Szeged, Hungary (June 2014 – May 2017). These averages of *RH* and *T* were calculated from ten-minute records of 22 stations situated on a study area of about 8 km × 5.5 km. For the derivation of *e* averages we used the measured *T* and *RH*. For more details about the study area and data source see Unger et al. (2018).

The patterns of the three-summer RH and T averages have also mirror-like pictures (Fig. 1): dry/warm areas in the central parts and moist/cooler areas in the western, northern and south-eastern parts of the study area. Additionally, the island-like shape of the patterns is clearly recognizable with highest T and lowest RH values in the middle then the decreasing T s and increasing RH s toward the edges. Based on Fig. 1, we could reach the deceptive conclusion that the city core is drier than the rural areas.

On the contrary, the distribution of vapor pressure in the UCL does not follow the thermal field and differs radically from the previous ones (Fig. 2). It does not show a regular shape, the pattern of e is mosaic-like: the driest and wettest areas are in the north-western and south-eastern parts, respectively, but smaller dry and moist areas can be found in the city center, too. Furthermore, there are moist areas in the north and the south-eastern parts, while dry areas appear in the north-western, north-eastern and southern edges. This mosaic-like behavior of e implies that the moisture content distribution in UCL does not have any contact with the thermal pattern developed there but primarily depends on the smaller scale local moisture sources (irrigated parks, traffic, households, district heating plants, manufactories, etc.) and on the local conditions that inhibit or assist in air mixing promoting moisture accumulation or dilution.

Comparing Figs. 1 and 2 it is clearly visible that the usage of RH in intra-urban analysis hides the real spatial distribution of moisture in the city. Precisely, on the basis of the mean patterns on Figs. 1 and 2 we can state that the investigation of urban RH patterns is not really useful since it does not give any valid information about the actual moisture content distribution of the urban air. It is more proper to turn our attention to the studies investigating the absolute measures (e , T_d , P_v and q) of air moisture in urban environment.

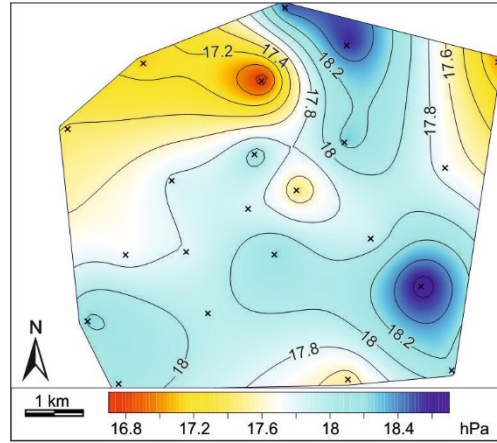


Fig. 2. Mean summer pattern of vapor pressure in the urban area of Szeged, Hungary (June 2014 – May 2017)

3. SHORT OVERVIEW ON STUDIES ABOUT ABSOLUTE MOISTURE CONTENT IN MID-LATITUDE CITIES

In the following, starting with a short historical review, we look at the findings of the absolute moisture amount in the UCL based on studies in cities located at mid-latitudes. For the first time, Kremser (1908) stated that humidity changes in the city air. Based on his investigation of 14-year data series from Berlin (Germany) and its surroundings, e was smaller in the city with 0.2 mmHg on average. Lessmann and Zedler's (1936) mobile measurement on a November day in 1935 gave rise to the first mapping of areal distribution of e with a largest difference of about 1.6 mmHg in Berlin.

Subsequently, according to our knowledge, no progress was made until Chandler's (1962) study in London (UK). Then the development has accelerated, both in terms of the

growing number of studies and in their versatility. It is not always possible to compare the urban effects identified in different cities as different humidity measures were utilized and insufficient information were given to convert them to a common measure (Oke et al. 2017).

Below we describe the main characteristics and key findings of the studies related to urban-rural differences (first group) as well as to humidity patterns that is to intra-urban differences (second group). These distinction by scales is based on the number of available measurement sites as well as their spatial distribution and density in the investigated urban regions.

3.1. Urban-rural differences

According to Oke et al. (2017) the urban-rural moisture differences in cities with mid-latitude climates have the following common characteristics:

- (i) "They are best displayed in 'ideal' (calm, clear) weather."
- (ii) "They are largest and spatially coherent at night but, during daytime they are complex and patchy."
- (iii) "There is a seasonal shift in the diurnal pattern; in summer, urban air is less moist than in the countryside by day, but more moist at night and in winter a city is commonly more moist at all times."

The main features of studies in the first group are summarized briefly in Table 1. These studies are different regarding their measurement methods (fixed sites, mobile), the studied measures (e , T_d , p_v) and the length of the examined period (from one night to 33 years). In addition we indicate which statements of Oke et al. (2017) are supported by the mentioned studies.

Chandler (1962) states that the cellular morphology of cities may trap pockets of air (in case of favorable conditions for urban heat island development). In this situation the *UCL* is free from excessive mixing, thus the high daytime humidity will be maintained. It was proven by the distribution of mean T_d values for about 23:30. In the central London T_d was exceptionally high.

According to Hage (1975) Edmonton (Canada) was found to be dry in the daytime but moist at night in all but especially in winter months. In winter p_v is usually higher in the city on the whole day. Annual maxima in p_v differences were found in March and August (moist) and in daytime in July (dry).

The *UCL* air in Chicago (US) could be more or less humid than that in the surrounding rural areas (Ackerman 1987). This study also found diurnal and seasonal cycles. The average urban-rural differences were positive at night and negative only in the forenoon in late spring and in early summer afternoons.

Lee (1991) found obvious seasonal and diurnal patterns of urban-rural humidity differences in case of London (UK). The mean monthly differences were between +0.9 and -0.3 hPa. The *UCL* is more humid than the rural area all day long in winter and spring while less humid only during daytime in summer.

Szeged (Hungary) was found to be more humid than its surroundings during the whole year (Unger 1993, 1999). The minimum of increased humidity is at 01 h and its maximum is at 19 h in the summer months. This type of regular diurnal variation does not exist except in case of these summer situations. The humidity difference increases from January–February to August and then decreases until November–December.

Holmer and Eliasson (1999) revealed that the urban moisture excess (*UME*) in Stockholm (Sweden) could develop from three different combinations of rural and urban

nocturnal e changes. This observation proves that different physical processes have effect on urban humidity, and these processes have different relationship with each other and the resulted e changes. They identified evaporation and condensation as an important factor for the development of *UME* but they also pointed out that the dry air advection caused by the urban heat island circulation could also modify the values.

Table 1 Main characteristics of studies focused on urban-rural humidity differences in absolute terms in chronological order (*fine* – clear and calm weather conditions, e – vapor pressure, T_d – dew point temperature, p_v – absolute humidity), as well as their confirmation of one or more statements by Oke et al. (2017)

Reference	Measurement type	Studied measure	Number of events, time	Confirm (i), (ii) or (iii)
Chandler (1962)	mobile traverse	T_d (°C)	1 night (October)	(i)
Hage (1975)	urban-rural station pair	p_v (gm ⁻³)	13 years	(iii)
Ackerman (1987)	urban-rural station pair	e , T_d (mb, °C)	7 years	(iii)
Lee (1991)	urban-rural station pair	e (mb)	10 years	(iii)
Unger (1993, 1999)	urban-rural station pair	e (mb, hPa)	3 years	-
Holmer and Eliasson (1999)	urban-rural station pair	e (hPa)	53 <i>fine</i> summer nights	-
Unkašević et al. (2001)	1 urban, 2 suburb, 1 rural stations	e (hPa)	5 years	(iii)
Charciarek (2003)	urban-rural station pair	e (hPa)	5 years	(iii)
Mayer et al. (2003)	3 urban stations, mobile traverses	e (hPa)	August, January	(iii)
Richards (2005)	urban-rural station pair	p_v (gm ⁻³)	24 days June-July (rain-free weather conditions biased toward fine and stable weather)	(ii)
Fortuniak et al. (2006)	urban-rural station pair	e (hPa)	6 years	(ii), (iii)
Sakakibara et al. (2006)	mobile traverses	e (hPa)	50 <i>fine</i> nights, 22 cloudy nights, 48 <i>fine</i> days (1 year)	(i), (iii)
Kuttler et al. (2007)	urban-rural station pair	e (hPa)	1 year	(iii)
Liu et al. (2009)	urban-rural station pair	e (hPa)	33 years	(ii), (iii)
Pongrácz et al. (2016)	intra-district mobile traverses, 1 suburban station	T_d (°C)	1 summer day	

Unkašević et al. (2001) manifested clear seasonal and diurnal patterns of urban-rural moisture differences in Belgrade (Serbia). They found humidity surplus in *UCL* compared to suburban and rural air at 07 and 21 h, autumn and winter, while in spring and summer the humidity had lower values in the *UCL*. They also clearly identified that at 14 h the *UCL* is drier in the whole year.

In case of Lodz (Poland) Charciarek (2003) found clear daily and seasonal cycle in e between urban and rural areas. In urban area the e is higher at nighttime, and in daytime only in the winter half-year. Maximal moisture surplus of urban area was measured after midnight in November and June, and in the afternoon and evening hours in November.

Mayer et al. (2003) could not find any significant spatial variation of e in the winter months in Munich (Germany). However they found that the summer variation of e is characterized by higher monthly mean values for all of their three measurement sites and the inter-site differences are considerable. Mayer et al. (2003) revealed that the diurnal variability of mean e values has different amplitudes and times of occurrence of their extreme values. The readings of their car traverses before, during and after a clear night showed an obvious small-scale spatio-temporal variability of e as a combined dependence on time and pattern of urban land cover.

In the case of Vancouver (Canada) there are no clear trend of urban humidity values, the urban-rural differences are between 1.7 and -3.3 gm^{-3} (Richards 2005). Median values for Δp_v between urban and rural sites were all negative, however, there was some tendency in the urban moisture island between 0 and 04 h.

Fortuniak et al. (2006) stated that urban-rural differences (Δe) in winter were usually around 1 hPa, but in summer they exceeded 5 hPa in extreme cases in Lodz (Poland). The highest negative differences occurred at night with a magnitude similar to the positive ones. They also found that it is very difficult to predict which type of humidity contrast will occur. According to their results the appearance of the highest positive Δe is at late night and the highest negative Δe is at early morning.

Based on the measurements in six different cities in Japan, Sakakibara et al. (2006) found that urban e had usually lower value than in rural areas. Urban-rural e differences on days with clear and calm daily weather conditions were two times larger than on cloudy or calm nights. They found that the mean value of e differences in summer was nearly twice as large as in winter. They also revealed that the connection between mean e differences and settlement population size is logarithmic.

Kuttler et al. (2007) revealed weak and intense *UME* during the year but the frequencies per month were different in Krefeld (Germany). A diurnal course of *UME* was also found only for summer. Weak or intense *UME* events usually occurred in the second half of the night. Most of these events had a duration of one hour, but in few occasions they found longer duration of weak and intense *UME* events up to 14 and 12 h, respectively.

In case of Beijing (China) annual urban-rural e differences were high at night and low in the morning and afternoon (Liu et al. 2009). In winter, for the 08, 14 and 20 hours urban e was higher than rural area and lower in the other seasons. They stated that the difference usually reached its maximum in summer, on the other hand, at 02 hours the difference was marginal. Based on their measurements urban e was basically higher than the rural one.

Pongrácz et al. (2016) revealed that T_d values in the afternoon are usually lower than in the evening in Budapest (Hungary). The difference relative to the suburb station decreased from 3–5°C (at about 14 h) to 1–2°C (at about 21 h).

3.2. Intra-urban patterns

The following is an overview of the main results that have been achieved so far related to the absolute humidity patterns in the urban areas. So now we turn to the studies in the second group that are more related to our recent investigation in Szeged (see Unger et al. 2018). The main features of studies of this group are summarized briefly in Table 2.

In case of Leicester (UK) Chandler (1967) proved that nighttime absolute humidity values were frequently higher in cities than in the rural areas nearby. There is also a remarkable conformity between the distribution of e and the extent and form of the city.

Kopec (1973) revealed that in clear and calm weather situations the humidity in urban area of Chapel Hill (US) were higher at night as well as lower in the morning and afternoon compared to suburban and rural areas. Based on their measurements, the maximal differences and the most complex patterns were in late afternoon and in contrary, and there were the minimal differences and less complex spatial patterns at night.

Table 2 Main characteristics of studies focused on urban humidity patterns in absolute terms in chronological order (e – vapor pressure, T_d – dew point temperature, q – specific humidity, p_v – absolute humidity)

Reference	Measurement type	Studied measure	Number of events, time
Chandler (1967)	mobile traverse	e (mb)	3 nights (August)
Kopec (1973)	mobile traverse	T_d (°F)	6 (midnight, morning, afternoon) (Sept., Oct.)
Goldreich (1974, 1999)	mobile traverse	q (gkg ⁻¹)	48 (morning, afternoon) (June, Dec.)
Henry et al. (1985)	mobile traverse	T_d (°C)	45 (morning, afternoon, evening) (Aug. – Oct.)
Moriwaki et al. (2013)	21-station network	p_v (gm ⁻³)	16 months (from July to next Oct.)
Dou et al. (2015)	24-station urban + 20-station nonurban networks	q (gkg ⁻¹)	summer (5 years)

According to Goldreich (1974, 1999) a distinct q island was found above the Central Business District in Johannesburg (South Africa) in summer and winter, especially at sunrise and in the early afternoon. The q island was most pronounced in the daytime in winter.

Henry et al. (1985) stated that over undeveloped land the T_d was higher in the morning and afternoon in Lawrence (US). In contrary, residential and educational-institutional land use categories had negative correlation with T_d values, while in the evening the significance of this relationship was minimal.

In Matsuyama Plain (Japan) the UDI was identified in the daytime during favorable weather conditions (Moriwaki et al. 2013). They explained this phenomenon by the difference in water vapor fluxes at urban and rural sites. Their measurements showed obvious appearance of UDI in the morning and late afternoon, when the sea breeze and land breeze altered each other and the wind speed declined. Their study also revealed that UDI intensity was larger in summer than in winter. They explained their results with the small latent heat fluxes and strong NW monsoon effect in winter, which enhanced the mixing of humidity.

In Beijing (China) the urban q values were lower than in the surrounding regions (Dou et al. 2015). Their measurements clearly illustrated that a multicenter distribution occurred and it was connected to the spatial distribution of urban impervious surfaces. According to their results these surfaces decrease the evapotranspiration and increase the runoff, thus decrease urban q levels. They also highlighted that the usually warmer urban boundary layer in the daytime is also more convective than the rural one, and it could increase upward moisture fluxes, resulting lower q in UCL than in the nearby rural areas.

4. CONCLUSIONS

Our results help to draw the attention to the deceptive use of *RH* in urban climate studies. With the usage of absolute vapor characteristics (e.g. e , T_d , p_v , q) it is more likely possible to reveal the real moisture characteristics of urban areas.

Our literature review revealed the contradictions and knowledge gaps in the field of urban moisture behavior. There are some basic tendencies in the urban-rural characteristics, as Oke et al. (2017) summarized, however the studies could not prove all of them in the same urban area. We also found some studies where none of these general tendencies could be found. In case of intra-urban patterns we could find only a few studies, and based on their results it is hard to outline any general characteristics. We can state that the highest moisture differences occur in late afternoon, the differences disappear at night and there are some connection between the most vegetated urban surfaces and moisture content.

Essentially, the results of this systematic review show the necessity of a detailed analysis of the urban moisture patterns. This evaluation should use long data series in order to represent various weather situations, and it has to obtain readings from numerous different built-up areas of an urban environment in order to identify the possible factors what leads different moisture content in the basically same urban land use situations. In the second part of our study (Unger et al. 2018) we aim to present an analysis that is capable to accomplish these criteria.

Acknowledgement: This study was supported by the Hungarian Scientific Research Fund (OTKA K-111768).

REFERENCES

- Ackerman B (1987) Climatology of Chicago area urban-rural differences in humidity. *J Clim Appl Meteorol* 26:427-430
- Chandler TJ (1962) Temperature and humidity traverses across London. *Weather* 17:235-241
- Chandler TJ (1967) Absolute and relative humidities in towns. *B Am Meteorol Soc* 48:394-399
- Charciarek T (2003) Daily course of vapour pressure and relative humidity differences between urban and rural site in Lodz. Fifth Int Conf on Urban Climate, Lodz, Poland, P.4.14.
- Cuadrat JM, Vicente-Serrano, Saz MA (2015) Influence of different factors on relative air humidity in Zaragoza, Spain. *Frontiers in Earth Science* 3, Article 10
- Dou J, Wang Y, Bornstein R, Miao S (2015) Observed spatial characteristics of Beijing urban climate impacts on summer thunderstorms. *J Appl Meteorol Climatol* 54:94-105
- Fortuniak K, Klysik K, Wibig J (2006) Urban-rural contrasts of meteorological parameters on Lodz. *Theor Appl Climatol* 84, 91-101
- Goldreich Y (1974) Observations on the urban humidity island in Johannesburg. *Isr J Earth Sci* 23:39-46
- Goldreich Y (1999) Absolute and relative humidity island in urban area. ICB-ICUC Sydney, CD ICUC7
- Hage KD (1975) Urban-rural humidity differences. *J Appl Meteorol* 14:1277-1283
- Henry JA, Dicks SE, Marotz GA (1985) Urban and rural humidity distributions: relationships to surface materials and land use. *J Climatol* 5:53-62
- Holmer B, Eliasson I (1999) Urban-rural vapour pressure differences and their role in the development of urban heat islands. *Int J Climatol* 19:989-1009
- Kopec RJ (1973) Daily spatial and secular variations of atmospheric humidity in a small city. *J Appl Meteorol* 12:639-648
- Kottek M, Grieser J, Beck C, Rudolf B, Rubel F (2006) World Map of the Köppen-Geiger climate classification updated. *Meteorol Z* 15:259-263
- Kremser V (1908) Der Einfluß der Großstädte auf die Luftfeuchtigkeit. *Meteorol Z* 25:206-2015
- Kuttler W, Weber S, Schonhefeld J, Hesselschwerdt A (2007) Urban/rural atmospheric water vapour pressure differences and urban moisture excess in Krefeld, Germany. *Int J Climatol* 27:2005-2015

- Lee DO (1991) Urban-rural humidity differences in London. *Int J Climatol* 11:577-582
- Lessmann H, Zedler P (1936) Ein Beitrag zum Berliner Stadtklima. *Biokl Bbl* 3:163-165
- Liu W, You H, Dou J (2009) Urban-rural humidity and temperature differences in the Beijing area. *Theor Appl Climatol* 96:201-207
- Mayer H, Matzarakis A, Iziomon MG (2003) Spatio-temporal variability of moisture conditions within the Urban Canopy Layer. *Theor Appl Climatol* 76:165-179
- Moriwaki R, Watanabe K, Morimoto K (2013) Urban dry island phenomenon and its impact on cloud base level. *Journal of JSCE* 1:521-529
- Oke TR (1987) *Boundary Layer Climates*. Second Edition. Routledge
- Oke TR, Mills G, Christen A, Voogt JA (2017) *Urban Climates*. Cambridge University Press
- Pongrácz R, Bartholy J, Dezső Z, Dian C (2016) Analysis of the air temperature and relative humidity measurements in Budapest-Ferencváros. *Hung Geogr B* 65:93-103
- Richards K (2005) Urban and rural dewfall, surface moisture and associated canopy level air temperature and humidity measurements for Vancouver, Canada. *Bound-Lay Meteorol* 114:143-163
- Sakakibara Y, Kitahara Y, Nakagawa K (2006) The relationship between urban-rural water vapor pressure differences and the population sizes of settlements in Saku, Nagano, Japan. *J Agric Meteorol* 82:1-8
- Unger J (1993) The urban influence on the diurnal and annual patterns of absolute humidity in Szeged, Hungary. *Acta Climatol* 27:33-39
- Unger J (1999) Urban-rural air humidity differences in Szeged, Hungary. *Int J Climatol* 19:1509-1515
- Unger J, Skarbit N, Gál T (2018) Absolute moisture content in mid-latitude urban canopy layer, Part 2: results from Szeged, Hungary. *Acta Climatol* 51-52:47-56
- Unkašević M, Jovanović O, Popović T (2001) Urban-suburban/rural vapour pressure and relative humidity differences at fixed hours over the area of Belgrade city. *Theor Appl Climatol* 68:67-73

ABSOLUTE MOISTURE CONTENT IN MID-LATITUDE URBAN CANOPY LAYER, PART 2: RESULTS FROM SZEGED, HUNGARY

J UNGER, N SKARBIT and T GÁL

*Department of Climatology and Landscape Ecology, University of Szeged, Egyetem u. 2., 6720 Szeged, Hungary,
E-mail: unger@geo.u-szeged.hu*

Summary: This study gives a comprehensive picture on the air humidity observation and mapping in urban canopy layer in Szeged, Hungary, analyzing three-year long vapor pressure dataset (e) calculated from observations of a 22-station urban network. The analysis was divided into two directions, namely the urban-rural and intra-urban ones where the latter was partly based on the local climate zone approach. (i) The general features of the annual and diurnal variations of urban-rural absolute humidity difference in cities with mid-latitude climates are also detectable in the case of Szeged. (ii) In the annual and seasonal e means there is no clear zone sequence that would follow the differences in the compactness or building height of the zones and even the built-up versus land cover distinction. (iii) The highest e values and their differences among stations appear in summer, while the lowest ones in winter and the values of transitional seasons are between them. In certain cases the intra-zone differences can exceed the inter-zone ones since the effect of microscale environment is essential. The decisive factors are the permeability of the surface and the vegetation cover. (iv) The diurnal course of the e pattern in normalized 4-hour time steps does not show a regular shape, the patterns are mosaic-like: in all time steps the driest and wettest areas are mainly in the north-western and south-eastern parts, respectively.

Keywords: vapor pressure, urban network, long dataset, urban-rural, intra-urban, local climate zones

1. INTRODUCTION

The first part of our study dealt with the main results of earlier studies related to urban absolute moisture content of the urban canopy layer (*UCL*) in mid-latitude climate regions (see Unger et al. 2018).

Our work in this second part presents a development in this research field compared to the previous ones as it is based on a rather long and spatio-temporally detailed intra-urban dataset from Szeged (Hungary). We analyze three-year long relative humidity and temperature data from 22 stations of an urban meteorological network, the installation of which was based on the surface classification scheme of Local Climate Zone (LCZ) system proposed recently by Stewart and Oke (2012). The applied dataset from the period of 2014–2017 provides a reliable basis for examining the seasonal and annual features, as well as the diurnal dynamics of the urban absolute moisture content in and around the city.

Based on the vapor pressure values calculated from relative humidity and temperature data of the urban network our analysis applies two approaches, namely the urban-rural and intra-urban ones:

(1) In the first approach the annual and diurnal variations of mean urban-rural humidity differences are analyzed comparing them to the earlier results mentioned by Oke et al. (2017);

(2) During the second approach (a) the mean annual and seasonal humidity conditions of LCZs, (b) the mean diurnal variation of humidity of LCZs by seasons and (c) the mean diurnal variation of intra-urban humidity patterns in summer are evaluated.

2. STUDY AREA, DATA AND METHODS

Szeged is located in the south-eastern part of Hungary (46.25°N, 20.15°E) at 79 m a.s.l. on a flat terrain with a population of 162,000 within an urbanized area of about 40 km². According to Kottek et al. (2006) it is in Köppen's climatic region Cfb (warm temperate climate, no dry season, warm summer) with annual mean temperature of 10.9°C, sunshine duration of 2049 hours and annual amount of precipitation of 514 mm (1981–2010, OMSZ 2015). Its urban area is characterized by a densely built midrise core, with openly spaced blocks of flats in the east-northern part of the city, as well as family homes and warehouses on the outskirts. The rural surroundings are mostly croplands (wheat, maize) with few scattered trees (Skarbit et al. 2017).

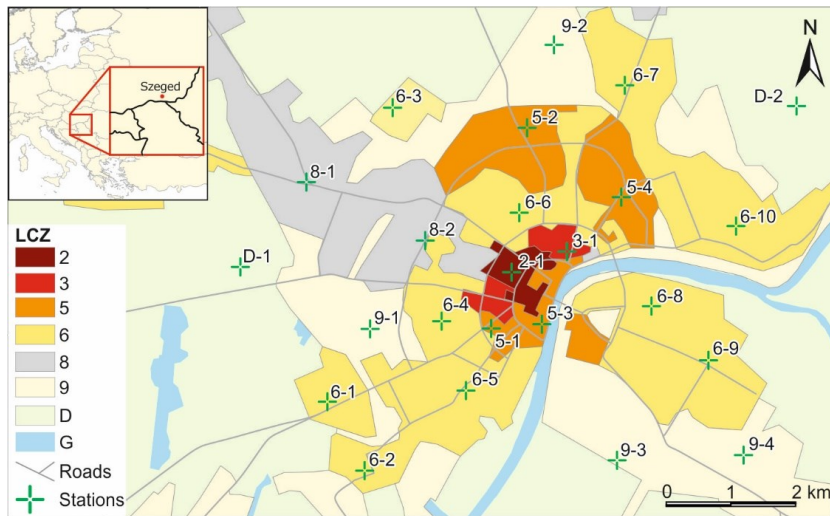


Fig. 1 Geographical location of Szeged and local climate zone map of the study area with station sites of the urban meteorological network (marked by green crosses and digits referring to the zones)

Within the framework of an EU project (URBAN-PATH 2018) an urban meteorological network with 24 stations was set up in Szeged representing different LCZs occurring in and around Szeged (Fig. 1). Two stations represent the rural area and 22 stations represent the different built-up areas (different LCZs) of the city (for more details see Unger et al. 2015). The network provides air temperature (T in °C) and relative humidity (RH in %) datasets of high temporal and spatial resolution across various weather conditions. In this analysis two stations (5-1, D-1) were excluded from the original network because of technical reasons. The remaining 22 stations represent the built and land cover LCZs occurring in Szeged with one exception: LCZ G, as there is no measurement station near the small water bodies in the area. Thus, the data used in the present study relate to LCZs 2 (compact midrise),

3 (compact low-rise), 5 (open midrise), 6 (open low-rise), 8 (large low-rise), 9 (sparsely built) and D (low plants) (Fig. 1).

As a first step, we calculated ten-minute averages of the measured 1-minute T and RH data of 22 stations from June 1, 2014 to May 31, 2017. In order to avoid the problem related to the effect of temperature on relative humidity (see Unger et al. 2018) and present the absolute moisture content of the urban canopy layer, the vapor pressure (e) values were calculated from the T and RH data, as a second step. During this procedure the vapor saturation pressure (e_s) was determined by:

$$e_s = A \cdot 10^{\left(\frac{m \cdot T}{T + T_n}\right)}$$

where A , m and T_n are constants depending of the state of water (Vaisala 2013). After, using the obtained ten-minute RH and e_s values the e was calculated by the following equation:

$$RH = \frac{e}{e_s} \cdot 100\%$$

To compare the general humidity modifying effects of different LCZs in Szeged, monthly hourly means, monthly and seasonal means, as well as seasonal minimum and maximum means were used. In case of LCZs 2, 3 and D the averages derived from data of only one station, however, for LCZs 5, 6, 8 and 9 the average of data from several stations were used according to the size of these zones.

We used data from selected stations to examine and compare the diurnal variation of seasonal averages by LCZs. In this analysis LCZs 2, 3 and D were represented by one station. Similarly, from the LCZ 8 we used also one station (8-2) because the other station has large data gaps in autumn, winter and spring. From the zones where this was possible more than one station was selected in order to reveal the intra-zone differences which may occur in e variations. These stations were 5-2 and 5-4 from LCZ 5, 6-1, 6-3 and 6-9 from LCZ 6 as well as 9-2 and 9-4 from LCZ 9.

During the investigation of the temporal dynamics of the seasonal humidity patterns normalized time steps were applied in order to avoid the disturbing effect of different length of nights. It means that the time period from sunset to sunrise was divided into 12 parts and from sunrise to the next sunset also into 12 parts called them as ‘normalized hours’. The diurnal change of the seasonal e pattern was examined in 4-normalized-hour time steps: at sunrise, four and eight hours after sunrise as well as at sunset, four and eight hours after sunset, but only in summer as an example. The patterns were based on the above mentioned 22 stations’ data using Kriging interpolation method with 100 m resolution.

3. RESULTS AND DISCUSSION

3.1. Annual and diurnal variations of mean urban-rural humidity differences

In the first part of our study (Unger et al. 2018) we already mentioned three statements of Oke et al. (2017) about the common characteristics of the urban-rural moisture differences in cities with mid-latitude climates. To confirm their statement (iii) they cited an example from the results of Hage (1975) who evaluated a 13-year dataset of an urban-rural station pair in Edmonton (Canada) having continental climate with cold winters (Köppen type D, Kottek et al. 2006). Based on this example (see also their Fig. 9.4) they mentioned three features of

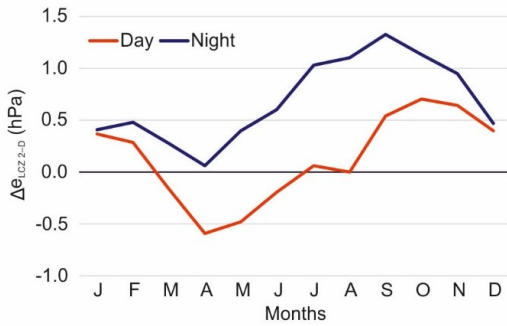


Fig. 2 Annual and diurnal variations of mean urban-rural (LCZ_{2-D}, 2-1 ↔ D-2) vapor pressure difference in Szeged (June 2014 – May 2017)

the annual and diurnal variations of urban-rural absolute humidity difference as typical ones for mid-latitude cities. We now compare these features with those of Szeged using data also from a station pair based on our three-year dataset: station 2-1 from the city center and station D-2 represents the urban and rural conditions, respectively (Fig. 2).

According to Oke et al. (2017) the “nocturnal absolute humidity difference is positive throughout the year with largest differences in August and the smallest in winter and

spring” is the first feature. The e variation at night in Szeged is consistent with this feature except for the time of the maximum difference (September instead of August) because of the longer warm season. The second feature is the following: “Annual course of daytime difference changes from a deficit (city drier) in the warmer part of the year, to excess in the colder part.” Similarly, in our case the city is drier between March and July, then the urban-rural daytime difference disappears and from September to February it changes its sign that is the rural areas are drier. The third feature, that is, “in winter there is a little diurnal change in the magnitude of the excess, but mid-summer there is a strong diurnal shift from a large daytime deficit to an equally large nocturnal excess” is also valid in Szeged with certain time deviations. Namely, the largest daytime deficit and the largest nocturnal excess occur in April and September, respectively.

So the general features of the annual and diurnal variations of urban-rural absolute humidity difference in cities with mid-latitude climates are also detectable in the case of Szeged.

3.2. Inter-zone comparison of mean annual and seasonal humidity conditions

Based on the three-year dataset we calculated annual and seasonal means, as well as means of maximum and minimum vapor pressure by LCZ classes. Table 1 contains these e means, the maximum differences between the zones (Δe_{max}) and information about the zones between which this maximum occurred.

As expected the largest e means occur in summer while the smallest ones in winter (Table 1). In the transitional seasons the values are between them with a bit higher e means in autumn followed the warmest period of the year. The largest mean difference (1.3 hPa) appears in the daily minimum vapor pressure in summer as a difference between urban (LCZ 3) and rural (LCZ D) areas while the smallest one (0.3 hPa) is in winter also between the e minimums.

There is no clear zone sequence neither in the seasonal nor in the annual means that would follow the differences in the compactness or building height of the zones and even the built-up versus land cover distinction. Furthermore, there is no detectable order of sequence between the zones that would be valid for all seasons.

Table 1 Annual and seasonal vapor pressure (e , hPa) means by LCZs in Szeged, Hungary (June 2014 – May 2017)

Means (2014–17)		LCZ class							Δe_{\max}	max LCZ _{X-Y}
		2	3	5	6	8	9	D		
Summer	e_s mean	17.9	17.5	17.8	18.1	17.8	18.1	17.2	0.9	6, 9 – D
	e_s mean max	20.2	19.8	20.1	20.7	20.1	21.0	20.4	1.2	6 – 3
	e_s mean min	15.7	15.2	15.5	15.6	15.5	15.3	14.4	1.3	3 – D
Autumn	e_a mean	12.1	11.3	11.7	11.9	12.2	11.8	11.6	0.9	8 – 3
	e_a mean max	13.9	13.0	13.6	13.9	14.1	13.9	13.8	1.1	8 – 3
	e_a mean min	10.5	9.9	10.1	10.1	10.6	9.8	9.7	0.9	2 – D
Winter	e_w mean	6.4	6.1	6.2	6.2	6.2	6.2	6.5	0.4	D – 3
	e_w mean max	7.3	6.9	7.1	7.2	7.1	7.1	7.5	0.6	D – 3
	e_w mean min	5.5	5.2	5.4	5.3	5.3	5.2	5.5	0.3	2, D – 3, 9
Spring	e_{sp} mean	10.3	10.0	10.3	10.4	10.3	10.3	10.2	0.4	6 – 3
	e_{sp} mean max	11.9	11.7	12.0	12.2	12.0	12.2	12.3	0.6	D – 3
	e_{sp} mean min	8.7	8.4	8.7	8.6	8.6	8.4	8.2	0.5	2, 5 – D
Annual	e_{an} mean	11.6	11.1	11.5	11.7	11.8	11.6	11.4	0.7	8 – 3

3.3. Inter- and intra-zone comparison of mean diurnal course of humidity by seasons

Figs. 3-5 present the seasonal daily variations of vapor pressure by LCZs based on normalized hourly means. In order to reveal any intra-LCZ deviations that may arise as a result of local circumstances we selected data from more than one station from the zones where this was possible (two, three and two stations from LCZ 5, 6 and 9, respectively).

In summer the highest mean values approach the 20 hPa and their range is 4.3 hPa (15.4–19.7 hPa) during the day (Fig. 3). As expected, summer has the highest values and the largest range among the seasons. The smallest values are at sunrise, but the upward trend in the first part of the daytime breaks at about 4 hours after sunrise showing an early morning peak in almost all zones. This peak is the diurnal one except of station 9-2. Then a local decline can be observed until sunset. Then a slight increase appears, forming a second maximum in most cases (e.g. 5-4, 6-9, 9-4). In the case of remaining stations the decline continues until sunrise (e.g. 2-1, 3-1, 5-2). Appearance of the two peaks is caused by the daily dynamics of the urban boundary layer (*UBL*). At morning the insolation rapidly increases the evaporation, later the near surface moisture is transported to the higher part of the *UBL* by convection. Near sunset when the *UBL* collapses due to the cessation of insolation this moisture of the higher part of the *UBL* descends near to the surface.

The stations in the suburb (9-2, 6-9) have the largest values during the whole 24-hour period while the smallest values can be found partly in the rural area (low plants, D-2) and partly, for surprise, in the housing estate (compact midrise, 5-2).

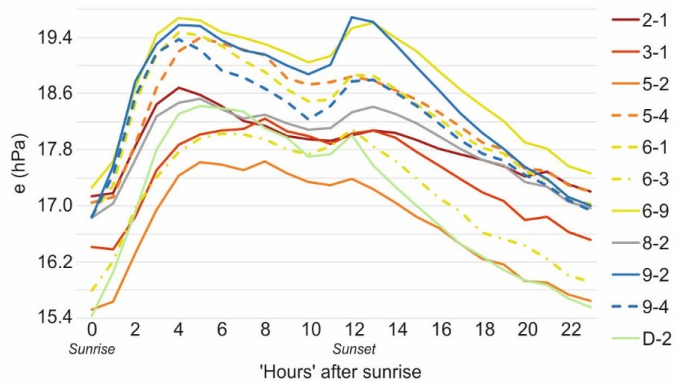


Fig. 3 Daily variations of normalized hourly mean vapor pressure (e) in summer by LCZs in Szeged, Hungary (June 2014 – May 2017)

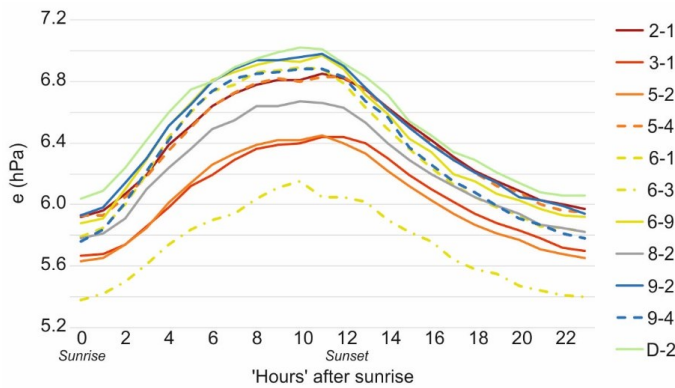


Fig. 4 Daily variations of normalized hourly mean vapor pressure (e) in winter by LCZs in Szeged, Hungary (June 2014 – May 2017)

Considering the intra-zone differences in LCZ 5 the hourly e means of station 5-2 are much lower (~ 2.5 hPa) during the whole day than the means of station 5-4. The reason of this deviation is the difference in the microscale environments, as station 5-2 is surrounded by mostly impervious surface,

while the immediate environment of station 5-4 is dominated by vegetation, particularly by trees.

In LCZ 6 stations 6-9 and 6-1 have almost equal values until 6 hours after sunrise, after that the maximal deviation between them is only 0.8 hPa. Station 6-3 has lower values than stations 6-9 and 6-1 with about 1.6 and 1.1 hPa in average, respectively. These differences are also caused by the vegetation nearby the stations since stations 6-1 and 6-9 are surrounded by more dense vegetation than station 6-3.

As far as LCZ 9 is concerned values of stations 9-2 and 9-4 are almost equal except in the period from sunrise+6 hours to sunset+4 hours with a maximum difference of 0.9 hPa at sunset. Station 9-4 is located near to dense vegetation and in its close proximity there is a partly swampy area (former river bed) thus the alteration of increased evaporation at this time causes the momentary higher values (Fig. 3).

In winter, compared to summer, the e values are much lower (they are smaller than 7.1 hPa) and the range is more narrow (1.6 hPa) (Fig. 4). The diurnal courses follow a fairly regular shape from a sunrise minimum to a sole peak between 10 hours after sunrise and sunset in all zones. It is remarkable that the two peaks of the daily cycle disappear. In this season the moistest zone is the rural one (D-2), this is followed by the outer zones (LCZs 9 and 6, except station 6-3) with the compact and open midrise zones (stations 3-1, 5-4). The extended and compact low-rise zones (stations 8-2, 3-1) have smaller values, then, as a real exception, the station 6-3 in the north-western part of the city follows with its extra small values distinctly separating from the others. The absence of the two peaks indicates that the daily development and collapse of the *UBL* is not as dynamic as in summer.

To examine the intra-zone differences two zones can be considered (LCZs 5 and 6) as in LCZ 9 there is minor deviation in the diurnal course between stations 9-2 and 9-4. In LCZs 5 and 6 larger differences appear, which are 0.3–0.4 hPa and 0.4–0.9 hPa, respectively. In this season values of stations 6-1 and 6-3 are almost equal all of the hours. The appearing alteration is attributable to the differences in the impervious/pervious surfaces and vegetation in the microscale environments. The small variation inside zones highlights that in winter the micro scale differences of water availability and transpiration sources are not as important factors as in summer. The basic reason of this phenomenon is the more humid conditions (due to the less energy for evaporation) in this season (Fig. 4).

In the transitional seasons the e values are a bit higher (1.5–2 hPa) in the autumn following the summer, as in the spring following the winter (Fig. 5). Their values are between 8.6 and 13.4 hPa with the almost equal ranges (2.8 hPa and 3.2 hPa in spring and autumn, respectively). The highest daytime values in autumn (in LCZs 6 and 9) have two peaks similar to the summer ones while the peaks in spring are less pronounced. The appearance of two peaks indicates that in the transition seasons the daily cycle of *UBL* is similar to the summer situation.

The intra-zone variations are more noticeable compared to winter, since in the transition seasons the increase (or decrease) of energy income of the surface will lead to increase (or decrease) the humidity difference in various micro environments, and, additionally the availability of evaporable water is not equal within the whole urban area (even within a zone).

In LCZ 5 the character of the difference between the two stations is similar to the summer one in both seasons but the deviation is smaller, it does not exceed 0.8 hPa and 1 hPa in spring and autumn, respectively (Fig. 5). In case of LCZ 6 the daily courses of stations 6-9 and 6-1 are more separated in spring, the maximum difference is of 0.5 hPa, while the values of station 6-3 are not much lower than the ones of station 6-1 with the difference ranging from 6-9 is 0.7–1.1 hPa. It can be assumed that the changing vegetation causes the different seasonal differences. Considering LCZ 9 there is minor deviation (< 0.1 hPa) in the diurnal course between stations 9-2 and 9-4 in autumn but in spring the deviation is a bit larger, mainly in the daylight hours (0.3–0.6 hPa) due to the more active vegetation life (Fig. 5).

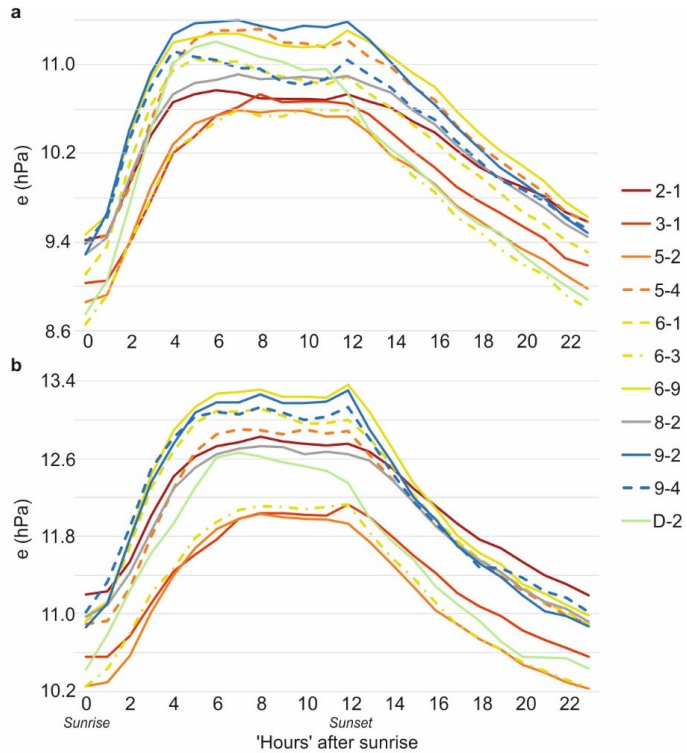


Fig. 5 Daily variations of normalized hourly mean vapor pressure (e) in spring (a) and in autumn (b) by LCZs in Szeged, Hungary (June 2014 – May 2017)

3.4. Mean diurnal variation of intra-urban humidity patterns in summer

According to the previous section the largest mean seasonal LCZ-difference in e appears in summer (4.3 hPa) which means that the most picturesque intra-urban deviations are expected in the summer urban patterns based on the dataset from 22 stations mentioned

in Section 2. Therefore, now we present the mean diurnal course of intra-urban humidity patterns only in summer as an example.

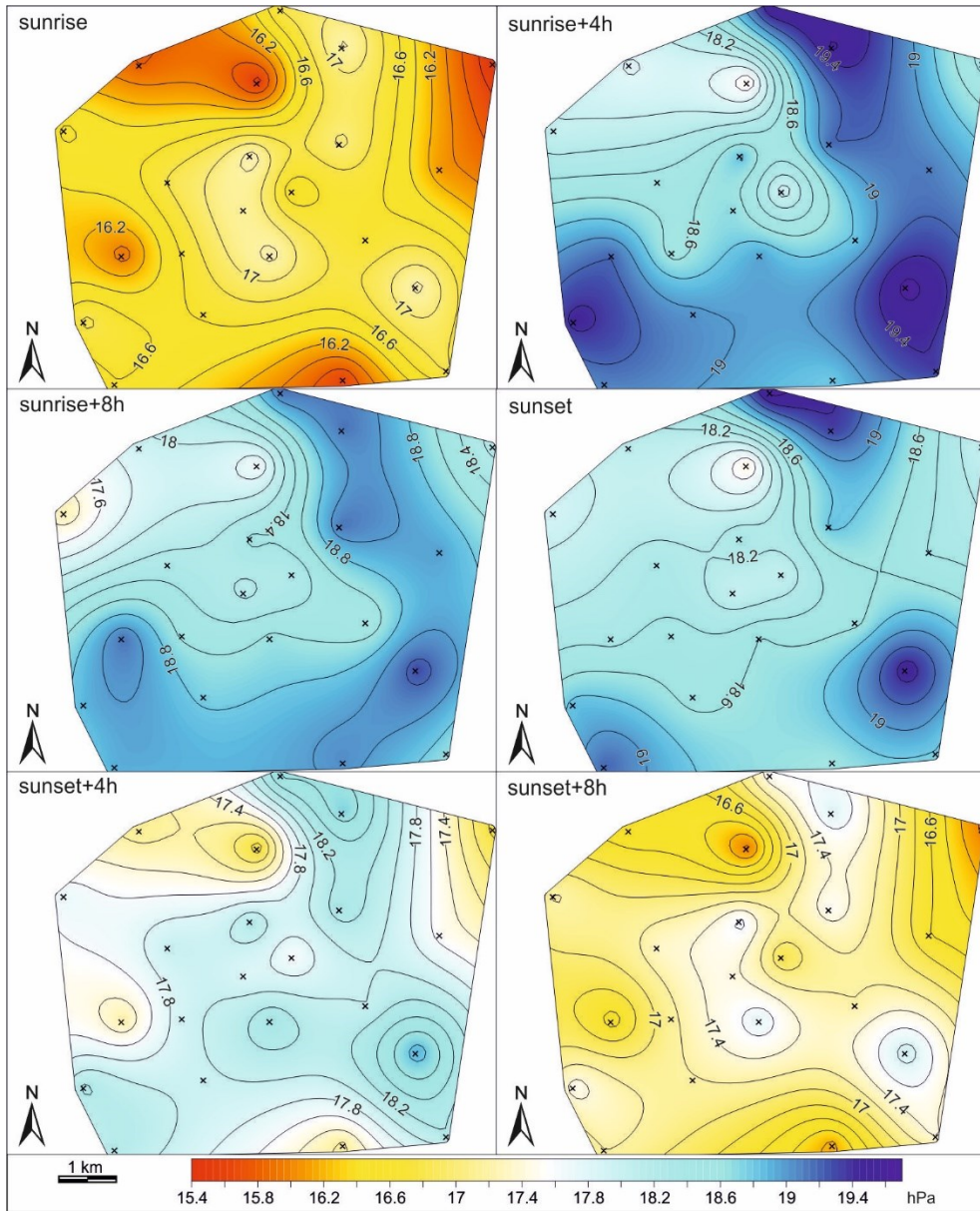


Fig. 6 Diurnal course of the mean summer patterns of vapor pressure in the urban area of Szeged, Hungary in normalized 4-hour time steps (June 2014 – May 2017)
(station sites are marked by crosses)

Fig. 6 shows this diurnal course in normalized 4-hour time steps from sunrise to 4 hours before the next sunrise. Generally, as in the mean summer case (see Fig. 2 in Unger et al. 2018), the distribution of *UCL* vapor pressure does not show a regular shape, the *e* pattern is mosaic-like: in all time steps the driest and wettest areas are in the north-western and south-eastern parts, respectively. That is, there are no detectable trace of the urban dry island phenomenon. This result confirms the statement of Unger et al. (2018), namely the urban dry island is a phenomenon that is mostly caused by the areal change of temperature dependent relative humidity.

As the dew formation on the gradually cooled surface during the night removed some of the moisture from the near-surface air the driest situation occurs at sunrise. At this time the lowest values (< 15.6 hPa) can be found in the north-western outskirts and north-eastern rural areas, while the highest ones (> 17.2 hPa) are in the city center as well as in the northern and south-eastern outskirts.

Then, due to the intensive evaporation from the wet surface supported by the rising sun, the moisture content of the air increased drastically until 4 normalized hours after sunrise to reach the highest values in the 24-hour period (18–19.6 hPa). The areas with highest humidity appear in the eastern and south-western outskirts while the inner and north-western areas are a bit drier.

Similar patterns can be observed after 8 hours and at sunset but with a bit lower air moisture content: the *e* values range between 17.4 and 19.2, as well as between 17.6 and 19.4 hPa, respectively.

After sunset, due to the increasingly cool surface, the moisture is partially extracted from the air resulting very similar patterns to the first one at sunrise, although their *e* values are not at the minimum: they ranges between 16.8 and 18.8 hPa, as well as between 16 and 17.8 hPa, respectively (Fig. 6).

4. CONCLUSIONS

In this study the seasonal and annual, as well as the diurnal absolute moisture contents were analyzed in the urban canopy layer of Szeged, Hungary. The analysis consisted of two approaches, namely urban-rural and intra-urban ones, the latter was partly based on the local climate zone surface classification system. The general features of the annual and diurnal variations of urban-rural absolute humidity difference in Szeged are consistent with the features of mid-latitude cities. The nocturnal absolute humidity difference is positive throughout the year while the diurnal course changes its sign. The largest daytime deficit and nocturnal excess occur in April and in September, respectively.

The largest *e* means occur in summer while the smallest ones in winter and in the transitional seasons the values are between them with a bit higher *e* means in autumn. There is no clear sequence in the annual and seasonal mean values of local climate zones that would follow the differences in the compactness or building height of the zones and even the built-up versus land cover distinction. The intra-zone differences can be larger than the inter-zones. Consequently, the effects of the microscale environment of the measurement sites are crucial. The permeability of the surface and vegetation cover of the immediate surrounding can cause the different values of the stations within the same zones. The higher impervious surface indicate lower, while natural surfaces, mostly the proximity of trees indicate higher values.

The mean diurnal course of intra-urban humidity patterns in summer shows mosaic-like ones. In all time steps the driest and wettest areas are mainly in the north-western and south-eastern parts, respectively. The driest situation occurs at sunrise and after that, due to the intensive evaporation from the wet surface supported by the rising sun, the moisture content of the air increases. The city core is drier from 4 hours after sunrise to 4 hours after sunset than the outskirts. After sunset, due to the cooling surface the *e* patterns are very similar to the first one at sunrise.

Acknowledgement: This study was supported by the Hungarian Scientific Research Fund (OTKA K-111768).

REFERENCES

- Hage KD (1975) Urban-rural humidity differences. *J Appl Meteorol* 14:1277-1283
- Kottek M, Grieser J, Beck C, Rudolf B, Rubel F (2006) World Map of the Köppen-Geiger climate classification updated. *Meteorol Z* 15:259-263
- Oke TR, Mills G, Christen A, Voogt JA (2017) *Urban Climates*. Cambridge University Press
- OMSZ (2015) Climate dataseries 1901–2010, Szeged. Hungarian Meteorological Service (OMSZ), Budapest (in Hungarian). http://met.hu/eghajlat/magyarorszag_eghajlata/eghajlati_adatsorok/
- Skarbit N, Stewart ID, Unger J, Gál T (2017) Employing an urban meteorological network to monitor air temperature conditions in the ‘local climate zones’ of Szeged (Hungary). *Int J Climatol* 37/S1:582-596
- Stewart ID, Oke TR (2012) Local Climate Zones for urban temperature studies. *B Am Meteorol Soc* 93:1879-1900
- Unger J, Gál T, Csépe Z, Lelovics E, Gulyás Á (2015) Development, data processing and preliminary results of an urban human comfort monitoring and information system. *Időjárás* 119:337-354
- Unger J, Skarbit N, Gál T (2018) Absolute moisture content in mid-latitude urban canopy layer, Part 1: a literature review. *Acta Climatol* 51-52:37-45
- URBAN-PATH Project (2018) Evaluations and Public Display of Urban Patterns of Human Thermal Conditions. <http://urban-path.hu/>. Last accessed: 20 November 2018
- Vaisala (2013) Humidity conversion formulas. Calculation formulas for humidity. https://www.vaisala.com/sites/default/files/documents/Humidity_Conversion_Formulas_B210973EN-F.pdf. Last accessed: 12 December 2018

EVALUATION OF A WRF-LCZ SYSTEM IN SIMULATING URBAN EFFECTS UNDER NON-IDEAL SYNOPTIC PATTERNS

G MOLNÁR, T GÁL and AZ GYÖNGYÖSI

*Department of Climatology and Landscape Ecology, University of Szeged, Egyetem u. 2., 6720 Szeged, Hungary,
E-mail: molnarge@geo.u-szeged.hu*

Summary: The modelling of meteorological variables under non-ideal (e.g. characterized by cyclonal activity) synoptic patterns is always challenging. It is particularly true, when the simulations are performed on local or neighborhood scale. In this study, the spatio-temporal distribution of urban heat island of Szeged was predicted by the Weather Research and Forecasting (WRF) model during two period with different meteorological background. During the first, a thick and permanent fog layer was located over the Carpathian Basin. The second one was dominated by a Mediterranean low that has caused high sums of precipitation. The comparison of modelled and observed variables suggested that the computed outputs showed robust consistency with the observations during the rainfall event. On the foggy days, however, WRF had difficulties to capture the daily variability of urban heat island intensity. It was due to the large underestimations of moisture circumstances.

Keywords: urban heat island, Weather Research and Forecasting model, numerical modelling, local climate zones, modified static canopy parameters

1. INTRODUCTION

Urban dwellers have been experiencing an increasing amount of thermal load in expanding urbanized areas. The influence of specific surface geometry on energy budget results in major distinctions on local climate related to less-developed surroundings. One of the well-known manifestation of this phenomenon is the urban heat island (UHI), a temperature increment measured over areas with high rate of built-up. UHI has negative effects, for example, on economy (e.g. elevated energy consumption due to air conditioning in summer) (Vardoulakis et al. 2013), health care (e.g. elevated cardiovascular morbidity and mortality) (Tan et al. 2010), and air quality (e.g. elevated tropospheric ozone production) (Fallmann et al. 2016). The projected tendencies of climate change triggers positively the modification of climatic parameters on urban scale, which draws even more attention to comprehensive monitoring of local environmental issues.

In cities with temperate climate, UHI is particularly strong in the summertime nights under anticyclonic conditions. In case of high cloud fraction or precipitation, UHI becomes less pronounced or completely missing (Morris et al. 2001). At this time, thick clouds attenuate the incoming solar radiation and decrease the net solar energy at the surface. Less solar energy can store in urban fabrics, so that less energy is emitted in the night-time, which mitigates the temperature contrast between areas with different built-up ratio. The fog belongs to a special group of low-level clouds. This phenomenon develops directly over the surface and attenuates not only the shortwave part of radiation but also reflects the outgoing longwave radiation. If the fog layer is thick enough, the top of the fog behaves like an active

surface in terms of radiation. During fog events, the latent heat flux of surface energy budget dominates over the sensible flux and heat storage terms, and so UHI will be negligible.

The elevated number of cloud condensation nuclei from anthropogenic activities leads to higher probability of cloud (and fog) formation and precipitation in urban areas (Oke 1987, Bokwa et al. 2018). The typical annual days of fog in Szeged is around 50-55, which is the consequence of the geographic location and the relatively high frequency of high-pressure synoptic patterns in autumn and winter months. Due to the projected effects of climate change, the frequency of high precipitation events will likely be increased in the forthcoming decades (Kis et al. 2017) over the Carpathian Basin. Furthermore, Péliné Németh et al. (2016) suggested that wind speed is projected to be decreased in autumn and winter months, which also triggers the physical mechanisms lead to fog formation.

The Weather Research and Forecasting (WRF; Skamarock 2008) is a non-hydrostatic, mesoscale numerical meteorological model that has been designed for both research and weather prediction purposes. In order to represent the physical processes at city scale, three urban schemes (Single Layer Urban Canopy Model (SLUCM) of Kusaka et al., 2001, Kusaka and Kimura 2004, Building Effect Parameterization (BEP) of Martilli et al. 2002, Building Energy Model (BEM) of Salamanca et al. 2010) are available for the simulations. The urban schemes have been coupled with the Noah land surface scheme (Tewari et al. 2004) through the land cover fraction parameter that partitions the grids to urban and non-urban parts. For non-urban parts, Noah calculates, for example, the heat fluxes and then adds them to the urban scheme where the urban fluxes have already been determined. The sum of the two sub-fluxes gives the final value of the fluxes.

WRF has many options to take boundary layer processes and microphysics into account. One of the most important challenge in fog and precipitation predictions is to find the optimal combination of physical schemes (Tudor 2010). Beside the appropriate representation of physical processes, the selection of initial and boundary conditions is also crucial (Bergot et al. 2005). Several studies (e.g. Rémy and Bergot 2010, Gao et al. 2018) have successfully applied data assimilation techniques to enhance their fog forecast scores instead of using initial data from global models. It was also highlighted that the assimilation of near-surface temperature and specific humidity has the greatest influence on the simulations. Steeneveld et al. (2015) highlighted that the grid configurations also impact the quality of fog analysis and forecast. Most of the studies employed a horizontal resolution of 5 km and below for the finest domain.

Up to now, we only have experiences on the behavior of WRF in urban scale under calm weather conditions. Our earlier analyses have indicated that the coupled WRF-SLUCM with an adjusted urban parameter-set has been able predict most of the features of UHI. However, it is important to test our model under various synoptic patterns to be convinced of the strengths and shortcomings of the physical setting and static database. For this reason, in this study we intended to investigate the spatio-temporal variation of UHI during a foggy and rainy period. The simulated UHI was compared to the observations of a local urban climate monitoring system (Lelovics et al. 2014). This monitoring system consist 24 stations in Szeged representing different local climate zones (LCZs, Stewart and Oke 2012) in the city (Fig. 1).

2. STUDY AREA

Szeged (46.25°N; 20.15°E) is located in the middle of Great Hungarian Plain, at 79 m a.s.l. The city with an administration area of 280 km² is spread on both banks of the River Tisza (Fig. 1). Szeged has a population of 162,000 that makes it the third most populated city of Hungary. The annual mean temperature and precipitation is around 10–12°C and 500–600 mm. During the year, Szeged is influenced by both oceanic and continental climate with different rates, but in general the latter is slightly dominant due to the Köppen–Geiger's climate classification Cfb (warm temperate climate, no dry season, warm summer) (Kottek et al. 2006).

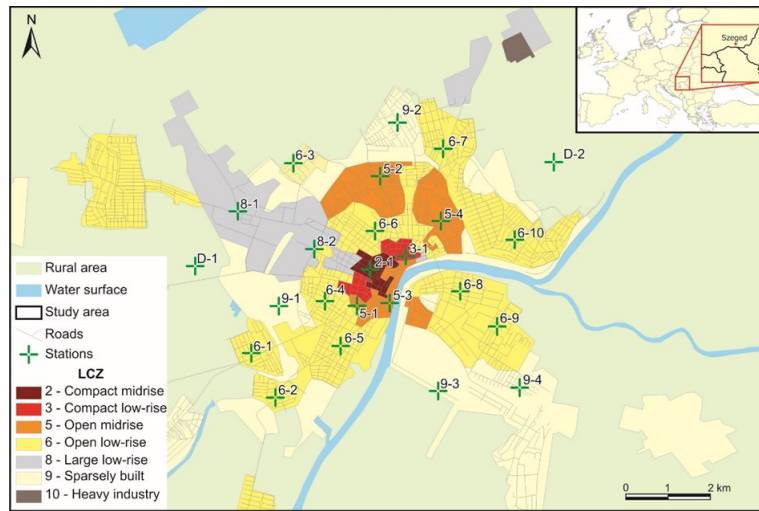


Fig. 1 Spatial distribution of local climate zones over the study area (crosses mark the sites of urban climate monitoring system)

The urbanized area consists of a well-developed and highly built-up city centre with commercials, educational and administrative buildings. In the inner residential belt, apartment houses and block of flats (mostly to the northwest) are found. On the right side of River Tisza, the residential area includes gardening houses with a larger amount green spaces. At the outermost parts with scattered cottages and logistics, the urban landscape is shifted gradually by the surrounding agricultural areas.

3. BRIEF DESCRIPTION OF MODIFIED STATIC DATABASE

The accurate representation of sophisticated urban geometry is essential in quantifying the physical processes within any urban area. Since each city is unique by its specific geographical, economical, and demographical features, it is required to create such static database that fits particularly well for the area of interest. To do so, several of the urban parameters (UCP) of SLUCM and BEP (Table 1) were tailored for Szeged by using three-dimensional building database and remote sensing data. For taking the climate-modifying effect of surface built-up elements on local (i.e. few hundred meters to kilometer) scale into

account, a local climate zone-based land-use categorization was incorporated to WRF. By default, the model employs only three urban land-use categories, which largely simplifies the diversity of buildings. In contrast with the default case, LCZ classification allows ten urban classes to derive a more realistic land-use data. The classes are based on the height and compactness of buildings. Additionally, the LCZ system also includes further seven non-urban categories (e.g. dense trees, bare soil, water) that describes the natural coverage of surface.

Table 1 The modified SLUCM parameters according to the LCZ system

UCP/LCZ name and designation	LCZ 2 Compact midrise	LCZ 3 Compact low-rise	LCZ 5 Open midrise	LCZ 6 Open low-rise	LCZ 8 Large low-rise	LCZ 9 Sparsely built
Urban fraction	0.90	0.82	0.58	0.66	0.75	0.25
Vegetation fraction	0.10	0.18	0.42	0.34	0.25	0.75
Building height [m]	13.6	7.9	15.4	5.4	6.6	5.0
Road and roof width [m]	5.1	4.3	5.3	3.2	5.5	2.9
Surface albedo of road, roof, walls	0.15	0.14	0.12	0.16	0.16	0.17
Thermal conductivity of road [Jm ⁻¹ s ⁻¹ K ⁻¹]	0.70	0.70	0.70	0.70	0.70	0.70
Thermal conductivity of roof [Jm ⁻¹ s ⁻¹ K ⁻¹]	1.04	1.01	1.20	1.01	1.24	1.01
Thermal conductivity of walls [Jm ⁻¹ s ⁻¹ K ⁻¹]	1.02	1.01	1.10	1.02	1.20	1.01
Heat capacity of road [Jm ⁻³ K ⁻¹]	1.95·10 ⁶	1.98·10 ⁶	1.95·10 ⁶	1.98·10 ⁶	1.94·10 ⁶	1.98·10 ⁶
Heat capacity of roof [Jm ⁻³ K ⁻¹]	1.97·10 ⁶	1.97·10 ⁶	1.97·10 ⁶	1.97·10 ⁶	1.97·10 ⁶	1.97·10 ⁶
Heat capacity of walls [Jm ⁻³ K ⁻¹]	1.63·10 ⁶	1.62·10 ⁶	1.72·10 ⁶	1.62·10 ⁶	1.86·10 ⁶	1.61·10 ⁶
Emissivity of road	0.93	0.93	0.93	0.93	0.93	0.93
Emissivity of roof	0.91	0.92	0.87	0.92	0.86	0.92
Emissivity of walls	0.92	0.93	0.90	0.93	0.87	0.93

There is an option in the model in which particular thermodynamic parameters (e.g. albedo, emissivity, heat conductivity) can be assigned to the predefined land-use types. During the compilation of such data, there is a lot of impediments to be resolved. For instance, it is necessary to have detailed information of road, wall, and roof materials. Another important feature is the age and condition (e.g. leaf litter and moss coverage, wetness) of these materials that can be determined with difficulty or neglected in most cases. In this study, we made an attempt to construct the dataset of most relevant thermodynamic-related SLUCM parameters for each LCZ. In the first step, it was assumed that the dominant built-up materials are concrete and asphalt for roads and pavements, brick for walls, and ceramic (representing tiles) and concrete for roofs. Then such small areas were allocated that are representative for the given LCZ. By knowing the relative occurrence of the materials in the LCZs, the final value of a thermodynamic parameter (e.g. heat capacity) can be calculated as follows:

$$C_{LCZ_x} = C_{asphalt} \cdot M_{asphalt} + C_{brick} \cdot M_{brick} + C_{ceramic} \cdot M_{ceramic} + C_{concrete} \cdot M_{concrete}$$

where C_{LCZ_x} is the heat capacity of wall, road, or roof in a given LCZ in $J\ m^{-3}K^{-1}$ (x stands for building facets, i.e. wall, road, or roof), $C_{asphalt}$, C_{brick} , $C_{concrete}$, $C_{ceramic}$ is the standard heat capacity of asphalt, brick, concrete, and tile, respectively, in $J\ m^{-3}K^{-1}$, $M_{asphalt}$, M_{brick} , $M_{concrete}$, $M_{ceramic}$ is the relative fraction of asphalt, brick, concrete, and ceramic (tile) coverage. The standard values of the built-up materials are based on the physical look-up table of Wang and Kuo (2001). Overall, 14 SLUCM parameters (Table 1) were modified in each LCZ and applied to the simulations.

3. MODEL CONFIGURATION

The model integrations were performed with WRF model version 3.8.1. Three one-way nested domains were employed (Fig. 2.), with a horizontal resolution of 13.5 km for D01 (80×75 grids), 4.5 km for D02 (121×94), and 1.5 km for D03 (106×79).

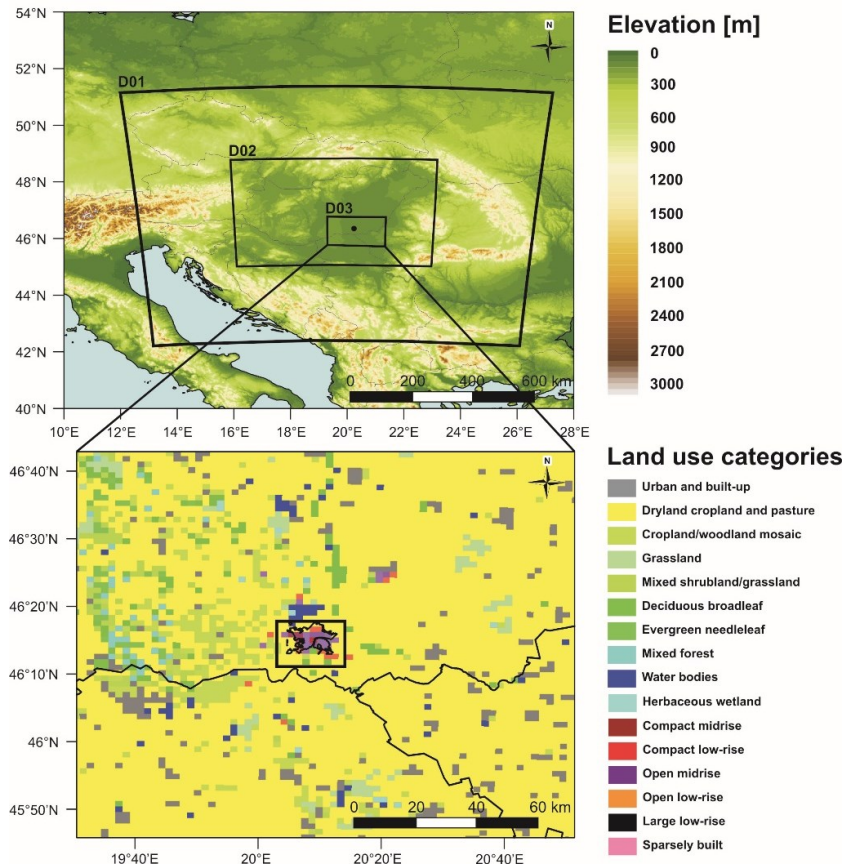


Fig. 2 Adopted domain configuration (the bottom map contains the LCZ classification for D03)

44 sigma vertical levels were prescribed, with higher density below 2 km for accounting even more precisely the turbulent and microphysical processes within the urban boundary layer. Centers for Environmental Prediction (NCEP) Global Forecast System (GFS) $0.25^\circ \times 0.25^\circ$ database provided the initial and boundary conditions, with a 3-h temporal resolution. Each simulation started at 00 UTC, one day before the period of interest, so that the first 24 hours was considered as spin-up time. In order to quantify the influence of urban geometry on local meteorological mechanisms, we have switched on the urban scheme of SLUCM. Further on, Noah land surface (sub)model (Tewari et al. 2004) was responsible for describing the surface-atmosphere interactions, RRTMG scheme (Iacono et al. 2008) for long- and shortwave radiation, revised MM5 scheme (Jiménez et al. 2012) for surface layer processes, BouLac scheme (Bougeault and Lacarrere 1989) for boundary layer processes, WSM-5 class scheme (Hong et al. 2004) for microphysics, and Kain-Fritsch scheme (Kain 2004) for cumulus convection. The Kain-Fritsch scheme was not considered for the innermost domain, since the model is able to explicitly simulate the cumulus convection at this mesh size.

The investigation concentrated on those periods when the background synoptic pattern had remarkable forcing on urban effects. During the first period, an extended anticyclone were located over Eastern Europe and Hungary, with typical mean pressures around 1035 hPa. As a result of adequate moist content in the bottom troposphere and weak synoptic winds, thick fog layer formed over the Carpathian Basin and lasted many days of which two days (21 and 22 December, 2016) has been selected for the analysis. Our second case is quite different from the previous one: a strong Mediterranean low has swept across Hungary from southwest, causing remarkable precipitation sums and high wind speeds. The peak of the cyclone activity fell between 22 and 23 October, 2017, so the influence of precipitation on UHI was examined on these days.

Table 2 Geographical information about the stations that are used for the evaluation

N°	LCZ	Station ID	Latitude	Longitude	Elevation [m a.s.l.]
1.	LCZ 2	2-1	46.2549°N	20.1611°E	82
2.	LCZ 5	5-1	46.2643°N	20.1402°E	80
3.	LCZ 5	5-2	46.2749°N	20.1646°E	79
4.	LCZ 5	5-4	46.2818°N	20.1832°E	80
5.	LCZ 6	6-4	46.2650°N	20.1470°E	80
6.	LCZ 6	6-5	46.2386°N	20.1350°E	81
7.	LCZ 6	6-8	46.2666°N	20.1722°E	78
8.	LCZ 6	6-9	46.2590°N	20.1834°E	78
9.	LCZ 6	6-10	46.2775°N	20.1892°E	79
10.	LCZ 9	9-2	46.2863°N	20.1535°E	79
11.	LCZ 9	9-4	46.2458°N	20.1901°E	79
12.	LCZ D	D-1	46.2562°N	20.0903°E	80

The simulated near-surface air temperature (T_{nWRF}) and relative humidity (for the fog case) was verified against the observations of urban climate monitoring system. From the modelled variables, we considered only those that are closest to the given monitoring site and characterized by same land-use category (i.e. they are in same LCZ). For example, station D-1 was chosen to represent the rural measurements. The corresponding rural pair in the simulations is the value in the nearest grid to station D-1. By following this assumption, the mean UHI intensity in a given LCZ can be calculated as

$$\Delta T_{LCZ_x} = \sum_{i=1}^m \frac{1}{m} (T_{n_i} - T_{n_{LCZ D}})$$

where ΔT_{LCZ_x} is the modelled or observed UHI intensity in a given LCZ, T_n is the modelled or observed near-surface temperature in a given LCZ, $T_{n_{LCZ D}}$ is the modelled or observed rural near-surface temperature, m is the number of stations in a given LCZ. Precipitation measurements occur solely at station D-1, therefore the verification of precipitation sums was performed only for the rural site. Towards an efficient and comprehensive comparison, the sampling frequency of outputs was set to 10 minutes. Some of the stations indicated missing values during one of the periods, thus they were omitted from the analysis. The fundamental metadata of the remaining stations are summarized in Table 2.

4. RESULTS AND DISCUSSION

4.1. “Fog case”

4.2.1. Evaluation of near-surface temperature

As it can be seen in Fig. 3, the observed near-surface air temperature (T_{nOBS}) remains below the freezing point in all LCZs during the entire simulation period. An additional common feature was the almost uniform ranges of T_{nOBS} between -0.5°C and -2.5°C , with the highest peaks after 12 UTC on 22 December. In rural LCZ D, however, the mean T_{nOBS} was $1\text{--}1.5^{\circ}\text{C}$ lower than in urban ones. Higher temperatures within the city could be the consequence of such anthropogenic activities as transportation or heating of buildings. Due to the thick fog layer and lack of insolation, the diverse urban geometry has low impact on local meteorology, therefore only a slight inter-LCZ variability exists. If we consider T_{nOBS} on the two days, it is clearly seen that the daytime warming stage was utterly disappeared. Usually, the fog intensifies with inconstant speed and depends on the availability of moist supply. The measured time-series of T_n suggest that the increase of fog thickness could be permanent and conserves T_{nOBS} at a given level. In order to confirm this, the evolution of moist-related variables (e.g. relative humidity) should also be taken into consideration.

The modelled near-surface temperature (T_{nWRF}) that varies between -4°C and 4°C shows quite different patterns from the observations in each LCZ. On average, T_{nWRF} overestimates T_{nOBS} , especially during the day (Fig. 3). The daytime positive biases peaks around 12 UTC, with a magnitude of $5\text{--}6^{\circ}\text{C}$ and minor distinctions between the first and second day. T_{nWRF} at night can be typified with 2 stages. The first stage covers the first 5-6 hours when the warm biases decrease in each LCZ, and what is more in LCZ 5 and LCZ 9 the overestimation shifts to a slight underestimations of about 0.5°C . By comparing the static SLUCM parameters and T_{nWRF} in different LCZs, it is revealed that the cooling rate is proportional to the built-up rates of LCZs. In LCZ 2 with a mean urban fraction of 90%, the maximum of T_{nWRF} is about 3°C higher than in LCZ 9 with a mean urban fraction of 25%. During the second stage, covers the remaining night-time hours of the simulation period, the overestimations are even more obvious, although the aforementioned cooling potential is less significant. Then, the discrepancies in urban fractions are not a major factor in governing the nocturnal T_{nWRF} as earlier. Consequently, the daily temperature ranges on the second day are much (around 4°C) lower. A potential explanation for this may be that the emission of

longwave radiation is lower as a result of higher air moisture content and higher low-level cloud coverage. This also emphasizes that the overview of wetness conditions is crucial in this case.

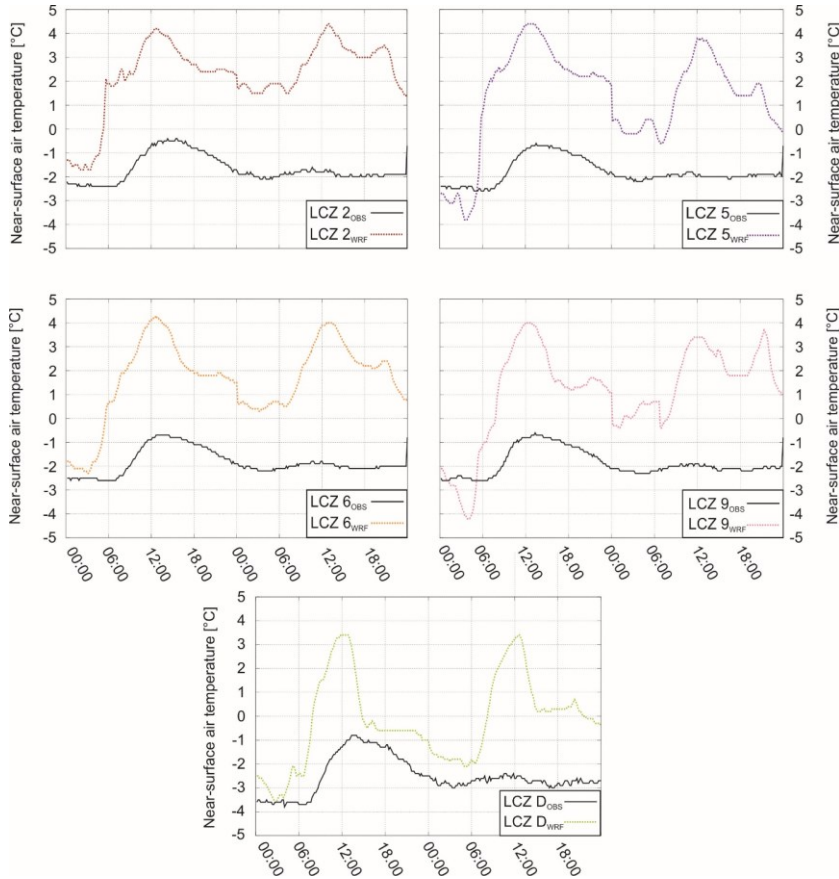


Fig. 3 Temporal variation of observed and modelled near-surface air temperature in each LCZ

4.1.2. Evaluation of UHI

The observed urban heat island intensity (ΔT_{OBS}) ranges within a narrow threshold between 0°C and 1°C (Fig. 4), which means tiny fluctuations either in space and time. A small decrease of 0.5°C, however, occurs on the second day because of the decreasing of T_{nOBS} around noon. Contrarily, the modelled intensity (ΔT_{WRF}) shows much higher spatio-temporal variability, with a range between -1°C and 4°C. Overall, ΔT_{OBS} is over-predicted, particularly in the night-time, with even 3–4°C. The largest uncertainties arise in LCZs 2 and 5 at 06 UTC, when the increasing of T_{n} is simulated to be faster in urban grids related to the rural counterpart. The positive biases in LCZs 5 and 9, however, decrease at this time due to the underestimation of T_{nWRF} .

In the daytime, particularly from 10 to 14 UTC, ΔT_{WRF} shows relatively good agreement with observations (Fig. 4). On the second day, however, slight underestimations

of daytime ΔT_{OBS} evolves in each LCZ. Beside the similarities, there are several differences that must be pointed out. In LCZs 2 and 6, for example, the strong UHI that predicted from 15 to 08 UTC stays at a constant level of 2.5–3.5°C. On the other hand, UHI in LCZ 5 has higher variability with a weak decrease after 01 UTC. When UHI is modelled to be positive, the mean magnitude is the lowest in LCZ 9, which is the result of low impervious and high pervious surface coverage.

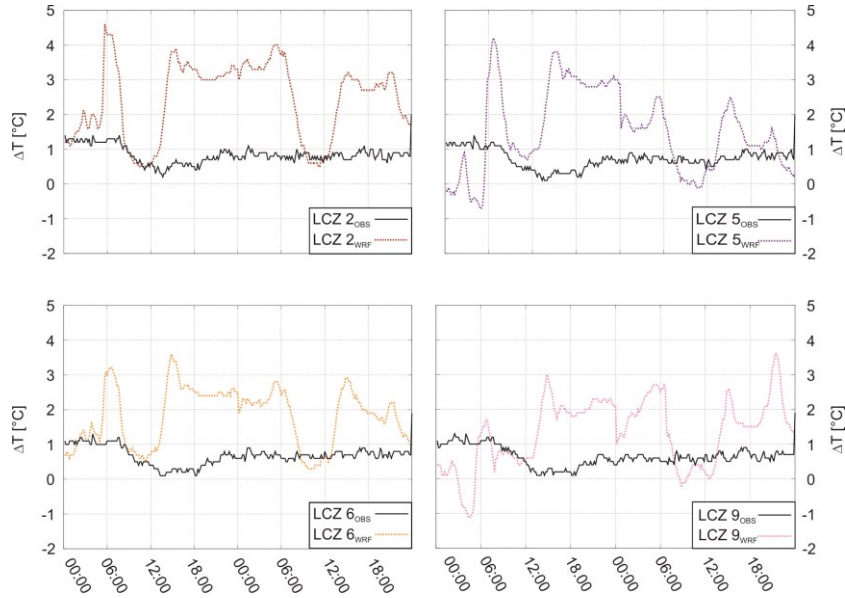


Fig. 4 Temporal variation of observed and modelled urban heat island intensity (ΔT) in each LCZ

Fig. 5 illustrates the spatial distribution of ΔT_{WRF} over the study area. As it is expected, ΔT_{WRF} at 12 UTC is around 0–1°C on both days, with minimal areal differences. Robust heat island, with more pronounced spatial variability, is simulated at 04 UTC (representing UHI before sunrise). On the first day of the period, the negative ΔT_{WRF} is limited to the northern and south-western periphery of Szeged, with values around 2.5°C. On the following day, at the same date, ΔT_{WRF} expands to the entire city. The hottest spots are located over the downtown (LCZs 2 and 5) and the northern parts with LCZ 6. The spatial distribution at 20 UTC (representing UHI after sunset) occurs analogously, with intensities over 2.5°C. When the two dates are compared, it can be seen that ΔT_{WRF} seems to be larger on 21 December. LCZs in the middle and the north-western parts that can be considered as a transition zone from urban to rural landscape are characterized by ΔT_{WRF} of 2°C and below. In parallel, the values are mostly under 0°C in the adjacent rural areas, showing a cooling to the previous day. Indeed, the nocturnal T_{nWRF} in LCZ D increases less compared to the urban LCZs, therefore the near-surface air layers in other rural grids can also cool below the mean of urban values. This contrast in cooling potential can lead to the relative difference in ΔT_{WRF} between the days at 20 UTC.

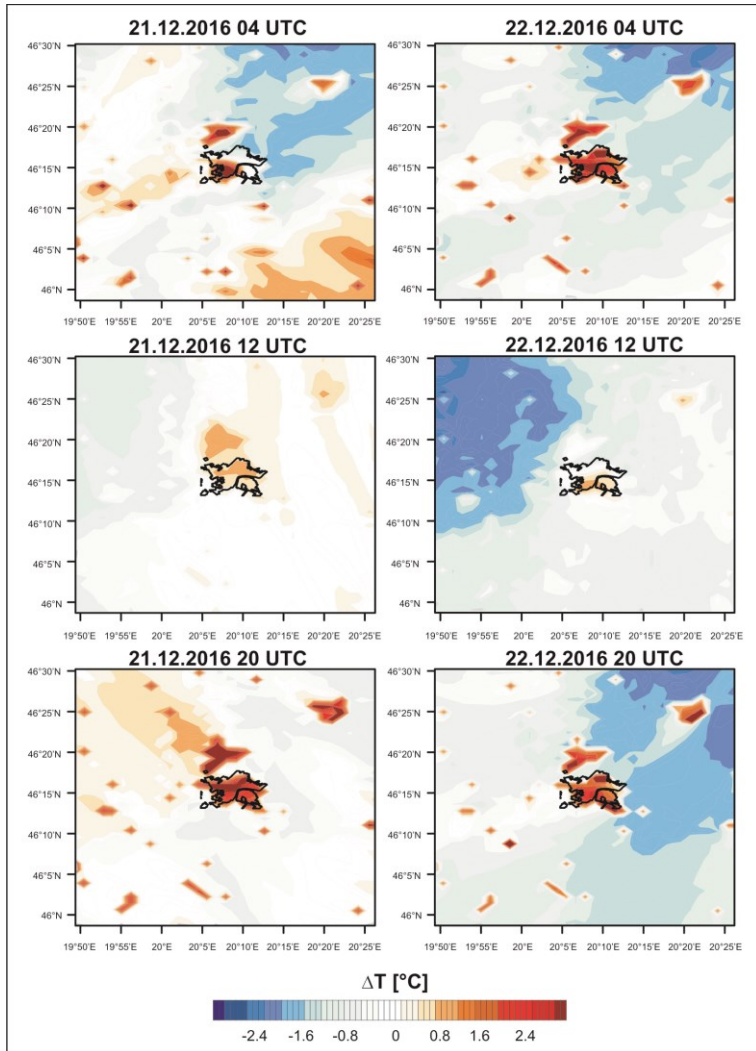


Fig. 5 Spatial distribution of modelled urban heat island intensity (ΔT) over the Szeged and the surroundings on six distinct dates

4.1.3. Evaluation of relative humidity and the analysis of net shortwave radiation flux

The presence of fog and mist in WRF simulations is further analysed on the temporal variability of relative humidity and net surface shortwave radiation flux (Fig. 6). Modelled shortwave flux has substantial daily variation with peaks around 300 Wm^{-2} at local noon (11 UTC). This flux is similar to the climatic mean value of December, referring to low amount of cloudiness. In LCZ D, the flux is about 25 Wm^{-2} lower than in the grid of station 5-1. It is may be the consequence of less transparent air column for solar radiation, due to higher absolute moisture content.

One of the major criterion for fog is that the relative humidity must be over 80%. By following this definition, the observations imply fog formation around the rural measurement site during the whole simulation period. The same is valid for station 5-1, however, the fog layer is likely to be broken up in the middle of the first day. The time-series of modelled relative humidity in each LCZ does not show reasonable agreement with the observations. The uncertainties as high value as 30–35% in the daytime. During the other stages of the era, the predicted relative humidity also remains under the observed standards. In the rural LCZ, the relative humidity was computed to be higher by 10%. At nights, the differences grows further, particularly from 15 to 10 UTC. Considering the criterion above, fog is predicted only for a small fraction of the simulation time, and exclusively for the rural grids.

The under-representation of moist content can be the reason why the model captures most of the features of T_n (and so ΔT) with relatively high biases. The well-balanced course of T_{nOBS} time-series are affected largely by the fog. Due to negligible solar radiation, the surface-induced thermal differences cannot be evolved. In the simulations, controversially, the overestimated insolation is able to store in urban fabrics in the daytime and being re-emitted to the overlying atmosphere in the night-time, creating significant daily variations of temperature.

Without proper representation of fog in initial and boundary conditions, the reconstruction of UHI under such synoptic patterns is quite challenging. A possible solution can be is the application of multiple models for initial conditions to find the most suitable option for the corresponding modelling purpose. For our case (and in many others), the assimilation of local measurement could give the “best guess” to derive the initial meteorological field.

4.2. “Precipitation case”

4.2.1. Evaluation of near-surface temperature

During the days with remarkable precipitation, T_{nOBS} fluctuates between 10°C and 18°C (Fig. 7). At the early stage of the first day, when the cyclone does not modify the progress of urban effect, a regular daily pattern of T_{nOBS} develops, with minima (maxima) around 06 UTC (14 UTC). On the second day, however, a gradual cooling occurred due to lack of insolation, moderate rainfall, and cold advection. WRF captures well the transition of T_{nOBS} between the days with distinct meteorological background. Focusing on the first day,

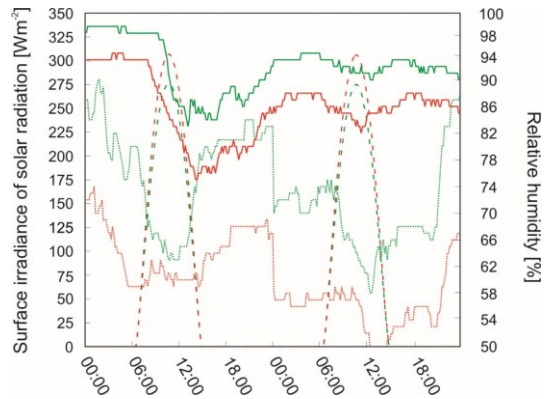


Fig. 6 Temporal variability of observed (solid lines) and modelled (dotted lines) relative humidity in LCZ D (green) and station 5-1 (red). The dashed lines represent the temporal variability of surface irradiance of solar radiation in LCZ D (green) and station 5-1 (red)

the minimum of T_{nWRF} is simulated properly in LCZs 2 and 5 but with different signals elsewhere: as against to the cold biases in LCZ D, warm biases evolves in LCZs 6 and 9. The daytime values are consistently overestimated by 1°C to 2°C in each LCZ. In many aspects, T_{nWRF} indicates a better agreement with the observations on the second day, with absolute biases under 1°C. From 18 UTC, a slight warming appears in all LCZs, which is not underpinned by the observations and can be linked to the misinterpretation of rainfall length.

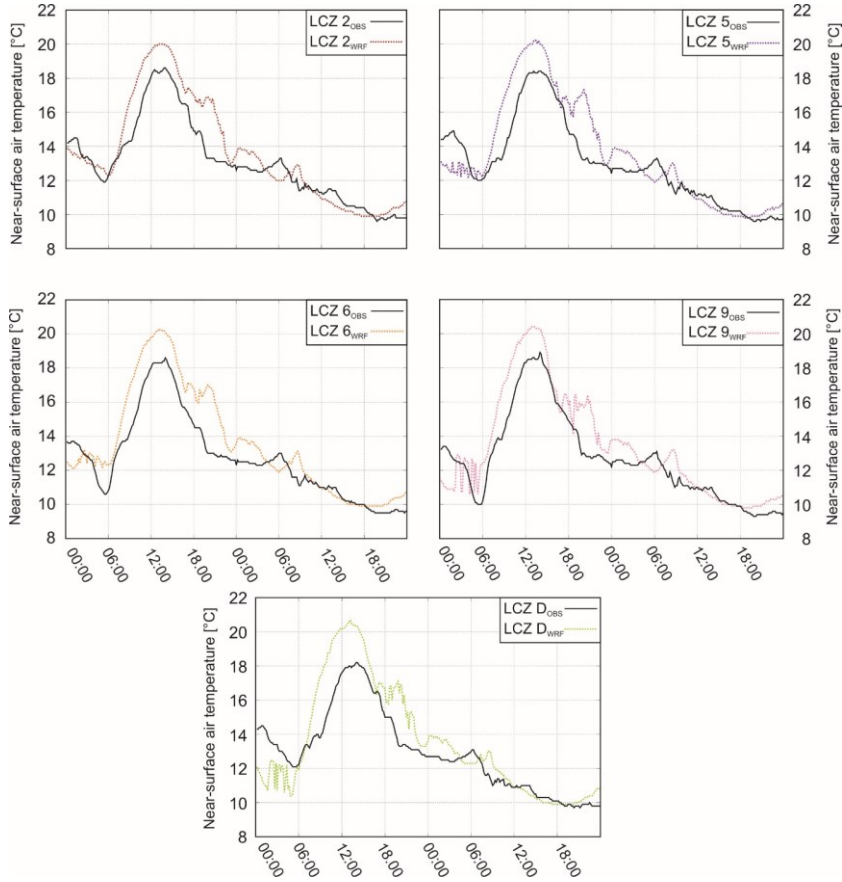


Fig. 7 Temporal variation of observed and modelled near-surface air temperature in each LCZ

Fig. 8 confirms that the weather conditions were not favoured for the development of urban heat island; ΔT_{OBS} scatters between -1°C and 1°C and becomes invariant as the precipitation event begins. The largest uncertainties of ΔT_{WRF} arises at the first hours of the simulation, when the rain has not started to fall. After sunset of 22 October, there are overestimations of 2–3°C, particularly in LCZs 6 and 9. The negative biases, predicted in the middle of the day, are considerably in those LCZs where ΔT is observed to be higher during this period. As it is discussed earlier, this general under-prediction stems from lower modelled cloud coverage (higher modelled incoming solar radiation) and so higher T_{nWRF} .

In Fig. 9 the thermal differences of ΔT_{WRF} over urban and non-urban parts of the study area are illustrated. The shifting in the synoptic situation and its influence on the shape of

urban heat island is captured well by WRF. In the dawn of the first day (04 UTC), a well-pronounced UHI is simulated, with intensities around 2°C. As it is expected, no considerable difference in ΔT_{WRF} is depicted during the day. After sunset, the urban effect amplifies again, but with less magnitude due to the arrival of cyclonic system. As the time goes by, ΔT_{WRF} increases to 0°C and UHI is entirely blurred. In other words, the inhomogeneity of surface geometry has slightly visible and sensible impact on the distribution of local meteorological variables. Without insolation, the single income term of energy budget is the anthropogenic heat. In autumn, the most common form of heat release from human activity is the heating of buildings. Under such weather conditions, the urban boundary layer is well-mixed, so this additional energy surplus cannot be cumulated over areas with higher built-up and does not increase of urban-rural thermal contrast.

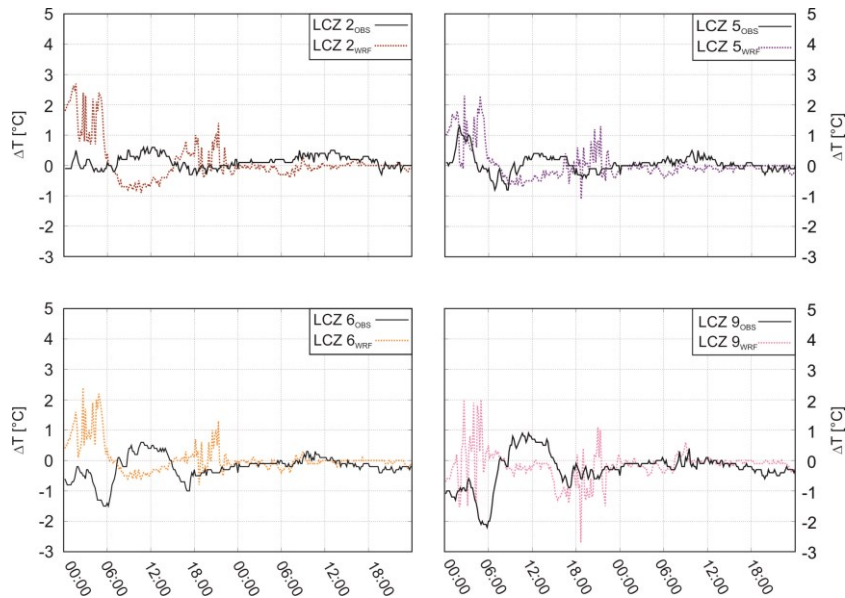


Fig. 8 Temporal variation of observed and modelled urban heat island intensity (ΔT) in each LCZ

Fig. 10 shows the evolution of precipitation field over Hungary during the second day of the simulation period. The largest amount of precipitation is modelled around 00 UTC, with hourly sums around 5 mm. As the centre of the cyclone (mean sea level pressure around 1004 hPa) approaches Szeged (around 12-13 UTC), the rainfall intensity decreases to 2–3 mm, however, still remarkable moist convergence is predicted at the western side of the centre. The dissipation of the system starts in the late afternoon, the hourly sums stays below 1 mm at 20 UTC. Later, the rainfall ceases according to the simulations.

The predicted hourly precipitation sums is evaluated through the measured values at station D-1 (Fig. 11). Under the evaluation process, three types of biases are introduced. The “standard” bias means the modelled bias (observed value subtracted from the modelled one) when the precipitation at a given hour is included both in the observations and outputs. Bias_{COND1} (always positive) refers to the case when the precipitation is modelled but not measured. Bias_{COND2} (always negative) refers to the case when the precipitation is measured but not modelled. Following this assumption, it is revealed that the rainfall in WRF is

simulated first at 18 UTC (on 22 October), but it is not supported by the observations. In real, the precipitation starts to fall in the next hour, which is not caught by WRF. In the hours afterwards, the hourly rainfall sums is mostly underestimated with about 1–2 mm. At 22 UTC a significant positive bias of 7 mm occurs. From 05 to 17 UTC, hourly sums over 1.5 mm is predicted, without the confirmation of the observations. At the end of the simulation period slight underestimations are illustrated. This can be the reason why T_n is simulated to be higher in contrast with T_{nOBS} .

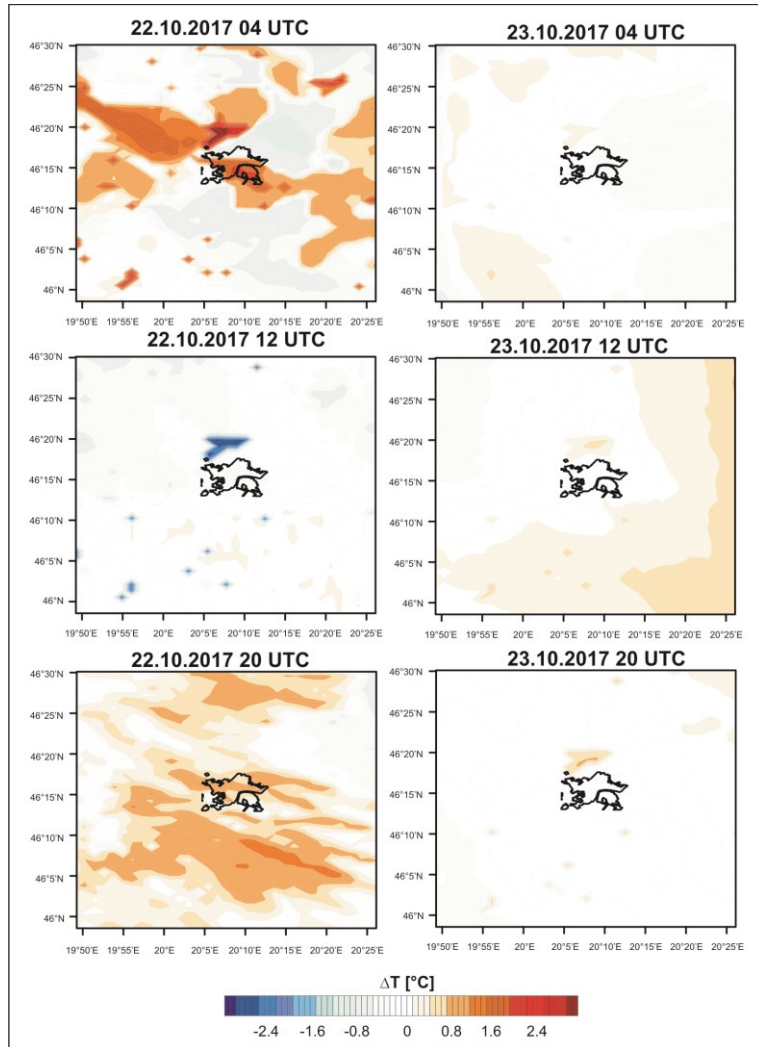


Fig. 9 Spatial distribution of modelled urban heat island intensity (ΔT) over the Szeged and the surroundings on six distinct dates

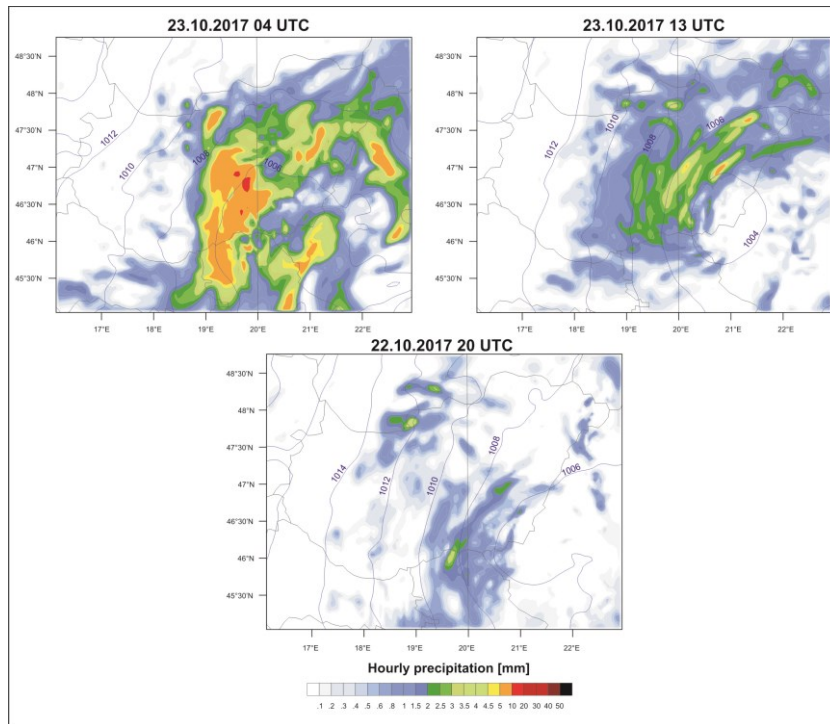


Fig. 10 Spatial distribution of modelled hourly sums of precipitation and mean sea level pressure over Hungary on three distinct dates

5. CONCLUSIONS

In this study, the urban heat island effect was simulated with WRF under non-ideal (i.e. fog and precipitation) meteorological conditions. It was analysed that whether the model is able to predict the influence of strong synoptic forcing on the evolution of thermal and moisture-related variables in the complex urban canopy layer. The modelled outputs of near-surface air temperature, urban heat island intensity, relative humidity, and precipitation sums was evaluated against the observations of our urban climate monitoring system.

During the first simulation period, thick fog layer covered the Carpathian Basin. Due to lack of insolation, the observed near-surface air temperatures had low temporal variation and ranged -3°C and 0°C . On the other hand, the predicted diurnal variabilities exceeded 5°C . The overestimations in the daytime, however, slightly decreased on the second day. At nights, the near-surface air temperature was simulated

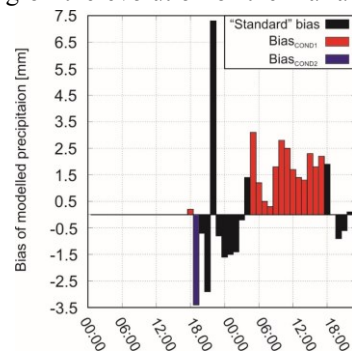


Fig. 11 Comparison of observed and modelled hourly precipitation sums at station D-1

better on the first day, with absolute biases lower than 1.5°C. According to the observations, only a weak urban effect was created under this synoptic pattern. As a result of the higher predicted temperatures in each urban LCZ related to the rural LCZ D, the urban heat island intensity was found to be 1.5–2°C higher in the simulations. Spatially, UHI has developed with the highest simulated magnitudes over areas classified as LCZs 2 and 5. LCZs with lower artificial surface coverage (e.g. LCZs 9 and D) were characterized by less pronounced urban effect. The relatively errors of WRF can be contributed to the under-prediction of air moisture content. While the observed relative humidity was around 80%, the observed values remained below this threshold, in fact, during the entire period. It means that the fog was almost totally excluded from the simulations, which has caused the remarkable variations of temperature and heat island intensity.

The second simulation period coincided with the pass of a Mediterranean low over Szeged, characterized by significant rainfall. It can be concluded that WRF has performed much better in terms of all variables. The largest uncertainties of near-surface temperature evolved on the first day when the precipitation event has not started yet. Then, the nocturnal values were caught adequately, although some underestimations of 1.5–2°C occurred during the daytime. On the next day, when the cyclonal system had more effect on the local meteorology, WRF predicted reasonably better the overall pattern of near-surface temperature in all LCZs. The drastic shift in urban effect between the two days of this period was also predicted with small biases. Due to intense rainfall, the simulated heat island intensity decreased 2–2.5°C in the downtown and stagnated around 0°C during the entire day. The evaluation of modelled hourly sums of precipitation suggested that pass of the rain field was captured appropriately in most of its aspects. Overall, more precipitation was simulated as it may be expected from the observations. The largest positive biases were created on the second day from 04 to 17 UTC. Meanwhile, the rainfall was modelled but not recorded by the measurements. This mistake has not caused significant biases in temperature, since the attenuation of solar radiation could be equal both in WRF and the observations.

As a conclusion, during the precipitation case, the model with our settings modelled the urban effect with relatively good agreement with the observations. The simulation of the synoptic pattern with thick fog layer, however, were followed by significant uncertainties. The evaluation of relative humidity in an urban and rural station confirmed that the existence of fog or mist was not reproduced by the model at all. The forecast of fog is one of the most difficult modelling challenge. Since this phenomenon acts typically on local scale, the horizontal resolution of grid and the selection of parameterization schemes is particularly crucial. If the global model that provides the initial and boundary conditions for WRF is not able to represent some of the important feature of the atmosphere over the region of interest, the simulation of WRF can also be inaccurate. To overcome this problem, it is advisable to use more model for reproducing the initial meteorological field and find which of those the best choice under a specific synoptic situation is. Moreover, the assimilation of local measurements can also be a reliable solution. For this reason, we aim to execute a 3-dimensional variational data assimilation of near-surface temperature and relative humidity, measured by our urban climate monitoring system. Hopefully, it can contribute to a better representation of the initial meteorological field, particularly under strong external synoptic forcing.

Acknowledgement: This work has been granted by the Hungarian Scientific Research Fund (OTKA K-111768).

REFERENCES

- Bergot T, Carrer D, Noilhan J, Bougeault P (2005) Improved site-specific numerical prediction of fog and low clouds: A feasibility study. *Weather Forecast* 20:627-646
- Bokwa A, Wypych A, Hajto MJ (2018) Role of fog in urban heat island modification in Kraków, Poland. *Aerosol Air Qual Res* 18:178-187
- Bougeault P, Lacarrere P (1989) Parameterization of orography-Induced turbulence in a mesobeta-scale model. *Mon Weather Rev* 117:1872-1890
- Fallmann J, Forkel R, Emeis S (2016) Secondary effects of urban heat island mitigation measures on air quality. *Atmos Environ* 125:199-211
- Gao X, Gao S, Yang Y (2018) A comparison between 3DVAR and EnKF for data assimilation effects on the Yellow Sea fog forecast. *Atmosphere-Basel* 9:346
- Hong SY, Dudhia J, Chen SH (2004) A revised approach to ice microphysical processes for the bulk parameterization of clouds and precipitation. *Mon Weather Rev* 132:103-120
- Iacono MJ, Delemere JS, Mlawer EJ, Shephard MW, Clough SA, Collins WD (2008) Radiative forcing by long-lived green-house gases: Calculations with the AER radiative transfer models. *J Geophys Res* 113:D13103
- Jimenez PA, Dudhia J, Gonzalez-Rouco JF, Navarro J, Montavez JP, Garcia-Bustamante, E (2012) A revised scheme for the WRF surface layer formulation. *Mon Weather Rev* 140:898-918
- Kain JS (2004) The Kain-Fritsch convective parameterization: An update. *J Appl Meteor* 43:170-181
- Kis A, Pongrácz R, Bartholy J (2017) Multi-model analysis of regional dry and wet conditions for the Carpathian Region. *Int J Climatol* 37:4543-4560
- Kottek M, Grieser J, Beck C, Rudolf B, Rubel F (2006) World map of the Köppen-Geiger climate classification update. *Meteorol Z* 15:259-263
- Kusaka H, Kondo H, Kikegawa Y, Kimura F (2001) A simple single-layer urban canopy model for atmospheric models: Comparison with multi-layer and slab models. *Bound-Lay Meteorol* 101:329-358
- Kusaka H, Kimura F (2004) Coupling a single-layer urban canopy model with a simple atmospheric model: Impact on urban heat island simulation for an idealized case. *J Meteorol Soc Jpn* 82:67-80
- Lelovics E, Unger J, Gál T, Gál CV (2014) Design of an urban monitoring network based on Local Climate Zone mapping and temperature pattern modelling. *Clim Res* 60:51-62
- Martilli, A, Clappier A, Rotach MW (2002) An urban surface exchange parameterization for mesoscale models. *Bound-Lay Meteorol* 104:261-304
- Morris CJG, Simmonds I, Plummer N (2001) Quantification of the influences of wind and cloud on the nocturnal Urban Heat Island of a large city. *J Appl Meteorol* 40:169-182
- Oke TR (1987) *Boundary Layer Climates*, 2nd ed. Routledge, London
- Péliné Németh Cs, Bartholy J, Pongrácz R, Radics K (2015) Analysis of climate change influences on the wind characteristics in Hungary. *Időjárás* 120:53-71
- Rémy S, Bergot T (2010) Ensemble Kalman filter data assimilation in a 1D numerical model used for fog forecasting. *Mon Weather Rev* 138:1792-1810
- Salamanca F, Martilli A (2010) A new building energy model coupled with an urban canopy parameterization for urban climate simulations—part II. Validation with one dimension offline simulations. *Theor Appl Climatol* 99:345-356
- Skamarock WC, Klemp JB, Dudhia J, Gill DO, Barker DM, Duda MG, Huang XY, Wang W, Powers JG (2008) A description of the advanced research WRF version 3. NCAR Tech. Note NCAR/TN-475+STR
- Steenefeld GJ, Ronda RJ, Holtslag AAM (2015) The challenge of forecasting onset and development of radiation fog using mesoscale atmospheric models. *Bound-Lay Meteorol* 154:265-289
- Stewart ID, Oke TR (2012) Local Climate Zones for urban temperature studies. *B Am Meteorol Soc* 93:1879-1900
- Tan J, Zheng Y, Tang X, Guo C, Li L, Song G, Zhen X, Yuan D, Kalkstein AJ, Li F, Chen H (2010) The urban heat island and its impact on heat waves and human health in Shanghai. *Int J Biometeorol* 54:75-84
- Tewari M, Chen F, Wang W, Dudhia J, LeMone MA, Mitchell K, Ek M, Gayno G, Wegiel J, Cuenca RH (2004) Implementation and verification of the unified NOAA land surface model in the WRF model. 20th Conference on Weather Analysis and Forecasting/16th Conference on Numerical Weather Prediction
- Tudor M (2010) Impact of horizontal diffusion, radiation and cloudiness parameterization schemes on fog forecasting on valleys. *Meteorol Atmos Phys* 108:57-70
- Vardoulakis E, Karamanis D, Fotiadi A, Mihalakakou G (2013) The urban heat island effect in a small Mediterranean city of high temperatures and cooling energy demands. *Sol Energy* 94:128-144
- Wang SK, Kuo S (2001) *Handbook of Air Conditioning and Refrigeration*. McGraw-Hill, New York